Title

Optimization and Improvement of Pressure-driven Membrane Performance for Desalinated Water Production

Author

Jung, Bongyeon

Publication Date

2022

Peer reviewed|Thesis/dissertation

UNIVERSITY OF CALIFORNIA

Los Angeles

Optimization and Improvement of Pressure-driven Membrane Performance for Desalinated Water Production

A dissertation submitted in partial satisfaction of the

requirements for the degree Doctor of Philosophy

in Civil Engineering

by

Bongyeon Jung

2022

ABSTRACT OF THE DISSERTATION

Optimization and Improvement of Pressure-driven Membrane Performance for Desalinated Water Production

by

Bongyeon Jung

Doctor of Philosophy in Civil Engineering

University of California, Los Angeles, 2022

Professor David Jassby, Chair

With the limited amount of freshwater resources, water scarcity has been becoming a serious problem. Thus, alternative water resources such as seawater and wastewater have been attracting water suppliers' attention. To exploit these alternative water resources, membrane filtration that has an ability to remove ionic species plays an important role. Although high salt removal efficiency (> 99%) can be achieved when membrane (i.e., reverse osmosis membrane) is operated under a great condition, membranes have relatively low removal efficiency of neutral and small molecules. In addition, the operation and application of membrane filtration is often limited by accumulation of undesired materials on the membrane surface, so called membrane fouling. To mitigate membrane fouling, source water must be appropriately pre-treated prior to be fed into

membrane filtration unit. In addition, membrane must be intermittently cleaned to remove readily formed membrane fouling in a chemical/physical way, which will increase water production cost.

Herein, we investigated electrochemical approach to enhance removal of neutrally-charged boron ions in seawater with electrically-conductive reverse osmosis membranes. By applying cathodic potentials, water electrolysis was facilitated to elevate local pH near the membrane surface, which increased the boron removal efficiency. We also studied optimization of groundwater treatment train that includes pretreatment and membrane filtration. By evaluating performance of each water treatment technologies, obtained results was coupled into a mathematical model to identify an optimum treatment train with blending ratio that can produce potable water that meets drinking water standards. Lastly, we also studied impact of alternating current on mineral scale formation on the electrically-conductive membrane that treats natural groundwater. With application of alternating current on the membrane surface, electrokinetic mixing was induced, which resulted in a mitigated scale formation.

The Dissertation of Bongyeon Jung is approved.

Eric M.V. Hoek

Jennifer A. Jay

Sanjay K. Mohanty

David Jassby, Committee Chair

University of California, Los Angeles

2022

TABLE OF CONTENTS

LIST OF FIGURES

LIST OF TABLES

ACKNOWLEDGEMENTS

I would like to thank my advisor, Dr. David Jassby, for his mentorship and extensive guidance. Without his support, I could not have made this far.

I also would like to acknowledge all my lab mates for their enormous help and support.

VITA

2010 Bachelor of Science in Environmental Energy System Engineering

Kyonggi University, South Korea

JOURNAL PUBLICATIONS

Bongyeon Jung, Caroline Y Kim, Shiyan Jiao, Unnati Rao, Alexander V Dudchenko, Jefferson Testet, David Jassby, *Enhancing boron rejection on electrically conduction reverse osmosis membranes through local electrochemical pH modification*, *Desalination (2020)*

Bongyeon Jung, Dean Menk, Michael J. Watts, David Jassby, *Evaluation and Optimization of Treatment Technologies Treating Groundwater from the Arbuckle-Timbered Hills Aquifer in Oklahoma*, *ACS Environmental Science & Technology Water (2021)*

Unnati Rao, Yiming Su, Chia Miang Khor, **Bongyeon Jung**, Shencun Ma, David M Cwiertny, Bryan M Wong, David Jassby, *Structurual Dependence of Reductive Defluorination of Linear PFAS Compounds in a UV/Electrochemical System*, *Environmental Science & Technology (2020)*

Unnati Rao, Arpita Iddya, **Bongyeon Jung**, Chia Miang Khor, Zachary Hendren, Craig Turchi, Tzahi Cath, Eric MV Hoek, Guy Z Roman, David Jassby, *Mineral Scale Prevention on Electrically Conducting Membrane Distillation Membranes Using Induced Electrophoretic Mixing*, *Environmental Science & Technology (2020)*

Shengcun Ma, Fan Yang, Xin Chen, Chia Miang Khor, **Bongyeon Jung**, Arpita Iddya, Gaurav Sant, David Jassby, *Removal of As(III) by Electrically Conducting Ultrafiltration Membranes*. *Water Research (2021)*

Yiming Liu, Jingbo Wang, **Bongyeon Jung**, Unnati Rao, Erfan Sedighib, Eric M.V. Hoek, Nils Tiltond, Tzahi Y. Cath, Craig S. Turch, Michael B. Heeley, Y. Sungtaek Ju, David Jassby, *Hyper-saline produced water desalination via direct-heat vacuum membrane distillation, Water Research (2022)*

CONFERENCES PRESENTATIONS

Bongyeon Jung, Caroline Y Kim, Shiyan Jiao, Unnati Rao, Alexander V Dudchenko, Jefferson Testet, David Jassby, *Enhancement of Boron Removal Using Electrically Conducting Reverse Osmosis Membranes,* The North American Membrane Society (NAMS), 2019

Bongyeon Jung, Shengcun Ma, Chia Miang Khor, Noman Khalid Khanzada, Arezou Anvari, Unnati Rao, Eric M.V. Hoek, David Jassby, Retarded Scaling Formation on Electrically Conducting Nanofiltration Membranes, The North American Membrane Society (NAMS), 2020

Unnati Rao**,** Arpita Iddya, **Bongyeon Jung**, Chia Miang Khor, Zachary Hendren, Craig Turchi, Tzahi Cath, Eric MV Hoek, Guy Z Roman, David Jassby**,** Scaling Mitigation in Membrane Distillation through Electrokinetic Mixing**,** The North American Membrane Society (NAMS), 2019

David Jassby, Unnati Rao, Arpita Iddya, **Bongyeon Jung**, Chia Miang Khor, Zachary Hendren, Craig Turchi, Tzahi Y. Cath, Eric M.V. Hoek, Guy Ramon, Electrochemical Prevention of Mineral Scale on Electrically Conducting Membrane Distillation Membranes, International Congress on Membranes and Membrane Processes (ICOM), 2020

Yiming Liu, Jingbo Wang, **Bongyeon Jung**, Unnati Rao, Erfan Sedighib, Eric M.V. Hoek, Nils Tiltond, Tzahi Y. Cath, Craig S. Turch, Michael B. Heeley, Y. Sungtaek Ju, David Jassby, Evaluation of Direct Heated Vacuum Membrane Distillation Process using Module-scale Simulation, The North American Membrane Society (NAMS), 2021

Chapter 1.

Introduction

1.1 Membrane Filtration: A Promising Solution to Water Scarcity

Water is an essential ingredient for human beings: not only up to 60% of human body is composed of water, but also food (such as crops, meat, fruits, etc..) requires huge amount of water for its production, resulting in the food production sector taking up the largest portion of freshwater consumption (~75% of current human water use).[1–4] Although water is the most abundant resource on earth, majority of water (97%) exist in the form of seawater, and only marginal amount of water is readily available for direct use.[5–7] In addition, sources for fresh water (i.e., liver, lake, and groundwater) is not evenly distributed around the world, which makes arid and semi-arid regions (i.e., Middle East, and South African countries) suffer from the lack of water.[8–11] This water scarcity also occurs in well-developed countries, due to fast industrialization, water pollution, population growth, and climate change.[12–15] Industrialization takes place with more advanced manufacturing plants, which inevitably leads to more water and energy consumption and more wastewater generation that could potentially cause water pollution. Population growth obviously elevates the demand for potable water and daily water usage, and climate change has been influencing annual precipitation and evaporation patterns of water that changes water availability.

To meet the increasing demand of fresh water, water suppliers have been looking for alternative water resources that are less impacted by the aforementioned factors and relatively infinite in amount. Such resources can be seawater, wastewater, and brackish groundwater since these resources are continuously generated or naturally replenished.[16–22] In order to treat this type of water resources, membrane filtration is an essential technology to meet the growing demand for drinking and agricultural water.

1.2 Basics of Membrane Filtration

1.2.1 Classification of Pressure-driven Membranes

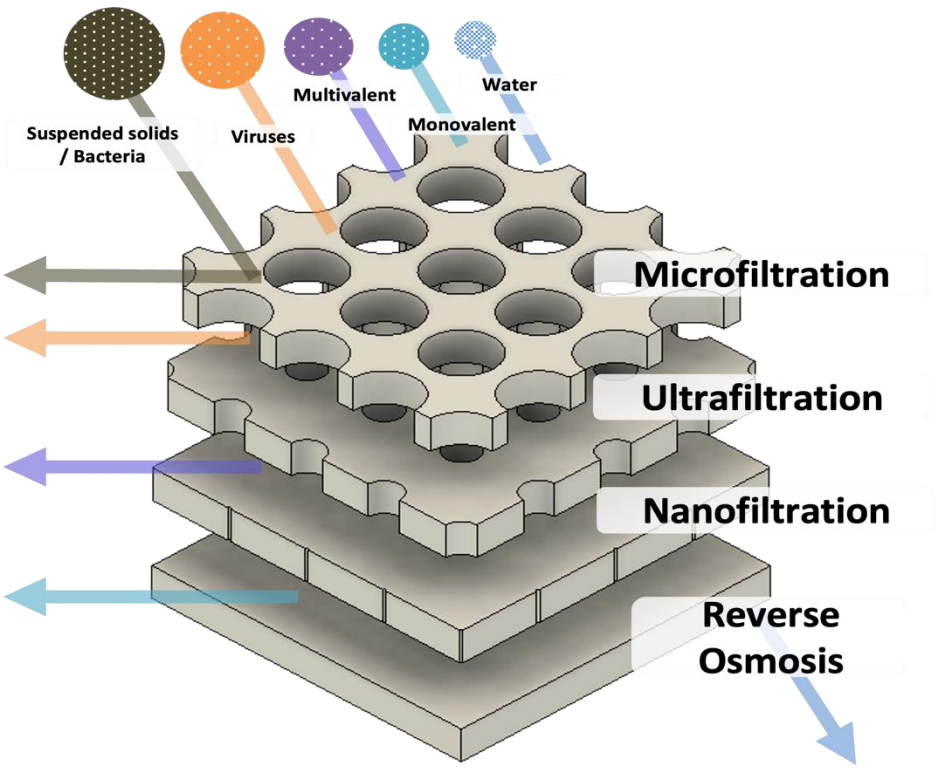

Figure 1.1. Classification of pressure-driven membranes

Polymeric membranes in water treatment plants can be classified based on their pore size (Figure 1).[23,24] Microfiltration (MF) membranes have the largest pore size followed by ultrafiltration (UF), nanofiltration (NF) and reverse osmosis (RO). MF and UF membranes rely on the physical separation (so called, size exclusion) owing to their relatively larger pore sizes than NF and RO.[25] Any materials greater than the size of membrane pores in the water will be retained. Thus, MF membranes have an ability to sieve large molecules (e.g., suspended solids and bacteria) in the feed, while UF membranes can not only remove suspended solids and bacteria, but also can separate viruses. NF and RO membranes that are often considered to be non-porous remove

matters not only by their size (size exclusion), but also by their charge (charge repulsion and Donnan exclusion).[26–30] Therefore, NF and RO membranes are able to separate much smaller molecules (i.e., ionic species) from water that can easily penetrate MF and UF membranes.

1.2.2 Microfiltration (MF) membranes

Collodion (nitrocellulose) MF membrane was first developed in 1920s.[31] However, the market was small, and its application was limited to small-scale industrial applications. First large-scale of MF membrane was employed to culture microorganisms in drinking water, which was conducted in Germany during World War II to monitor the contamination of water supply. MF membrane was used to filter any bacteria in the water. Then, the filtered membrane was immersed in a nutrient solution to multiply bacteria, making them easily counted by a microscope.[32]

MF membrane has a pore size ranging from 0.05 μm to 10 μm, which makes it suitable to remove particles having size > 0.1 μm from a liquid.[33] Owing to its open membrane structure, MF membrane requires low pressures (< 2 bar) for contaminant removal. Modern MF membrane is commonly applied in food/beverage, pharmaceuticals, wastewater treatment, desalination, semiconductor industry and biotechnology.[33–36]

MF membranes can be fabricated by multiple techniques: sintering, stretching, track-etching, and phase inversion.[37,38] Organic and inorganic materials that are commonly used for MF membranes synthesis are listed below:

Table 1.1. List of common organic and inorganic materials for MF membrane synthesis

Membrane characteristics	Materials
Hydrophobic polymeric membranes	Polytetrafluoroethylene (PTFE) poly(vinylidene fluoride) (PVDF) polypropylene (PP) Polyethylene (PE)

Hydrophilic polymeric membranes	Cellulose esters, polycarbonate (PC) polysulfone (PSf) poly(ether sulfone) (PES) polyimide (PI) poly(ether imide) (PEI) (aliphatic) polyamide (PA) polyehteretherketone (PEEK)
Ceramic membranes	Alumina (Al_2O_3) zirconia (ZrO_2) titania (TiO_2) silicium carbide (SiC)

1.2.3 Ultrafiltration (UF) membranes

Similar to MF membranes, first UF membranes were also synthesized by collodion in 1907 by Bechhold.[39] However, application of this type of UF membranes was limited to lab-scale studies until the breakthrough took place in 1960s. In 1963, Loeb and Sourirjan developed anisotropic cellulose acetate UF membranes using polymer precipitation method at University of California, Los Angeles (UCLA), and in 1969, successful application of UF membranes in an industry-scale appeared.[32]

UF membranes has a similarity with MF in processes and separation principle, but the difference lies in membrane pore size and asymmetric structure. While MF membranes have pore size ranging from 0.05 µm to 10 µm, UF membranes, in general, have a pore size in the 0.001 µm to 0.1 µm (10 Å to 1000 Å).[40,41] This smaller pores and asymmetric structure of UF membranes provide much higher hydrodynamic resistance than MF, requiring a higher applied pressure (1 – 10 bar).[42]

UF membranes are applicable to separate colloids and macromolecules in diameter of > 10 ~ 1000 Å from a solution. Such application includes food/dairy (i.e., milk, cheese, whey protein recovery etc..) industry, pharmaceutical, textile, paper, and leather industry.[43–47]

Due to UF membranes' relatively smaller pore diameter, the pore size distribution and separation properties of UF membranes are often characterized by molecular weight cut-off (MWCO) at which > 90% rejection of defined solutes is identified.

UF membranes are synthesized by a Loeb-Sourirajan technique (also called phase inversion or polymer precipitation process) which a casting polymer solution turns into solid phase. There are four different phase inversion methods: water precipitation, water vapor absorption, thermal gelation, and solvent evaporation.[48,49] Among these, water precipitation is a most common method for modern UF membrane fabrication. Loeb-Sourirajan's technique was not only a breakthrough for UF membranes, but also was a catalyst for the development of new membrane fabrication techniques. Interfacial polymerization (IP), one of most important non-porous membrane fabrication process in the modern society, is one of the examples, and will be covered in the following section.

Materials for UF membrane synthesis include organic and inorganic materials, and these are listed below:

Table 1.2. List of common organic and inorganic materials for UF membrane synthesis

Membrane characteristics	Materials
Polymeric materials	Polysulfone (PSf) Polyetheresulfone (PES) Sulfonated polysulfone Poly(vinylidene fluoride) (PVDF) Cellulose acetate Polyimide Poly(ethere imide) Aliphatic polyamides Polyehteretherketone (PEEK)
Inorganic materials	Alumina (Al_2O_3) zirconia (ZrO_2)

1.2.4 Nanofiltration (NF) membranes

NF membranes are developed as a variant of reverse osmosis (RO) membranes in late 1970s. During the RO membrane fabrication process, it was found that various post treatment (i.e., heat curing) condition could produce a relatively larger pores leading to lower monovalent (Na^+ and Cl^-) rejection while requiring lower operating pressure. Prior to being named as NF, it was called as loose RO, intermediate RO/UF, or tight UF membrane, since its separation properties laying between RO and UF.[32]

NF membranes were originally synthesized with cellulose acetate (CA) and its derivatives by a phase inversion method.[50] However, CA membranes were prone to biological degradation and exposure to chemicals and high temperature, resulting in degraded water flux and salt rejection.[51,52] Thus, looking for a new material that is non-cellulosic and biologically, chemically, and thermally stable was warranted. For this reason, new NF membranes were made with three different layers: top selective layer, microporous interlayer, and nonwoven polyester layer. This configuration is now known as thin film composite (TFC). Unlike CA membranes being fabricated with a sing-step process (i.e., phase inversion), fabrication of TFC membranes is a two-step process: phase inversion of microporous interlayer, and IP of selective layer.

NF membranes have a MWCO of 200 – 1,000 Dalton (Da), corresponding to pore sizes from 5 to 20 Å Compared to MF and UF membranes, NF membranes require much more operating pressures (150 psi) owing to its much smaller pore sizes. However, the operating pressure is still much lower than the pressure in reverse osmosis system (250 psi – 800 psi). Therefore, NF membranes are widely used as a water softening method, a pretreatment step, or a primary separation method in which high level of divalent ion removal is required with a relatively low energy input.[53–55]

Salt removal mechanism by NF membranes includes size exclusion (steric hinderance), electrostatic (Donnan) exclusion, and dielectric exclusion.[56–58]

1.2.5 Reverse Osmosis (RO) membranes

Osmosis is a naturally occurring process which solvent moves toward an area having lower solute concentration through a semi-permeable membrane from an area having higher solute concentration. Concentration gradient (concentration imbalance between each side of membrane) drives the solvent more from one side to the other, resulting in an osmotic pressure. In 1850s, osmotic phenomena were studied with ceramic membranes, and it was proven that membranes were capable of separation of small solutes from water. [59]

RO is a process which solvent moves against the concentration gradient by applying a pressure greater than osmotic pressure. Thus, more solutes remain in the one side, and the other side becomes relatively solute-free. The term RO was first patented for the purpose of desalting water in 1931. In 1959, Reid and Breton showed the feasibility of cellulose acetate films to perform desalination. Although the cellulose acetate films had a great salt removal efficiency (> 98%), their commercialization was limited by low water flux.[60,61] In 1962, a breakthrough was made by Loeb and Sourirajan at UCLA.[62,63] They developed an anisotropic cellulose acetate membrane through the phase-inversion method. The resulting membrane had much higher water flux (10 times) with a similar salt removal efficiency with the Reid and Breton's membrane. This type of membrane was widely applied in 1960s until IP method was developed by Cadotte in 1972. Cadotte's membrane was made of same material (i.e., cellulose acetate) with Loeb and Sourirajan's, but the IP method provided a better water flux and salt rejection. The RO membrane made *via* IP method was first commercialized in 1975 by Fluid Systems.[64–66] Then, Cadotte made

TFC RO membrane out of m-phenylenediamine (MPD) and trimesoyl chloride (TMC) through the IP method, which is a standard method for RO membrane fabrication until now.

RO membranes are the tightest pressure-driven membranes. Unlike other types of membranes (MF, UF, and NF), RO membranes are generally considered as non-porous membrane. Salt removal mechanism includes size exclusion (steric hinderance), electrostatic (Donnan) exclusion, and dielectric exclusion.

1.3 Transport Mechanism in Membrane Filtration

1.3.1 Transport Mechanism of Microporous Membranes

MF and UF membranes can be classified as microporous membranes owing to their relatively large pore size than NF and RO membranes. Thus, a principal solute removal mechanism for MF and UF membranes is a size exclusion (or steric hinderance) that particles larger than the pore size are retained by the pores.

Darcy's law can be used to describe the convective water flow through capillary or porous medium:

$$J = A \times \Delta P \quad (1)$$

Where is J water flux, is A permeability constant, is ΔP pressure difference across the membrane. Constant A is a function of membrane's structure (porosity and pore size distribution) and viscosity of liquid passing through the membrane. Since UF membranes generally have smaller pore sizes, A value (water permeability constant) of UF is smaller than the A value of MF. For laminar flow (when Reynolds number < 2,000) and membrane having capillary pores, Hagen-Poiseuille equation can be applied with an assumption of identical pore radius:

$$J = \frac{\varepsilon r^2}{8 \eta \tau} \times \frac{\Delta P}{\Delta x} \quad (2)$$

where ε is surface porosity, r is pore radius, η is dynamic viscosity of permeating liquid, τ is tortuosity (unity for cylindrical pores), and Δx is membrane thickness. Equation (2) clearly shows a linear relationship between water flux and the driving force (i.e., transmembrane pressure, ΔP). Instead of Hagen-Poiseuille equation, Kozeny-Carman relationship can be used for membranes packed with spheres:

$$J = \frac{\varepsilon^3}{K\,\eta\,S^2\,(1-\varepsilon)^2} \times \frac{\Delta P}{\Delta x} \quad (3)$$

where ε is volume fraction of the pores, K is Kozeny-Carman constant that is a function of pore shape and tortuosity, and S is internal surface area.

Although actual pore structure of MF and UF membranes are neither of cylindrical or spherical, Hagen-Poiseulle or Kozeny-Carman equations are widely used to describe the water flux through the membrane.

1.3.2 Transport Mechanism of Dense Membranes

It has been more than 60 years since the TFC membranes have developed and extensively studied. However, it is still unclear how exactly the membranes retain salt while allowing water passage. The most widely accepted theory of transport mechanism in dense membranes (i.e., NF and RO) is a solution-diffusion model. In the solution-diffusion model, a component moves toward the membrane by driving forces (such as concentration gradient, transmembrane pressure, electrical potential gradient, temperature). Then, the component absorbs into the membrane, and diffuses toward the other side of membrane. And finally, the component desorbs and moves away from the membrane.

The solution-diffusion can be described mathematically from a simple equation:

$$J_i = -L_i \frac{d\mu_i}{dx} \quad (4)$$

where J_i is a flux of a component i, L_i is a proportionality coefficient, $\frac{d\mu_i}{dx}$ is a chemical gradient of component i across the membrane. Under the condition where driving forces are limited to concentration and pressure gradient, the chemical potential can be rewritten as:

$$d\mu_i = RTd\ ln(\gamma_i n_i) + v_i dp \quad (5)$$

where R is universal gas constant, T is absolute temperature, γ_i is activity coefficient, n_i is mole fraction of component i, v_i is the molar volume of the component i, and p is the pressure. For incompressible phases, volume does not change with pressure. Thus, integrating Equation (5) gives:

$$\mu_i = \mu_i^o + RT\ ln(\gamma_i n_i) + v_i(p - p_i^o) \quad (6)$$

where μ_i^o is the reference chemical potential of component i at reference pressure p_i^o. The reference pressure, p_i^o, can be expressed with the terms of vapor pressure of i, p_i^{sat}. Then, Equation (6) becomes:

$$\mu_i = \mu_i^o + RT\ ln(\gamma_i n_i) + v_i(p - p_i^{sat}) \quad (7)$$

With an assumption that there is no pressure gradient within the membrane and a linear gradient of chemical potential across the membrane, combination of Equation (4) and (5) gives:

$$J_i = -\frac{RTL_i}{n_i}\frac{dn_i}{dx} \quad (8)$$

Mole fraction of component i, n_i, can be expressed in terms of component i's concentration:

$$c_i = \rho\ m_i\ n_i \quad (9)$$

where ρ is molar density, is m_i molecular weight of component i. By combining Equation (8) and (9),

$$J_i = -\frac{RTL_i}{c_i}\frac{dc_i}{dx} \quad (10)$$

RTL_i/c_i can be replaced as diffusion coefficient D_i according to Fick's law ($J = -D\frac{dc}{dx}$). By integrating the Equation (10) over the membrane thickness (l),

$$J_i = \frac{D_i}{l}\left(C_{i,o,m} - C_{i,l,m}\right) \quad (11)$$

where $C_{i,o,m}$ is the concentration of component i at the feed-side of membrane and $C_{i,l,m}$ is the concentration of component i at the permeate-side of membrane.

Since it was assumed a linear chemical potential gradient within the membrane, chemical potential in the bulk solution is equal to the chemical potential near the feed-side membrane.

$$\mu_{i,o} = \mu_{i,o,m} \quad (12)$$

Equation (12) can be rewritten using the Equation (7):

$$\mu_i^o + RT\, ln\left(\gamma_{i,o} n_{i,o}\right) + v_i(p_o - p_i^{sat}) = \mu_i^o + RT\, ln\left(\gamma_{i,o,m} n_{i,o,m}\right) + v_i(p_o - p_i^{sat}) \quad (13)$$

By rearranging the Equation (13),

$$ln\left(\gamma_{i,o} n_{i,o}\right) = ln\left(\gamma_{i,o,m} n_{i,o,m}\right) \quad (14)$$

or,

$$n_{i,o} = \frac{\gamma_{i,o,m}}{\gamma_{i,o}} n_{i,o,m} \quad (15)$$

Using Equation (9), Equation (15) can also be written as:

$$C_{i,o,m} = \frac{\gamma_{i,o}\, \rho_m}{\gamma_{i,o,m}} c_{i,o} \quad (16)$$

The term $\gamma_{i,o}\, \rho_m/\gamma_{i,o,m}$ can be replaced by a sorption coefficient K_i. Then,

$$C_{i,o,m} = K_i \cdot c_{i,o} \quad (17)$$

In the same manner of the above procedure, the chemical potential near the membrane in the permeate side is,

$$\mu_{i,l} = \mu_{i,l,m} \quad (18)$$

Which leads to

$$\mu_i^o + RT\, ln(\gamma_{i,l} n_{i,l}) + v_i(p_l - p_i^{sat}) = \mu_i^o + RT\, ln(\gamma_{i,l,m} n_{i,l,m}) + v_i(p_o - p_i^{sat}) \quad (19)$$

With a rearrangement,

$$ln(\gamma_{i,l} n_{i,l}) = ln(\gamma_{i,l,m} n_{i,l,m}) + \frac{v_i(p_o - p_l)}{RT} \quad (20)$$

Equation (20) can be rearranged as:

$$\frac{\gamma_{i,l} n_{i,l}}{\gamma_{i,l,m} n_{i,l,m}} = \frac{v_i(p_o - p_l)}{RT} \quad (21)$$

By introducing the relationship used in Equation (16) and (17),

$$n_{i,l,m} = \frac{\gamma_{i,l}}{\gamma_{i,l,m}} \cdot n_{i,l}$$

$$c_{i,l,m} = \frac{\gamma_{i,l} \cdot \rho_m}{\gamma_{i,l,m} \cdot \rho_o} \cdot c_{i,l}$$

$$K_i = \frac{\gamma_{i,l} \cdot \rho_m}{\gamma_{i,l,m} \cdot \rho_o}$$

Equation (20) becomes

$$\frac{\gamma_{i,l} \cdot c_{i,l} \cdot \rho_m}{\gamma_{i,l,m} \cdot c_{i,l,m} \cdot \rho_o} = \frac{K_i \cdot c_{i,l}}{c_{i,l,m}} = exp\left(\frac{v_i(p_o - p_l)}{RT}\right) \quad (22)$$

Or,

$$c_{i,l,m} = K_i \cdot c_{i,l} \cdot exp\left(\frac{-v_i(p_o - p_l)}{RT}\right) \quad (23)$$

By combining Equation (17) and Equation (23) with Equation (11), we have

$$J_i = \frac{D_i \cdot K_i}{l}\left[c_{i,o} - c_{i,l} \cdot exp\left(\frac{-v_i(p_o - p_l)}{RT}\right)\right] \quad (24)$$

The term $D_i \cdot K_i/l$ can also be replaced as permeability coefficient, P_i. Then, Equation (24) becomes,

$$J_i = \frac{P_i}{l}\left[c_{i,o} - c_{i,l} \cdot exp\left(\frac{-v_i(p_o - p_l)}{RT}\right)\right] \quad (25)$$

With an assumption that water flux (J_w) is much higher than solute flux (J_s) and membrane has a great selectivity, Equation (25) can be simplified. Under the osmotic equilibrium condition where no water flux exists, Equation (25) becomes

$$J_w = \frac{P_i}{l}\left[c_{i,o} - c_{i,l} \cdot exp\left(\frac{-v_i(\Delta\pi)}{RT}\right)\right] = 0 \quad (26)$$

where $\Delta\pi$ is osmotic pressure. By rearranging,

$$c_{i,l} = c_{i,o} \cdot exp\left(\frac{v_i \cdot \Delta\pi}{RT}\right) \quad (27)$$

By plugging Equation (27) into Equation (25), we have

$$J_w = \frac{P_i \cdot c_{i,o}}{l}\left[1 - exp\left(\frac{-v_i[(p_o - p_l) - \Delta\pi]}{RT}\right)\right] \quad (28)$$

The term $(p_o - p_l)$ cam also be express as transmembrane pressure Δp:

$$J_w = \frac{P_i \cdot c_{i,o}}{l}\left[1 - exp\left(\frac{-v_i(\Delta p - \Delta\pi)}{RT}\right)\right] \quad (29)$$

It was mathematically proven that most of operational conditions where dense membrane is used, value of $\frac{-v_i(\Delta p - \Delta\pi)}{RT}$ is very small. So, $1 - \exp(-x) \approx -x$ can be used. Then, Equation (29) is simplified to:

$$J_w = \frac{P_i \cdot c_{i,o} \cdot v_i}{lRT}(\Delta p - \Delta\pi) \quad (30)$$

Equation (30) can also be further simplified by replacing $\frac{P_i \cdot c_{i,o} \cdot v_i}{lRT}$ with water permeability constant, A:

$$J_w = A(\Delta p - \Delta \pi) \quad (31)$$

Water permeability constant A is also called as A parameter. Equation (31) implies that the water flux is proportional to applied pressure at a given osmotic pressure. With a given applied and osmotic pressure, the water flux changes accordingly to A parameter which is a function of membrane structure (such as material and polymer chemistry).

In a similar manner, salt flux (J_s) can be express in the same manner with the Equation (24).

$$J_s = \frac{D_s \cdot K_s}{l}\left[c_{s,o} - c_{s,l} \cdot exp\left(\frac{-v_i(p_o - p_l)}{RT}\right)\right] \quad (32)$$

Since the value of $\frac{-v_i(\Delta p - \Delta \pi)}{RT}$ is small as mentioned previously, $exp\left(\frac{-v_i(p_o - p_l)}{RT}\right)$ is close to unity. Then, Equation (32) becomes

$$J_s = \frac{D_s \cdot K_s}{l}\left(c_{s,o} - c_{s,l}\right) \quad (33)$$

Similarly, $\frac{D_s \cdot K_s}{l}$ can be replaced as salt permeability constant, B:

$$J_s = B\left(c_{s,o} - c_{s,l}\right) \quad (34)$$

Equation (34) implies that the salt flux is independent of applied pressure and is a function of concentration difference between feed and permeate stream.

1.4 Challenges in Membrane Filtration

Compared to the conventional water treatment processes, membrane filtration processes have multiple advantages; Membrane filtration requires small foot-print and small energy input (for

microporous membranes); The filtration processes can provide a wide range of water quality that can be adjusted based on the needs; The operation and maintenance are relatively simple.[67–69] However, operation of membrane filtrations is often limited by the deposit of undesirable matters on the membrane surface, so called membrane fouling. Membrane fouling is particularly challenging in membrane-based water treatment processes because the fouling could lower the water permeance and target pollutant (such as microorganism and salt) removal efficiency, resulting in the poor quality of the final water product. Additionally, membrane fouling elevates the water production cost owing to the reduced the lifespan of membrane and more frequent membrane cleaning.[70]

In case of nonporous membranes (i.e., NF and RO), their application could be energy-intensive in some cases, and the processes inevitably generate a concentrated waste stream (so called, brine) that needs to be further treated or appropriately disposed. This could be a limiting factor of the installation of membrane-based water treatment facility in the suburban area where power consumption of membrane filtration and generation/disposal of concentrated waste are not economically feasible.

Membrane fouling can be classified by reversibility of membrane performance (i.e., permeate flux and salt rejection prior to fouling event).[71–75] Reversible fouling represents a fouling that can be eliminated from the surface of membrane with a single or multiple appropriate methods (such as back-washing, chemical cleaning, air scouring, etc.). On the other hand, irreversible fouling is defined as the fouling that remains on the membrane surface even after fouling removal practices, resulting in a deteriorated water flux and/or salt removal efficiency. Membrane fouling can also be subdivided based on the constituent of fouling layers. Frequently encountered foulant in the water treatment include colloids, organic matters, inorganic salts, and microorganisms which each

fouling is labeled as colloidal fouling, organic fouling, inorganic fouling (or, scaling), and biofouling.

1.4.1 Membrane fouling

1.4.1.1 Colloidal Fouling

Colloids are defined as a mixture that more than two substances are mixed but not combined. In the water treatment system colloids are found as insoluble matters that exist in water and are separatable with an appropriate method. One of such examples is a membrane filtration treating surface water or treated secondary effluent.[76–78]

Colloidal particles in the bulk feed moves toward membrane surface by various mechanisms such as convection, Brownian motion, inertia, gravitational settling, and lateral migration. Then, colloids can cause a blockage of membrane pores. The extent of attachment of colloids to the membrane surface is known to be a function of water chemistry (pH, ionic strength, temperature, etc.) and membrane's properties (roughness, surface charge, hydrophilicity, etc.).[79,80]

Colloids having a similar size with diameter of membrane pores can be clogged at the entrance of membrane pores, which is called pore-blocking.[81–83] Colloids having greater than the pores in size can accumulate on the surface of membrane, so-called cake formation. Pore-blocking is a prior procedure of cake formation; Colloidal particles first interact with the membrane, which leads to pore-blocking; Then, newly incoming colloids will start piling up and forming layers of colloids by interacting with the old colloids that are readily attached on the membrane surface. Therefore, once the cake layer is formed on the surface of membrane, water transport and solute removal is mainly governed by the cake layer that covers the surface of membrane and is exposed to the feed water.

The effect of fouling on the permeances has been described by a model named "Resistance-in-series", which is a variant of Darcy's law (Equation 1).

$$J = \frac{\Delta P}{\mu \cdot R_{total}} \quad (35)$$

$$R_{total} = R_{membrane} + R_{cake} + R_{pore-blocking} + \cdots \quad (36)$$

where μ is fluid viscosity, R_{total} is a total resistance that hinders permeation, $R_{membrane}$ is a resistance from membrane itself, $R_{cake}$is a resistance caused by the cake layer, $R_{pore-blocking}$ is a resistance resulting from pore-blocking.

1.4.1.2 Organic Fouling

Every water body contains dissolved organic matter (DOM) which can be a mixture of materials naturally occurring and being artificially synthesized. When the organic matter originates from feces and remains from plants and animals, it is labeled as natural organic matter (NOM). If the organic compounds are made by anthropogenic activity (such as a production of pesticides, fuel additives, byproducts from pre-oxidation, etc.), it is named synthetic organic compounds (SOC).

NOM is a dominant organic fouling agent particularly in drinking water treatment processes. NOM is complex carbon-based compounds that could comprise a range of constituent ranging from small acids to larger humic and fulvic acid. NOM can be divided into humic acids, fulvic acids, and humin; humic acids become soluble at alkaline pH while fulvic acid is always soluble and humin is unsoluble. Although it remains unclear of exact mechanism of organic fouling event, it is speculated that absorption of NOM into membrane pores (resulting in pore narrowing and

pore blocking) and gel layer formation of NOM onto membrane surface lead to the reduction of water permeation.[84,85]

1.4.1.3 Inorganic Fouling (Scaling)

When membrane fouling is caused by inorganic species, the fouling event is named as inorganic fouling, or scaling. Unlike other types of membrane fouling, scaling occurs when the concentrations of sparingly soluble salts exceed their solubility limits. Therefore, scaling is mostly problematic in desalination processes using tight and nonporous membranes (i.e., NF and RO) where a feed is continuously concentrated by the production of permeate water.

Scale formation on the membrane surface requires a prior step of nuclei formation that can be either formed in the bulk solution or on the membrane surface. The former case is labeled as homogeneous nucleation, while the latter case is called heterogeneous nucleation. Once nuclei forms, it starts growing up with interactions with surrounding ion species. Then, small nucleus are further developed into inorganic crystals, which is called crystallization. The crystallization also can be divided into bulk crystallization and surface crystallization depending on where the crystallization takes place. In bulk crystallization, crystals formed in the bulk solution are transported to the membrane surface. In case of surface crystallization, crystals are formed on the membrane surface followed by a sequence of crystal growth.[86–89]

Although membrane filtration has been extensively studied since its advent, it remains unclear which pathway of crystallization dominates in scaling formation. In addition, there are conflicting studies that suggest the dominance of specific crystallization over the other. Some researchers believe that bulk crystallization governs the membrane scaling because heterogeneous crystallization models fail to explain the patterns for flux decline and scale growth. However, other

researchers believe surface crystallization is more critical pathway of scaling formation due to longer induction time of bulk crystallization than the residence time in the membrane module.[90]

The most abundant scaling species in the desalination process are calcium carbonate ($CaCO_3$) and calcium sulfate ($CaSO_4$), while small amount of strontium sulfate ($SrSO_4$), barium sulfate ($BrSO_4$), and silicate are also identified. In seawater desalination process, $CaCO_3$ is a primary scaling species, while both of $CaCO_3$ and $CaSO_4$ are primary constituent of mineral scale in the brackish water desalination process. [91–93]

1.4.1.4 Biofouling

When the loss of membrane performance is caused by the membrane surface covered by biological foulant (such as carbohydrates, micro-organisms, cell debris, etc.), the fouling event is labeled as biofouling. Biofouling includes the process of attachment, growth, and metabolism of biological materials on the membrane.

Among other type of membrane fouling, biofouling has been regarded as the most serious problem. It has previously reported that more than biofouling accounts for around 50% of entire membrane fouling occurred in NF and RO membranes treating surface water and wastewater. In addition, biofoulant, unlike other foulants, has a characteristic of self-replication under the favorable environment to cell metabolism. Traditional biofoulant encountered in memebrane-based water treatment facilities include proteins, carbohydrates, cells, and biofilms.[94,95]

Although there could be multiple detailed steps to describe the occurrence of biofouling on the membrane surface, the procedure can be essentially presented as two major stage process: conditioning and growth. During the initial stage, deposition of conditioning film (such as organic molecules) cause pore blocking and solute adsorption onto the membrane surface. Then, cell

proliferation takes place, followed by production of extracellular polymeric substances (EPS) which accounts for more than 90% of total dry mass in biofilms. The EPS makes the fouling layer become more irreversible, as well as protects the cells from antibacterial agents. The EPS consists of proteins, nucleic acids, polysaccharides, and lipids.[94]

rane

1.4.1.5 Concentration Polarization

Membrane fouling is one factor that reduces water permeation through a membrane. Another factor that causes a permeation reduction is an accumulation of ions near the membrane surface, resulting in a region where concentrations of solute are higher than that in the bulk. Thus, osmotic pressure near the membrane surface becomes greater than the pressure in the bulk, resulting in a greater driving force (i.e., concentration gradient) of back diffusion to the bulk. This phenomenon is called concentration polarization which inevitably occurs in the pressure-driven membrane filtration processes. Membrane fouling and concentration polarization have an interrelationship and are often synergetic when both are present simultaneously. For instance, membrane scaling can be promoted due to presence of concentration polarization where concentrations of scaling ions could exceed their saturation level. Another example is organic fouling facilitated by concentration polarization. Higher concentration of Ca^{2+} ions in the concentration polarization region could encourage organic fouling by bridging organic molecules with Ca^{2+} ions.[96–98]

1.5 Solutions to Tackle Challenges in Membrane Filtration

1.5.1 Pretreatment of feed water

Pretreatment of feed water is a widely employed method to reduce the tendency of membrane fouling, resulting in an extended lifespan of membrane. Since there are various pretreatment

technologies, single or combined treatments must be reasonably chosen based on a target foulant in the source water.

Conventional pretreatment methods include coagulation, disinfection, and media filtration. Coagulation and flocculation can be applied to remove suspended solids and colloids in feed water, resulting in reduced colloidal fouling on membrane surface. For biofouling prevention, oxidizing agent (such as chlorine) can be injected to the feed to inactivate aquatic organism. Granular media filtration can also be applied to remove suspended solids, as well as microorganisms and other contaminants in the water. Pretreatment with UF/MF membranes are relatively new and gaining a lot of interests due to their nearly 100% particulate removal efficiency.[99]

To minimize mineral scaling, scale inhibitor and feed water acidification are commonly used during desalination process.

1.5.2 Electrically conducting membranes

Electrically-conductive membranes are relatively new, and gaining interests owing to their versatile applications. Most common approaches to fabricate electrically-conducting membranes include modification of a porous substrate with electrically conductive materials and incorporation of mesh electrodes on conventional membranes. Electrically conductive materials for substrate modification can be carbon cloth, stainless steel, polyaniline, graphene, and carbon nanotubes (CNTs). [100]

When electrically-conductive membranes are operated with cathodic potentials, the charge density (i.e., negative charge) on the membrane surface can be significantly enhanced, resulting in a stronger repulsion of negatively charged NOM. Similarly, with relatively low cathodic potentials, charged organic molecules can be pushed away from the membrane surface by electrophoretic

effect, resulting in organic fouling mitigation. Organic foulants can also be degraded by electrochemical oxidation. When cathodic potentials are applied on electrically conducting membranes, reactive oxygen species such as H_2O_2 or OH radical can be generated.[101,102]

Electrically-conductive membranes are also effective to mitigate inorganic membrane scaling. W. Duan *et al.* previously reported a gypsum scaling prevention on CNT-RO membranes with 1.5 V anodic potentials. In the same study, electrochemical cleaning of calcium carbonate that was formed on the membrane surface was conducted, and effectively recovered the performance of membrane. L. Tang *et al.* also reported silica scale mitigation on electrically-conductive membrane distillation (MD) membranes. By applying cathodic potentials (constant 20 mA) intermittently, water electrolysis was facilitated, resulting in high-pH environment that can redissolve silica scaling formed on the membrane surface. In the most recent study, U. Rao *et al.* reported electrically-conductive MD membranes with alternating current can significantly reduce the formation of gypsum on the membrane surface. The proposed mechanism was by switching the polarity of electrodes, there was no sufficient time for co-location of ion-pairs that forms inorganic scaling. In the same study, with elevation of pH, silica scaling formation was also significantly mitigated by the application of alternating current.[103–105]

1.6 Research Objectives

In this dissertation, the overall objective was to optimize and improve pressure-driven membrane process that is used for desalination.

Chapter 2 reported a chemical-free approach to enhance boron removal efficiency during seawater desalination by employing electrically-conductive RO (ECRO) membranes. In sweater, boron exists in the form of electrically-neutral boric acid at pH of seawater (~8.5). Therefore,

typical RO membranes have relatively poor rejection of boron during the seawater desalination, resulting in the use of alkaline chemicals to convert boric acid to borate that is negatively charged. This process comes with a huge price tag due to increase in operational cost and capital cost. However, local pH modification by ECRO membrane provided an economical approach to enhance boron rejection without any assist of chemical dosage.

Chapter 3 explored multiple water treatment technologies that are widely adopted during groundwater desalination. Since no single treatment technologies can stand alone to produce potable water during groundwater desalination, multiple pretreatment options such as coagulation and media-filtration were investigated and combined with membrane filtration to produce potable water that meets United States Environmental Protection Agency (USEPA) drinking water standard. Various water quality parameters were monitored, and economical model was finally employed to identify optimized the groundwater desalination treatment train.

Chapter 4 investigated an impact of frequent polarity reversal on membrane scaling formation on electrically-conductive NF (ECNF) membranes. Membrane scaling is of great interest since it could significantly reduce the membrane performance (water permeation flux and salt rejection). ECNF membrane that was fabricated with an incorporation of carbon nanotubes under polyamide layer yielded significantly reduced the formation of scaling on the surface of ECNF under the condition of alternating current (i.e., 4 Vpp and 1Hz). ECNF was firstly tested with synthetic brackish groundwater, and then the application was further extended to natural groundwater that has more complicated water matrix. The impact of alternating current on scaling formation was monitored by the trend of water permeation flux and salt rejection of membrane.

In chapter 5, conclusions from the above chapters and future research directions are discussed.

Chapter 2.

Enhancing Boron Rejection on Electrically Conducting Reverse Osmosis Membranes Through Local Electrochemical pH Modification

2.1 Summary

Reverse-osmosis (RO) has become a prevailing technology for seawater desalination. While RO removes the majority of ions in seawater, the removal of small, uncharged contaminants remains challenging. Boron existing as uncharged boric acid ($B(OH)_3$) in seawater is partially removed during the RO process, requiring further treatment if the desalinated seawater will be used for certain crop irrigation. Boron removal efficiency is significantly improved under a high pH condition where non-charged $B(OH)_3$ turns into negatively charged borate ($B(OH)_4^-$). Therefore, RO desalination plants often exploit a double-pass configuration, where the pH of the RO permeate from the first pass is chemically increased above the pKa of $B(OH)_3$, and is treated again using RO membrane (the second pass). Although this process can achieve high boron removal efficiency, it incurs substantial operating and capital costs. In this study, commercial RO membranes are coated with carbon nanotubes forming an electrically conducting, porous layer. We explore the impact of applied cathodic potentials on boron and salt rejection, membrane flux, and fouling. We demonstrate that applying cathodic potentials can elevate the near-membrane pH, which dramatically increases boron rejection. However, the higher pH results in membrane scaling ($Mg(OH)_2$), although the formed scaling does not dramatically reduce membrane flux.

2.2 Introduction

As water demand increases and conventional water supplies shrink, global attention is being directed towards the utilization of alternative water resources such as greywater, wastewater, and seawater.[106,107] As a result there has been increasing emphasis on lowering water consumption in dry regions as well as minimizing environmental impacts due to nutrient runoff into watersheds. Furthermore, the large volumes of available seawater coupled to consumer's acceptance, makes desalinated seawater, in particular, an attractive source of drinking water.[107–110] Therefore, reexamination of technologies for reclaiming and reusing contaminated water for agricultural use is increasing in importance. Reverse osmosis (RO) is the fastest growing seawater desalination technology because of its excellent salt-rejecting capabilities and high energy efficiency.[111,112] As a result, RO desalination accounts for more than 60 % of global desalination capacity.[109]

Human consumption of desalinated seawater is often the first step along the long road desalinated seawater takes. Once the desalinated seawater is used for municipal purposes (the largest use of desalinated sweater), it is typically discharged as wastewater, which undergoes further treatment before it is either discharged into the environment or reused.[109] In many parts of the world, and increasingly in parts of the United States (such as Southern California), wastewater is reused for various applications, with irrigation being a primary use.[113] An extreme example is Israel, which reuses more than 80% of its wastewater to provide 50% of its irrigation needs, with a large fraction of this water being produced through RO seawater desalination.[114] A similar condition exists in other parts of the Middle East and North Africa, such as Iraq, Kuwait, and Saudi Arabia.[115,116]

Although modern RO membranes exhibit excellent ion rejection (monovalent ion rejection levels are in excess of 99.9% in well-operated plants), the rejection of small, uncharged molecules remains a challenge.[117,118] Boron is one of the constituents of concern during seawater desalination.

While the toxicity of boron to mammals is not a concern considering the low concentrations in seawater (4-5 mg/L), certain crops (e.g., citrus) are highly sensitive to boron. Because of this sensitivity, it is recommended that boron concentrations in irrigation water be below 0.5 mg/L.[109,119–121] Typical rejection levels of boron by RO membranes is 40 – 80%, resulting in RO permeate concentrations that exceed the recommended concentration for irrigation.[119,122–124] To reduce boron concentrations in RO treated seawater, wastewater generated from desalinated seawater is blended (i.e., diluted) with wastewater from other, non-boron containing sources (such as river water).[125] However, if the wastewater is composed of primarily desalinated seawater, irrigation with this water becomes problematic. With seawater desalination becoming an increasingly large component of drinking water, and as a result, in reclaimed water for irrigation, the presence of boron in desalinated seawater could become a problem in certain parts of the world.[126,127] Critically, it is important to note that standard wastewater treatment processes do not effectively remove boron.[122,128] In addition, other streams, including certain groundwater and industrial wastewater, may have elevated boron concentrations that are significantly higher than seawater. For example, groundwater in Michigan was found to have boron concentrations in excess of 6 mg/L, and wastewater derived from palm oil manufacturing showed concentrations as high as 15 mg/L.[129,130]

Boron in seawater (pH 8) is found in the form of boric acid ($B(OH)_3$), which is a small, polar, uncharged molecule (very similar to water). [131,132] Since boric acid is a weak Lewis acid, increasing the pH to a point above its pKa transforms boric acid to its negatively charged counterpart, borate: [133]

$$B(OH)_3 + H_2O \leftrightharpoons B(OH)_4^- + H^+ \ (pKa = 9.23)$$

Although boron can exist as a polynuclear species (e.g., $B_2O(OH)_6^{2-}$) at higher concentration (> 216 mg/L), these conditions are not typically relevant during seawater desalination.[124]

Polyamide-based RO membranes rely on a combination of charge- and size-based exclusion mechanisms to remove contaminants from water [118]. Because these membranes are designed to allow water (a small, polar, non-charged molecule) to pass through the membrane, they are inefficient at rejecting contaminants with similar properties, such as boric acid. Therefore, if boric acid can be transformed into borate, the rejection of this species increases significantly; when the pH of the feed solution was increased to 11, borate rejection reached levels as high as 99%.[123,134] To remove boron from seawater, a strategy known as double-pass RO is commonly used. In this process, seawater is treated by a seawater RO (SWRO) membrane; the permeate (i.e., permeate from the first pass) is first treated with alkaline chemicals to increase the pH, and then treated again using brackish water RO (BWRO) membranes (the double-pass).[106,135] Increasing the pH of seawater during the first pass is limited by inorganic scaling from compounds such as brucite ($Mg(OH)_2$).[136,137] The double-pass strategy eliminates this concern, as divalent cations (such as Mg^{+2}), which are largely responsible for scaling, are removed in the first pass. However, the double-pass strategy incurs a heavy energy and chemical usage penalty [138–140]. The use of BWRO membrane in the second stage, instead of SWRO membrane, reduces the amount of energy consumption caused by an additional RO step since the energy requirement of BWRO is smaller than that of SWRO. Thus, an alternative method that allows for effective boron removal from seawater could significantly lower the cost of seawater desalination when this water could be reused for irrigation.

Electrically conducting membranes represent a new class of membrane materials with the ability to facilitate electrochemical reactions on the membrane surface.[141] These membranes are

made conductive through the inclusion of a percolating network of carbon nanotubes (CNTs) into the membrane structure. Several classes of electrically conducting membranes have been fabricated in this way, including RO, nanofiltration (NF), ultrafiltration (UF), and membrane distillation (MD).[142–144] Because of their electrical conductivity, these membranes can be used as anodes or cathodes in electrochemical systems; a counter electrode needs to be placed somewhere in the system, typically above the membrane with a mesh spacer separating them. When the membrane is used as a cathode and connected to an external potential source, water electrolysis can be facilitated on the membrane surface:

$$2H_2O + 2e^- \leftrightarrow H_2 + 2OH^-$$

Depending on the applied potential, the surface pH along the membrane can be increased to greater than 13.[145] By raising the pH along the surface of an RO membrane to above boron's pKa, it is possible to transform boron to its charged form ($B(OH)_4^-$), which will enhance its rejection by the membrane.

In this project, electrically conducting RO membranes were fabricated using commercially available SWRO membranes by depositing a percolating network of CNTs onto their surface. The membrane was connected to an external potential source and used as a cathode, with an anode (platinum-coated titanium wire) placed 3 mm above the membrane surface in a modified RO flat-sheet module. Various potentials were applied to the membrane and counter electrode (0 – 5 V cell potential) and the associated impact in boron concentration in the permeate was analyzed. In addition, the impact of the applied potential on membrane scaling, membrane flux, salt rejection, and permeate quality was analyzed.

2.3 Materials and Methods

2.3.1 Materials

Carboxylated multi-walled carbon nanotubes (CNT-COOH) were purchased from Cheap Tubes (length 10-30 μm and radius < 8 nm). RO membranes (RO4) were used in all experiments (Nanostone Water Inc., Oceanside, CA). Artificial seawater (AS), sodium dodecylbenzenesulfonate (NaDDBS), sodium chloride (NaCl), azomethine-H (~95%), ammonium acetate (≥98%), ethylenediaminetetraacetic acid disodium salt dehydrate (EDTA), thioglycolic acid (98%) and polyvinyl alcohol (PVA, M.W. 146,000 -186,000) were purchased from Sigma-Aldrich and used as received. Detailed information provided by a manufacturer on the constituents AS are listed in Table 1.

Table 2.1. Concentration of ions in artificial seawater

Constituent	**Concentration (mg/L)**
Chloride	19,000 – 20,000
Sodium	1,0700 – 11,000
Sulfate	2,660
Potassium	300 – 400
Calcium	400
Carbonate	140 – 200
Boron	5.6
Magnesium	1,320
Strontium	8.8
Insoluble matter	≤ 0.05 %
Trace elements	< 0.5

In order to achieve the concentration depicted in Table 1, 38 g of AS salt was dissolved in 1L of deionized water (DIW). L(+) Ascorbic acid (99%) was purchased from Acros and used as received. 10.0 N sodium hydroxide (NaOH), acetic acid and boric acid were purchased from Fisher Scientific.

2.3.2 Membrane fabrication

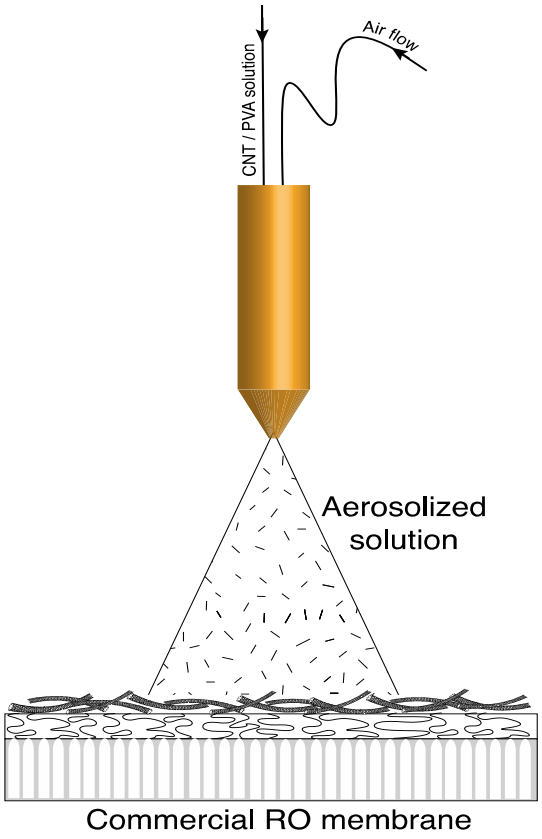

The fabrication process of electrically conducting RO membranes followed the following method: 1 wt% of PVA solution was prepared by dissolving 1 g of PVA in 100 mL of DIW with heating and stirring. To make a 1 wt% CNT-COOH suspension solution, 1 g of CNT-COOH and 10 g of NaDDBS in 1 L of DIW were sonicated for 30 minutes. Then, the CNT-COOH suspension solution was deposited onto the RO membrane using an air brush spraying method to a final thickness of approximately 2 μm (Figure 1). Then, a single layer of 1 wt% PVA solution was spray-deposited to ensure that the CNT layers are anchored to the membrane surface. The composite membrane material was then washed with DIW and dried at 90 ℃ for 10 minutes.

Figure 2.1 Illustration of spraying-assisted CNT and PVA deposition onto a commercial RO

2.3.3 Analytical methods

Boron concentrations were monitored using a colorimetric method (azomethine-H method).[146] In brief, 0.9 g of azomethine-H and 2 g of L(+) ascorbic acid were dissolved in 100 mL of DIW, and stored in the dark. In order to prepare a buffer-masking solution, 250 g of ammonium acetate were dissolved in 500 mL of DIW and then 125 mL of acetic acid, 6.7 g of EDTA, and 60 mL of thioglycolic acid were added while mixing. All of the solutions for Azomethine-H method were stored in a plastic bottle in order to prevent boron leaching from laboratory glassware made of borosilicate glass.[147] To a 5 mL of sample requiring analysis, we added 4 ml of the buffer-masking solution, and 2 ml of azomethine-H solution, which were mixed in the dark for 1 hour. Boron concentrations were quantified using a UV-vis spectrophotometer (PerkinElmer, Lambda 365) at 410 nm. Sodium concentrations were measured using inductively coupled plasma-mass spectrometry (ICP-MS, PerkinElmer, NexION 2000). Chloride concentrations were measured using ion chromatography (IC, Thermo Fisher, Dionex Integrion HPIC). pH and conductivity were measured using a benchtop pH meter (Thermo Scientific, Orion 720A) and a portable conductivity meter (Orion A321).

In order to characterize the membrane surface, a scanning electron microscopy (SEM, ZEISS, Supra 40VP) equipped with an energy-dispersive X-ray detector (EDAX), atomic force microscope (AFM, Brunker, FastScan), and a contact angle goniometer (Rame-hart, model 250) were employed. Membrane conductivity was measured using a 4-point conductivity probe (Mitsubishi, MCP-T610). The electrochemical properties of the membrane (open circuit potential, surface potential, and cyclic voltammetry) were determined using a potentiostat (CH Instrument, CHI600e)

2.3.4 Design and Operation of RO system

A process diagram of the RO filtration system employed in this work is illustrated in Figure 2. Real-time monitoring of pressure, pH of feed and permeate streams, conductivity in permeate, current and voltage was performed using open-source custom-built software.[148]

A membrane coupon with an effective area of 0.004 m^2 (8 cm x 5 cm) was placed in a flow cell and compressed with DIW until stable permeate flux was achieved. Then, the feed tank was filled by a model solution (NaCl or AS solution) and 0.1 N of NaOH was continuously injected into the feed to maintain pH 8. The pressure in the system was constantly held at 500 psi throughout this research. The system was operated at 2.33 cm/s which corresponds to a Reynolds number of 79. Experiments were conducted in concentration mode, i.e., the permeate was not returned to the feed tank.

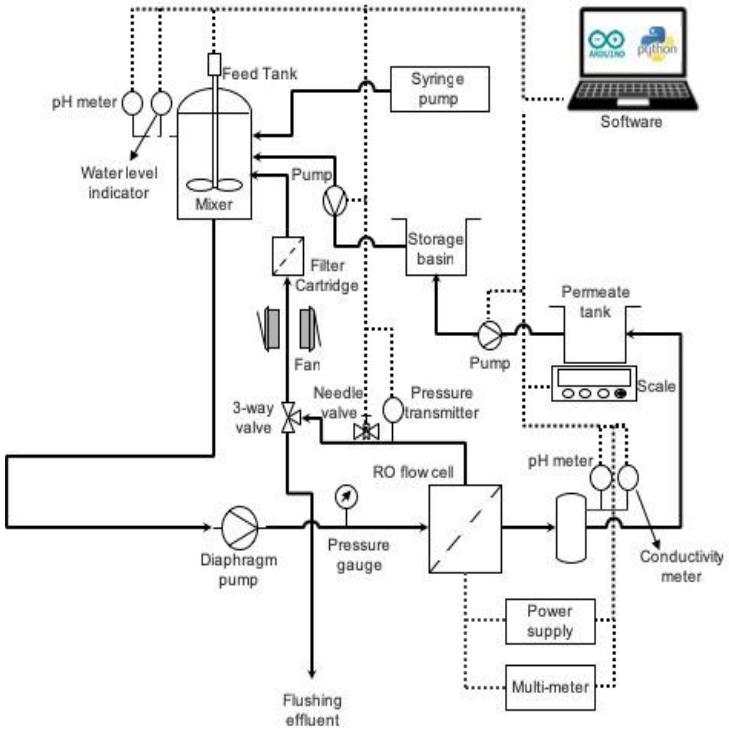

Figure 2.2. Schematic diagram of RO filtration system. The solid line represents water flow; the dashed-line represents

Voltage in a range of 0 to 5 V cell potential was applied to the electrically conducting RO membranes and a counter electrode, which was prepared by sputter-coating platinum (Pt) on a titanium (Ti) wire. Each experiment was conducted with a new counter electrode. Water samples (15 mL) were collected from the feed tank and permeate stream after 1 hour of each voltage application. Conductivity and pH of

samples were measured as soon as sample collection was done.

To investigate whether membrane scaling could be reversed, acid cleaning was performed using 10 mM hydrochloric acid (pH 2) after 33 hours of treating AS. The same cross-flow velocity was applied during the chemical cleaning process. The acid cleaning was performed for one hour.

2.4 Results and discussion

2.4.1 Membrane characterization

Pristine RO membranes exhibited a flux of 30.04 ± 1.80 LMH (pure water), 5.17 ± 0.06 LMH (35 g/L NaCl + boron mixture), and 5.53 ± 0.24 LMH (AS solution), while CNT-coated membranes exhibited a flux of 33.37 ± 1.18 LMH (pure water), 5.66 ± 0.16LMH (35 g/L NaCl + boron mixture), and 5.23 ± 0.14 LMH (AS solution), demonstrating that the addition of the porous CNT layer did not dramatically impact membrane flux. When the 35 g/L NaCl + boron mixture was used as a feed, pristine RO membranes and CNT-PVA-coated membranes exhibited 96.87 ± 2.28% and 96.69 ± 1.27% of salt rejection, respectively. This value is lower than the 99.5% that was reported from the manufacturer. It should be noted that experiments were conducted with a 35 g/L of NaCl + boron mixture at 500 psi in this study while manufacturer tested membranes with 32 g/L of NaCl at 800 psi. For boron rejection, pristine RO membranes and CNT-PVA coated membranes exhibited 74.83 ± 0.70% and 63.99 ± 2.12% rejection, respectively. When the AS solution was used as a feed, pristine RO membranes had 98.55 ± 0.57% of initial salt rejection and

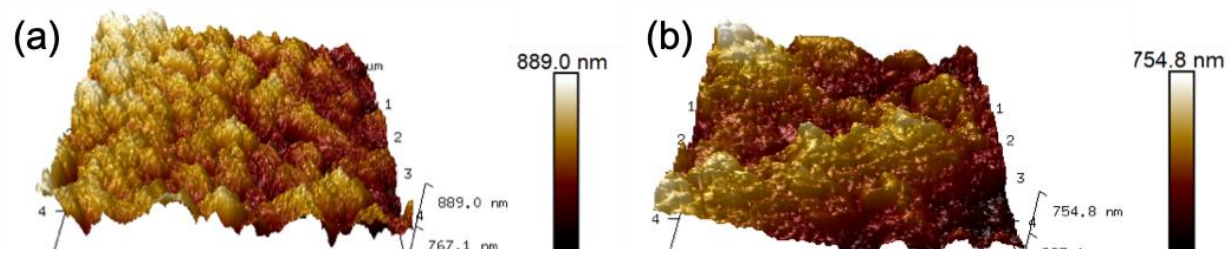

Figure 2.3. (a)AFM images of RO and (b) CNT-PVA-deposited membrane (5 μm by 5 μm of scan area).

81.30 ± 3.08% of initial boron rejection, while CNT-PVA-coated membranes exhibited 98.07 ± 0.90% of initial salt rejection and 77.58 ± 0.20% boron rejection. It is unclear why boron rejection by the uncharged CNT-PVA membrane is lower than the pristine RO membrane, particularly since the salt rejection and water flux were nearly identical.

Pristine RO membranes had relatively flat surface morphology compared to the rough surface of CNT-PVA-coated membranes (Figure 3a,c). Cross-sectional SEM images of the CNT-PVA-

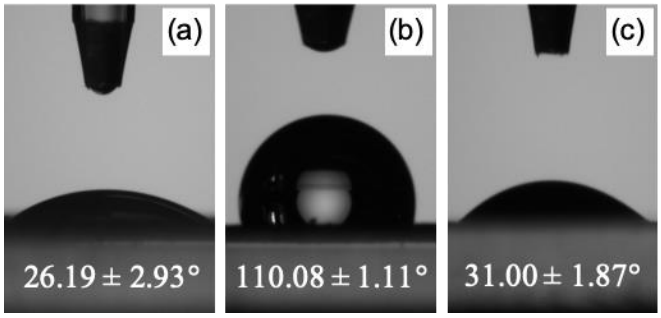

Figure 2.4. (a) Contact angle measurement of RO, (b) CNT only deposited, and (c) CNT-PVA-deposited membranes.

coated membrane confirmed that the membrane had a ~2 μm thick CNT layer (Figure 3d). Surface roughness of the pristine RO and CNT-PVA-coated membranes were investigated using AFM (Figure 4a,b). Pristine RO membranes showed 63.83 ± 33.31 nm of root-mean-square (RMS) roughness while CNT-PVA-coated membranes showed 138.0 ± 31.75 nm RMS roughness.

Contact angle measurements were conducted to obtain an insight into the surface hydrophilicity of the membranes (Figure 5a - c). Pristine membrane showed a contact angle of 26.19 ± 2.93°. The RO membrane coated with only CNTs, had a contact angle of 110.08 ± 1.11°, even though the CNTs were functionalized with -COOH groups, although the content of -COOH group was only 7 %. However, this surface hydrophobicity was significantly reduced to 31.0 ± 1.87° by coating a PVA layer on top of the CNTs. Based on the 4-point conductivity probe measurements, the CNT-PVA-coated membranes had a sheet resistance of 61.63 ± 7.49 Ω/□.

Table 2.2 Contact angles of pristine, CNT-only and CNT-PVA RO membranes

Type of membrane	Pristine RO	CNT-only RO	CNT-PVA RO
Contact angle (°)	26.19 ± 2.93°	110.08 ± 1.11°	31.0 ± 1.87°

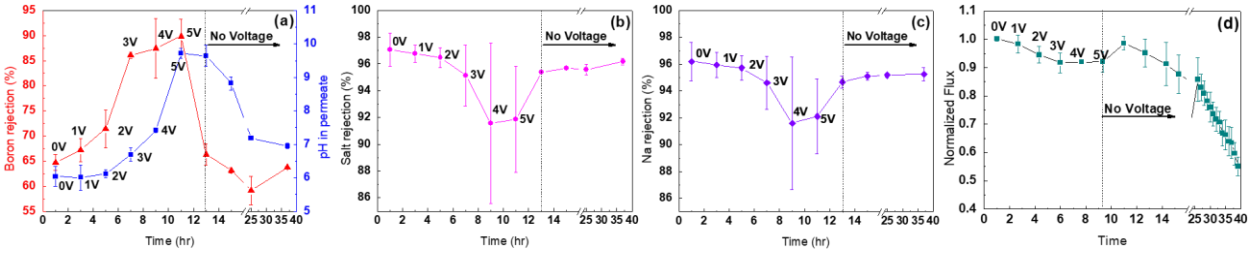

Figure 2.5. (a) Boron rejection and permeate pH as a function of the applied cell potential with NaCl + boric acid feed. (b) Salt rejection as a function of the applied cell potential. (c) Na^+ rejection as a function of the applied cell potential. (d) Normalized flux of NaCl + boric acid mixture with 5 V cell potential (triplicate runs).

In order to measure surface potential of CNT-PVA-coated membranes, open circuit potential measurements against a Ag/AgCl reference electrode were conducted in two model solutions (35 g/L NaCl + boric acid mixture and AS solution) while an external potential was applied to the membrane/counter electrode. When no voltage was applied, CNT-PVA-coated membranes had relative surface potentials of 0.24 ± 0.06 V in 35 g/L NaCl + boron mixture, and 0.29 ± 0.04 V in AS solution (Figure S1a). As the applied cell potential increased, the membranes showed increasing surface potentials vs. Ag/AgCl, reaching -1.71 ± 0.06 V vs. Ag/AgCl in 35 g/L NaCl + boron mixture and -1.71 ± 0.04 V vs. Ag/AgCl in AS solution when a cell potential of 5 V was applied (Figure S1a). Cyclic voltammetry (CV) was employed to observe electrochemical reactions on the membrane surface. Potentials ranging from 1.0V to -2.0 V vs. Ag/AgCl were applied to a PVA-CNT-coated membrane in 35 g/L NaCl + boron mixture and AS solution. As

can be seen (Figure S1b), an electrochemical reaction (i.e., water electrolysis) occurred at potentials as low as -0.4 V vs. Ag/AgCl in both solutions.

2.4.2 Performance of electrically conducting membranes using NaCl + boron

To mimic the level of total dissolved solids (TDS) in seawater, 35 g/L of NaCl along with 5 ppm of boron was first used to test boron rejection on CNT-PVA coated RO membranes. The application of an electrical potential increased boron rejection, with increasing potentials leading to higher boron rejection (Figure 6a). Boron removal efficiency at 5 V cell potential was 90.05 ± 0.95%, while the rejection without potential was only 63.99 ± 2.12%. The enhancement in boron rejection is a result of the elevated local pH along the membrane surface brought about by water electrolysis when an applied potential was greater than 1.2 V, with higher potentials leading to more OH^- generation and higher pH. Since OH^- ions have a smaller stokes radius (0.46 Å), they can easily penetrate RO membranes.[149] Therefore, a high permeate pH (10.83) at 5 V cell potential was observed compared to the pH at 0 V (6.55) (Figure 6a). The CNT-PVA-coated RO membranes exhibited 96.68 ± 1.27% of initial salt rejection at 0 V (Figure 4b). However, the rejection gradually decreased when the applied potential increased. At the end of experiments, 92.65 ± 0.93% of salt rejection was observed at 5 V cell potential (Figure 6b). ICP-MS and IC measurements of Na^+ and Cl^- concentrations in the permeate show that the rejection of both ions declined with increasing applied potentials (Table S1). While the "sodium pump" effect may be responsible for a small part of the observed decrease in Na^+ rejection, it is not capable of explaining the majority of the decline. To confirm whether this drop in rejection was a result of damage to the RO membrane, we continued to measure salt and Na^+ rejection once the applied potential was stopped (Figures 6b,c). As can be seen, salt rejection recovered to 96.18 ± 0.25%, and boron rejection

declined to 63.99 ± 2.12%, indicating that no significant damage was sustained by the RO membrane.

Over the 9-hour period where voltage was applied (from 0 to 5 V cell potential), a 10% flux decline was observed (Figure 6d). We attribute this flux decline to the increasing salt concentrations in the feed stream, as the system was operated in concentration mode, and no obvious fouling agents were present in the feed.

2.4.3 Performance of electrically conducting membranes using artificial seawater

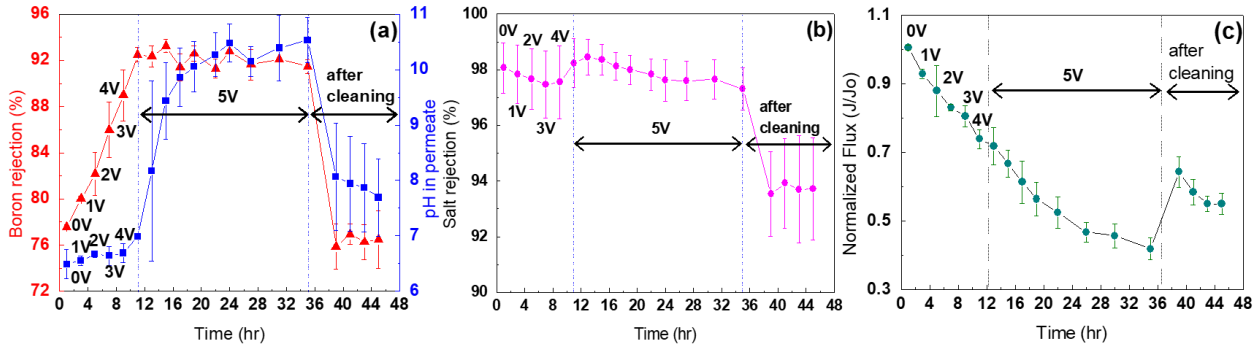

Figure 2.6. (a) Boron rejection and permeate pH over time and as a function of cell potential while treating a solution of AS. (b) Salt rejection as a function of cell potential and time. (c) Normalized flux as a function of time and applied potential.

The same experimental procedure used for the NaCl + boric acid solution was applied to towards the treatment of AS. However, the duration of membrane filtration (33 hr) was extended to monitor the formation of scaling on the surface of the membrane. Compared to boron rejection in the NaCl solution, the membranes exhibited approximately 14% higher boron rejection (77.58 ± 0.2%) when no voltage was applied. However, in general, a similar trend of boron removal efficiency was observed when AS solution was used as a feed, with increasing boron rejection corresponding to increasing applied potentials (Figure 7a). At 5 V cell potential, an average boron

rejection of 93.31 ± 0.53% was achieved. Boron rejection declined slowly over time, although the exact reason why remains unclear. It is possible that scale development on the membrane surface contributed to this phenomenon. Unlike the trends in permeate pH observed in the pure NaCl solution (Figure 6a), changes in permeate pH while treating the AS solution were slow to appear (Figure 7a). It is likely that the buffering capacity of the solution, a result of dissolved bicarbonate, reduced the presence of free hydroxide ions. However, as the experiment progresses, and scaling occurred (see discussion below), carbonate was consumed (to form $CaCO_3$), and the buffering capacity diminished, which led to the observed temporal changes in pH. The overall salt rejection of the membranes showed an average of 98.07 ± 0.73% at 0 V (Figure 7b). Although salt rejection from the NaCl + boric acid mixture declined with an increasing potential (Figure 4b), salt rejection of AS improved as soon as 5 V cell potential was applied (Figure 7b). However, salt rejection did decline over time. Over the course of a 33-hour treatment period, flux through uncoated and CNT-PVA coated RO membranes (without voltage applied) declined to 49.25 ± 8.95% and 47.30 ± 0.85%, of their initial value, respectively (Figures S2a,b). Over the same time period, flux of CNT-PVA coated RO membranes with applied potentials declined to 40.84 ± 3.83% of its initial value (Figure 7c). It should be noted that experiments were conducted in concentration mode. Therefore, some of the flux decline can be attributed to higher salt concentrations in the feed stream (i.e., higher osmotic pressure). In order to confirm this, flux of CNT-PVA coated RO membranes in a fresh AS solution and a concentrated AS solution was measured. With a concentrated solution, the membrane exhibited 68.15 ± 1.99% of relative flux to the fresh AS solution (Figure S3a). While a larger average flux decline was observed when 5 V cell potential was applied, the decline was not dramatically worse than the controls. That being said, it is likely that the increased flux decline observed under the 5 V conditions is a result of slightly more severe mineral scaling brought about

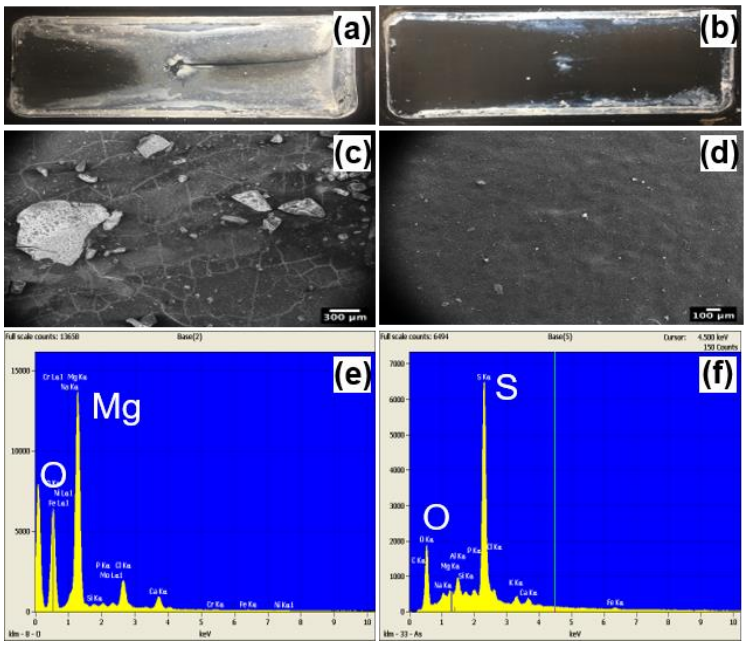

Figure 2.7. (a) The surface of electrically conducting membrane after 33 hours of operation; (b) The surface of electrically conducting membrane after acid cleaning; (c) SEM image of brucite scaling on the membrane surface; (d) SEM image of membrane surface after cleaning by acid; (e) EDAX analysis of scaled membrane surface; (f) EDAX analysis of acid-cleaned membrane surface.

by the high pH along the membrane surface. Observation of the membrane after the experiment showed a surface covered by mineral scale (Figure 8a). The scaled surface was investigated using SEM and EDAX: SEM images reveal large crystal structures, as well as a cracked coating on the CNT layer (Figure 8b); EDAX analysis of the surface showed that the surface deposits were largely composed of magnesium (Figure 8c). This data is consistent with the presence of $Mg(OH)_2$, which readily forms at high pH.

In an attempt to recover membrane flux post-scaling, the scaled membrane was cleaned using an acid solution (10 mM HCl) for one hour. After acid-cleaning was conducted, boron rejection by electrically conducting membranes without a potential (77.25 ± 1.01%) was identical to its initial rejection value (77.58 ± 0.2%). However, salt rejection without a potential decreased from its initial value, from 98.07 ± 0.90% to 93.93 ± 1.61%. Again, it should be noted that the experiments were conducted in concentration mode, where the higher feed concentrations of the feed lead to lower salt rejection.

This was also confirmed by comparing the salt rejection of CNT-PVA coated membranes (with no potential) with a fresh AS and a concentrated AS solution. With a concentrated AS solution, the membrane exhibited 96.29 ± 0.52% salt rejection, while the membrane achieved 99.33 ± 0.10% rejection with a fresh AS solution (Figure S3b). However, because the boron rejection values did not change, we can carefully conclude that the underlying RO membrane did not sustain any significant damage during the treatment or cleaning process.

Images of the membrane surface post acid cleaning show the process removed the vast majority of mineral scale (Figures 8d,f). EDAX analysis of the membrane surface post cleaning showed that the dominant atomic species were sulfur and oxygen, which can be attributed to the sulfonate groups on the polysulfone support of the RO membrane (Figure 8f); we confirmed this by analyzing the uncoated and a pristine PVA-CNT membrane, which showed an identical EDAX elemental signature (Figures S4a,b). The acid cleaning restored membrane flux to 64.24 ± 4.51% of its initial value. Importantly, the feed during this part of the experiment was the concentrated AS generated during the previous part of the experiment (i.e., while voltage was applied). A pristine CNT-PVA membrane used to treat this feed exhibited a flux that was 68.15 ± 1.99% of the flux generated while treating a fresh AS solution, demonstrating that acid cleaning was indeed successful at recovering membrane flux (Figure S3a).

2.4.4 Cost analysis of boron treatment using CNT-PVA coated RO membranes

In RO-based seawater desalination, the main costs of the process can be divided into two main categories: capital and operational costs. These two costs can vary depending on a number of factors such as the scale of the plants, the configuration of desalination process, the types of membranes used, the quality of feed and product water, etc..[106140150] Therefore, care must be taken

when comparing water production costs between different processes. However, with some assumptions, insight into the economic benefit of one process over the other can be obtained.

It was reported that the total costs associated with a single-pass RO desalination plant range between 0.38 – 0.52 $/m^3 of product water.[151,152] Feed water containing between 4 – 5 mg/L of boron treated by a single-pass RO process, results in a final boron concentration ranging between 0.8 – 1 mg/L. We used a software tool designed by DOW FILMTEC, called Reverse Osmosis System Analysis (ROSA), to simulate boron removal in a single-pass RO system. With a conventional pretreatment option (assuming a silt density index < 5), and standard operation condition (i.e., 800 psi of pressure), 1.26 mg/L of boron was expected to remain in the treated water when seawater having the same composition of ions listed in Table 1 was treated at pH 8.5; the estimated boron concentrations in the final product estimated by ROSA was fairly close to the reported value of 0.8 – 1 mg/L. On the other hand, if the pH of the feed stream was increased to 9.7, ROSA predicted that boron concentrations in the permeate would decline to an acceptable 0.38 mg/L. The estimated consumption of NaOH (100%) to increase the pH to this level was 94.85 g/m^3. Considering the price of NaOH (100%) is $0.72/Kg, the addition of NaOH required to elevate pH 9.7 solely adds $0.1366/m^3 of product water.[140] In contrast, the CNT-PVA coated RO membranes consumed only 0.015 kWh/m^2 which corresponds to $9.87 × 10^{-4} /m^2 (assuming an average price of industrial electricity in the United States of $0.0658/kWh as of June of 2019). Assuming an average flux of 15 LMH, the energy consumption translates into an additional cost of $0.0658/m^3 of treated water, which ~50% less than the cost of a pH-modified single-pass RO system.

2.5 Conclusion

In this work, the performance of an electrically charged CNT-PVA coated RO membrane was evaluated in terms of boron removal, salt rejection, and membrane flux using two model solutions (35 g/L NaCl + boric acid, and AS). Unlike conventional SWRO processes, no chemical pH adjustment was used, yet over 90% of boron removal was achieved when 5 V cell potential was applied to the CNT-PVA coated RO membranes in both model solutions. This enhancement was achieved through locally modified pH on the membrane surface when electrical potentials were applied. However, active generation of OH^- ions on the surface of CNT-PVA coated RO membranes caused $Mg(OH)_2$ scaling, which led to flux decline. Acid cleaning was able to restore membrane flux, which demonstrates that while scaling does occur, it is not an insurmountable problem during seawater desalination. performed and flux recovery was observed. Since a double-pass system is commonly used to eliminate boron in desalination plants, utilizing CNT-PVA coated RO membranes may be an economical choice which does not require an additional RO unit. If CNT-PVA coated RO membranes are employed in the seawater desalination process, $\$0.071/m^3$ (corresponding to 13.61 – 18.63% of water cost) would be saved compared to a single pass system coupled with feed pH adjustment. However, it should be noted that other factors affecting water production costs (e.g., the cost of chemical transport, implementational and operational cost of chemical dosage and handling, the cost of CNT deposition ($\$2.34/m^2$), etc.) must be considered to more precisely estimate and compare unit water production costs. Further research with regards to the use of appropriate scaling inhibitor should be done in order to fully take advantages of CNT-PVA coated RO membranes for efficient boron removal in seawater.

2.6 Acknowledgement

This work was completed as part of US-Israel Agricultural Research and Development (US-5051-17). The authors acknowledge the use of ICP-MS core facility within the UC center for Environmental Implications of Nanotechnology in CNSI at UCLA.

2.7 Supporting information

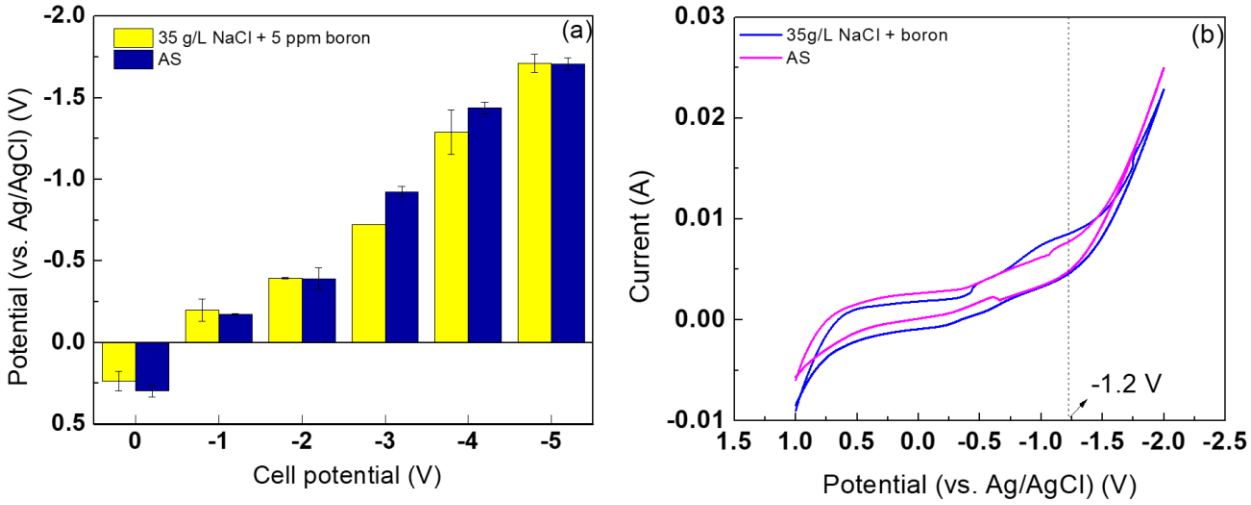

Figure S 2.1. Electrochemical properties of CNT-PVA-coated membranes; (a) Open circuit potentials of CNT-PVA-coated membranes against an Ag/AgCl reference electrode in two model solutions. (b) Cyclic voltammetry of CNT-PVA-coated membranes in two model solutions (scan rate at 50 mA/s).

Table S 2.1 Charge balance in the permeate

Applied potential	Cations			Anions				SUM
	H	Na	SUM	OH	Cl	$B(OH)_4$	SUM	
0 V	9.12E-04	15.865	15.866	1.10E-05	15.712	7.74E-05	-15.71	0.15
1 V	9.89E-04	17.473	17.474	1.01E-05	17.094	7.88E-05	-17.09	0.38
2 V	7.67E-04	18.346	18.347	1.30E-05	18.329	8.99E-05	-18.33	0.02
3 V	2.02E-04	23.617	23.618	4.95E-05	23.696	1.66E-04	-23.70	-0.08

4 V	3.89E-05	36.924	36.924	2.57E-04	37.548	7.76E-04	-37.55	-0.62
5 V	1.91E-07	36.330	36.330	5.25E-02	36.676	3.20E-02	-36.76	-0.43
0 V	2.26E-07	21.450	21.450	4.42E-02	21.603	9.81E-02	-21.75	-0.30
0 V	1.51E-06	21.327	21.327	6.61E-03	21.360	4.19E-02	-21.41	-0.08
0 V	9.66E-05	22.049	22.049	1.04E-04	22.226	1.00E-03	-22.23	-0.18
0 V	1.12E-04	20.108	20.108	8.91E-05	20.232	7.78E-04	-20.23	-0.12

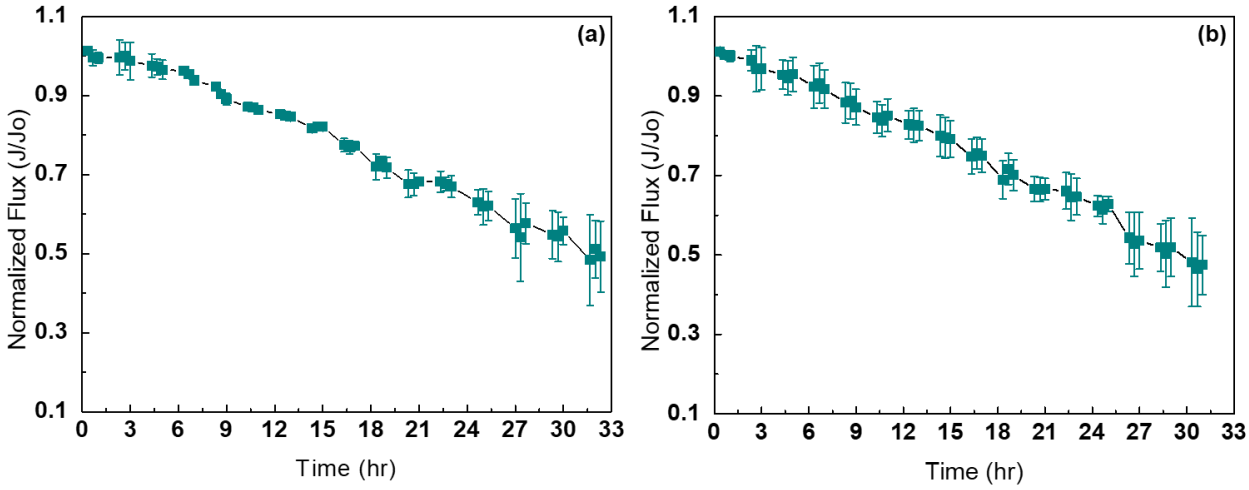

Figure S 2.2. (a) Normalized flux over time of uncoated RO membranes (artificial seawater solution as a feed) used). (b) Normalized flux over time of CNT-PVA-coated CNT membranes without voltages applied (artificial seawater solution as a feed).

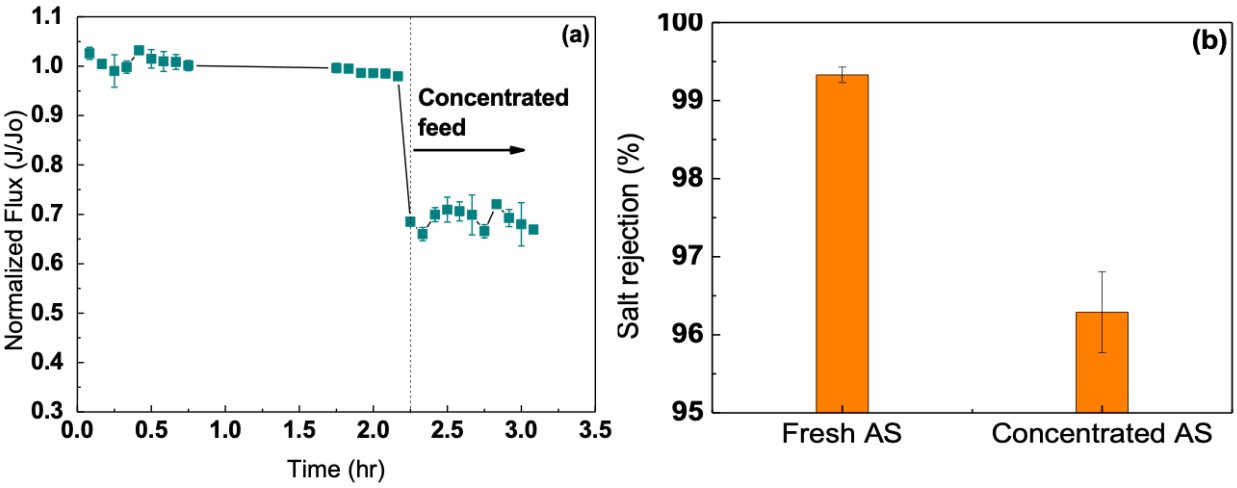

Figure S 2.3. (a) Normalized flux of CNT-PVA membranes with a fresh AS solution and a concentrated AS solution (b) Observed salt rejection of CNT-PVA-coated membranes (without a potential applied) in a fresh AS solution and a concentrated AS solution

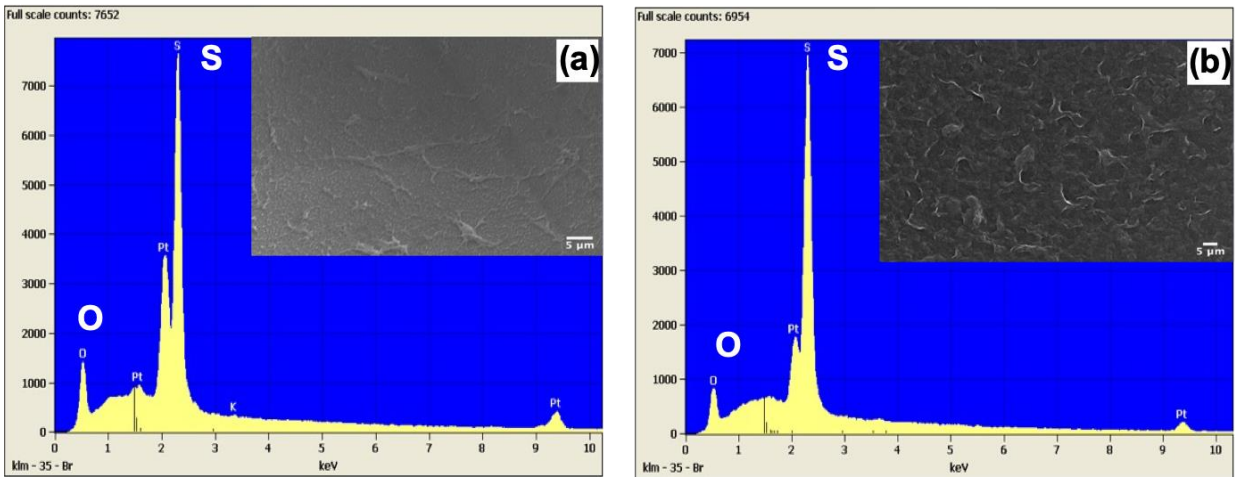

Figure S 2.4. (a) EDAX of uncoated RO membrane, (b) EDAX of CNT-PVA-coated RO membrane

Chapter 3.

Evaluation and Optimization of Treatment Technologies Treating Groundwater from the Arbuckle-Timbered Hills Aquifer in Oklahoma

3.1 Summary

Modern groundwater treatment processes often consist of pretreatment, membrane filtration, and disinfection steps. In order to achieve maximum water production and quality at the lowest possible production cost, treatment trains should be rationally designed based on contaminants present in the raw water, and the target application. In this study, synthetic and natural groundwater (obtained from the Arbuckle-Timbered Hills Aquifer in SW OK) containing elevated concentrations of fluoride (F), arsenic (As), iron (Fe), and total dissolved solids (TDS) were treated using a range of water treatment trains, with the goal of producing drinking water. The impact of coagulant ($Al_2(SO_4)_3 \cdot 18H_2O$, aluminum sulfate) dosage, filtration media (quartz sand, manganese greensand, and activated alumina), and membranes (i.e., nanofiltration (NF) and brackish reverse osmosis) were investigated in terms of removal efficiency of target contaminants. Then, a water reuse model was employed to determine the optimal treatment train configuration and blending regime that maximizes quality while minimizing treatment cost. The water reuse model determined that the optimal treatment train consists of aluminum sulfate coagulation, activated alumina filtration, and NF, and has a capability to produce potable water that meets drinking water guidelines at a production cost of \$0.212/m^3.

3.2 Introduction

Groundwater, which comprises 97% of global freshwater resources, provides more than 50% of drinking water consumption around the world.[153–155] Although groundwater is considered a reliable and useful drinking water resource, it often contains elevated concentrations of both naturally and anthropogenically-sourced undesirable ionic species such as F, As, and Cl.[156–159] Consumption of water containing concentrations in excess of regulatory limits can lead to adverse health problems. For example, consumption of drinking water with high concentrations of F can cause dental and bone fluorosis, although

small amounts of F helps to prevent dental cavities.[156,160,161] Consumption of drinking water with large amounts of As can cause skin, lung, kidney, and bladder cancer.[160,162] Elevated Cl concentrations in water are not associated with adverse health effects (within reason), although elevated Cl levels are associated with an unpleasant taste.[163] In order to provide safe, potable water to communities, the concentration of undesirable species in the source water should be mitigated by adopting appropriate water treatment processes.

The conventional drinking water treatment process consists of coagulation, followed by sedimentation, media-filtration, and disinfection.[164–167] Pressure-driven membrane filtration systems, such as brackish water reverse osmosis (BWRO) and nanofiltration (NF), are typically installed right before the disinfection step and are used to remove small, ionic species, such as Na, Cl, or hardness. However, NF and RO membranes cannot treat raw feed water, requiring pre-treatment that involves pre-filtration using looser membranes (e.g., ultrafiltration) or media filters.[167–169] The choice of pre-treatment is often determined by the specific feed water quality characteristics and desired % recovery, but is also dictated by the manufacturer's specifications that often revolve around turbidity (<1) NTU and silt density index (<4).[167,170,171]

In order to maximize water production that satisfies drinking water regulations and achieves the lowest possible cost, optimization of the water treatment process should be made based on the contaminants existing in the water resource. For example, S. Aoudj et al. compared defluoridation efficiency of two coagulants: iron salt (i.e., $Fe_2(SO4)_3$) and aluminum sulfate. It was concluded that coagulation by aluminum sulfate has a significantly higher F removal efficiency than by iron. In addition, F removal increased with respect to aluminum concentration when in the optimal pH range of 6 - 7 [172]. Similarly, it was reported that aluminum hydroxide ($Al(OH)_3$) had a higher F adsorption capacity than iron hydroxide ($Fe(OH)_3$).[173] Although aluminum sulfate coagulation is more effective for F removal, it was previously reported that another iron salt, ferric chloride ($FeCl_3$), has a higher removal rate of As.[174,175] Similarly, different filtration media have superior removal efficiency for specific water contaminants. For instance, manganese greensand (Grsand), which is glauconite greensand coated with manganese oxide, displays effective

removal of iron (Fe), manganese (Mn), and hydrogen sulfide (H_2S) from water [176–178]. Grsand manufacturers also report its effectiveness in F and As removal. Another widely used filter media, activated alumina (AA), is reported by the U.S. Environmental Protection Agency to be the best available technology for control of As and F to meet drinking water regulations [179–181]. To achieve removal of many mono- and di-valent ions (e.g., Cl^-, SO_4^{-2}, Na^+), membrane desalination (i.e., NF and RO) is often employed. In general, no single treatment process will be sufficient to meet all water quality targets, which results in the use of treatment trains, where each component of the train is used to remove specific targets. Ultimately, the choice of treatment train components will be dictated by the desired final water quality and cost.

Regional water reuse decision-support model (RWRM) is a simple mathematical model that only requires performance (i.e., removal rate of specific contaminants) and cost of unit processes in the treatment train considered.[182] The RWRM was developed to identify the most economical treatment train that produces product water that meets a variety of water quality targets. The most economical process design is determined by adjusting the blending ratios between the effluent of each unit process through iterative calculations.

The Arbuckle-Timbered Hills aquifer has the potential to serve as a source of potable water, but like many groundwater aquifers has elevated concentrations of undesirable species – in this case, fluoride, arsenic and total dissolved solids (TDS) that require treatment. In this study, a range of groundwater treatment technologies were evaluated for the treatment of synthetic and natural groundwater, with the goal of generating a drinking water-quality product. When the study began, natural groundwater was not yet available, and a synthetic solution was made based on a geological survey conducted in 1970s.[183] However, once natural groundwater was available, it was determined that its composition was somewhat different (different concentrations of total organic carbon (TOC), turbidity, iron, alkalinity and chloride), requiring a modified treatment approach. Aluminum sulfate was chosen as the coagulant to target the F and As ions in untreated groundwater. Three different adsorbents (i.e., sand, Grsand, and AA) were used for media filtration. NF and BWRO membranes were tested to compare their performance with regard to the quality of final product water. By analyzing the water quality after each treatment step, the treatment train was

optimized to produce potable water that meets drinking water standards, i.e., secondary maximum concentration level (MCL). Data generated in the experiments was fed into the RWRM to determine the optimal treatment train that generates the highest quality water at the lowest cost.

3.3 Materials and Methods

3.3.1 Feed water

The composition of the synthetic and natural groundwater is shown in Table S1. The concentrations of synthetic groundwater constituents were determined from a geological survey conducted in 1970s.[183] for groundwater obtained from the City of Lawton, OK, which sits atop the Arbuckle-Timbered Hills aquifer. Synthetic groundwater was prepared in the laboratory, with a composition that mimicked the natural groundwater.

To prepare the synthetic groundwater, 4.86 g of sodium chloride (NaCl, Fisher Scientific), 0.82 g of sodium sulfate (Na_2SO_4, Fisher Scientific), 0.24 mg of sodium metaarsenate ($NaAsO_3$, Sigma-Aldrich), 29.60 mg of iron (II) chloride ($FeCl_2$, Sigma-Aldrich), 0.25 g of calcium chloride ($CaCl_2 \cdot 2H_2O$, Sigma-Aldrich), and 0.14 g of sodium fluoride (NaF, Alfa Aesar) were dissolved in 8 L of DIW. NaF was dried in a vacuum oven (Thermo Scientific 3618 Vacuum Oven) before preparing a stock solution. The other chemicals were used as received. Prior to experimentation, feed water was degassed with nitrogen gas (N_2) overnight in order to mimic the anoxic condition of the groundwater aquifer. However, it is possible that under certain conditions (e.g., groundwater stored in open-aired equalization tanks), the water may become oxygenated; Such an instance is out of scope in this study.

3.3.2 Groundwater treatment train

Raw groundwater is first treated by coagulation followed by sedimentation. Then, the supernatant is treated by media-filtration (QS, Grsand, or AA). Last, effluent from the media-filtration column is filtered

by a desalination membrane (NF or BWRO) until a target water recovery is achieved. Schematic process diagram of the groundwater treatment train can be found in supporting information (Figure S1) Samples after each treatment step were collected and ten water quality parameters of samples were monitored during and after each treatment step.

3.3.3 Coagulation and sedimentation

Coagulation and sedimentation experiments were conducted using a standard jar tester (Phipps & Bird, PB-700 Jartester), with aluminum sulfate used as the coagulant (Sigma Aldrich) and used as received. In these experiments, a range of different aluminum sulfate loadings from 0 mg Al^{3+}/L to 50 mg Al^{3+}/L with increment of 10 mg Al^{3+}/L (corresponding to 0 mg/L, 63 mg/L, 127 mg/L, 190 mg/L, 254 mg/L, and 317 mg/L as $Al_2(SO_4)_3$) were added to water samples (1.25 L); in the synthetic groundwater experiments, the pH of each solution was adjusted to 6.0 through the addition of 1 N sodium hydroxide (NaOH, Fisher Scientific). Rapid mixing was carried out at 200 rpm for 1 minute, followed by slow mixing at 20 rpm for 15 minutes, and concluded by settling for 6 hours. After sedimentation, pH of the treated water was measured. The testing of natural groundwater followed the same procedure but without the pH adjustment.

3.3.4 Media-filtration

Quartz sand (QS) and AA (γ-Al_2O_3) were purchased from Sigma-Aldrich, and washed thoroughly with deionized water (DIW) to remove impurities before use. Grsand was purchased from the Inversand Company and pre-conditioned with 2,000 ppm of sodium hypochlorite (NaOCl, Sigma-Aldrich) as per the manufacturer's instruction. The regeneration of sorbents was not within the scope of this study. Filter media was packed inside a polyvinyl chloride (PVC) column (schedule 40) with a diameter of 1.05-inches and a

length of 24 inches. Filtration was conducted in an upward flow-orientation at a constant flow rate of 11.33 mL/min, with flow driven by a peristaltic pump (Masterflex).

3.3.5 Membrane filtration

Two types of desalination membranes were tested in this study; NF90 and BW30 flat sheet membranes were purchased from Dow-Filmtec. Membranes were stored at 4° C in a lightproof container filled with DIW. NF and BWRO membrane coupons (4 cm by 10 cm) were placed in a custom-built flow cell, and pressurized with DIW at 150 psi and 250 psi, respectively, for 24 hours. During testing, the system was operated at these operating pressures (i.e., constant pressure operation). The NF90 membrane had a DIW flux of 73.12 ± 5.46 LMH at 150 psi, while the BW30 membrane had a flux of 51.89 ± 5.83 LMH at 250 psi. The filtration system was operated in concentration mode, where the permeate was collected and not returned to the feed tank, which allowed the system to simulate a certain water recovery. Cross flow velocity was maintained at 2.33 cm/s, corresponding to Reynolds number of 79. Water recovery throughout the study was calculated using the equation:

$$Water\ recovery\ (\%) = \frac{V_P}{V_F} \times 100 \qquad (Equation\ 1)$$

where V_P is the total volume of water filtered by a membrane, and V_F is the initial volume of water in the feed tank. The removal efficiency of a specific aqueous constituent (R_i) was calculated by:

$$R_i\ (\%) = \frac{(C_{f,i} - C_{p,i})}{C_{f,i}} \times 100 \qquad (Equation\ 2)$$

where $C_{f,i}$ is the concentration of a specific constituent i in the bulk feed solution and $C_{p,i}$ is the concentration of the constituent i in the permeate.

3.3.6 Analytical methods

pH was measured using a portable pH meter (Thermo Scientific, Orion 720A) and turbidity was measured using a turbidity meter (Hach, 2100P). Alkalinity was measured using a digital titrator (Hach). Total dissolved solids (TDS) measurement followed the standard methods [184]. Total organic carbon (TOC) was measured by a TOC analyzer (Shimadzu, TOC-L). F and Cl concentrations were measured by ion-chromatography (IC, Thermo Fisher, Dionex Integrion HPIC). Total As and total Fe concentrations were measured by inductively-coupled plasma mass spectroscopy (ICP-MS, PerkinElmer, NexION 2000). Membrane surfaces were characterized using scanning electron microscopy (SEM, ZEISS, Supra 40VP) equipped with an energy-dispersive X-ray detector (EDAX).

3.3.7 Economic modeling

To determine the optimal treatment train and blending ratios, a simple model, RWRM, was employed [108]. In brief, the RWRM determines the most cost-effective blending ratios that produce water meeting specific quality requirements. Although the RWRM was originally developed to produce irrigation water, it can be easily adopted for other applications (such as drinking water) by adjusting the targeted water quality. The RWRM determines the treatment train and stream composition that minimizes the treatment cost while meeting water quality parameters. Details can be found in the Supporting Information.

3.4 Results and Discussion

3.4.1 Aluminum sulfate-based coagulation/flocculation/sedimentation treatment

Aluminum sulfate dosing was first optimized using synthetic groundwater. No significant change in TOC, pH, total As, turbidity, total Fe, and alkalinity was observed in the treated water when aluminum sulfate concentrations greater than 10 mg Al^{3+}/L were used (Figure S2). While F concentration decreased with increasing aluminum sulfate dosing, the decrease was accompanied with an increase in TDS levels.

Thus, we determined that 10 mg Al^{3+}/L of aluminum sulfate (63 mg/L as $Al_2(SO_4)_3$) was the optimal dosage for the pretreatment of synthetic groundwater. At this optimal dosage, the concentration of F exceeded the secondary MCL, which required further polishing. Further polishing of the water by granular filtration was performed, which is discussed in the following section.

The purpose of testing synthetic groundwater that is composed of anticipated contaminant concentrations was to predict the performance of treatment technologies treating natural groundwater.

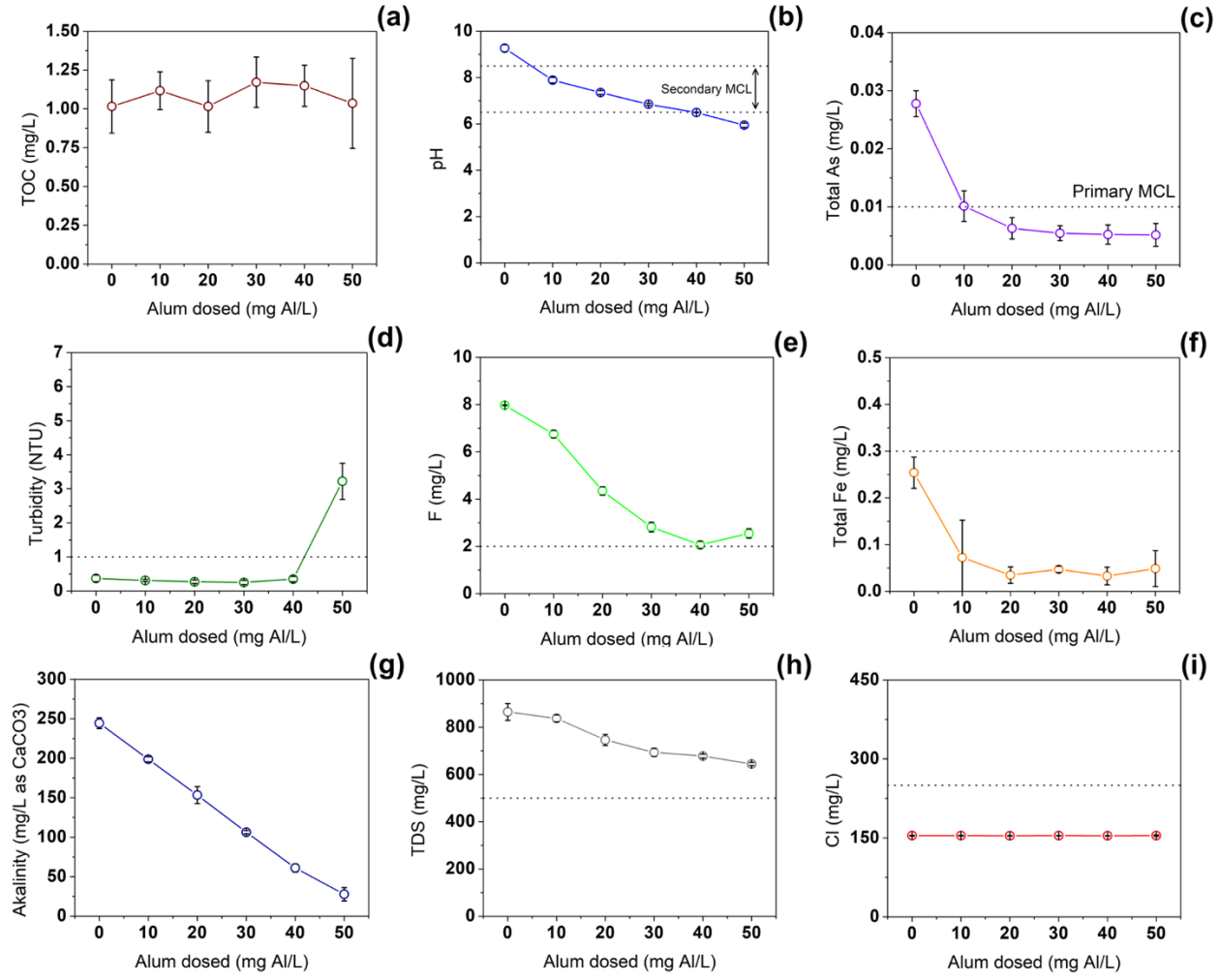

Figure 3.1. Average concentrations of TOC (a), pH (b), total As (c), turbidity (d), F (e), total Fe (f), alkalinity (g), TDS (h), and Cl (i) in natural groundwater after coagulation and sedimentation steps over a range of alum dosage (0 – 50 mg Al^{3+}/L). Error bars indicate standard deviation of triplicate trials. Horizontal dotted lines indicate the secondary MCL for specific water quality parameters, unless otherwise noted.

However, natural groundwater had different water quality (i.e., alkalinity) with the synthetic counterpart, which required re-optimization of coagulant dosage with natural groundwater. Therefore, tests were conducted to determine the optimal coagulant concentration for natural groundwater. Aluminum sulfate coagulation was not effective at removing TOC from the natural groundwater despite its effectiveness in synthetic groundwater, with natural groundwater displaying no clear trend of TOC removal with respect to aluminum sulfate dosage (Figure 1a). The difference in TOC removal between synthetic and natural groundwater could be explained by the composition of the TOC. While humic acid was the only source of TOC in the synthetic groundwater, the natural groundwater likely contains fulvic acids which are known to be more difficult to eliminate by aluminum-based coagulation.[185,186] After sedimentation, the pH of the treated groundwater was 7.88 ± 0.12, 7.35 ± 0.08, 6.84 ± 0.04, 6.49 ± 0.01, and 5.94 ± 0.09 with respect to the aluminum sulfate dosage scheme (Figure 1b). This decline in pH with increasing aluminum sulfate concentrations is known to be associated with the formation of aluminum flocs.[187–190] For the aluminum sulfate dosage of 10 mg Al^{3+}/L, total As concentrations were reduced to 0.010 ± 0.003 mg/L, with higher aluminum sulfate dosages reducing total As to below the primary MCL threshold of 0.01 ppm (Figure 1c). While the turbidity of synthetic groundwater significantly decreased with the addition of aluminum sulfate (Figure S2d), the turbidity of natural groundwater remained almost unchanged (Figure 1d), except at 50 mg Al^{3+}/L, where the turbidity of the treated water was elevated due to overdosing of the coagulant, in which colloids are restabilized.[191] Since turbidity in natural water arises from suspended particles, the small variation in turbidity with respect to the aluminum sulfate dosage could be related to its inability to effectively remove TOC by coagulation.[192] Aluminum sulfate coagulation reduced F concentrations to 6.75 ± 0.16 mg/L, 4.34 ± 0.18 mg/L, 2.82 ± 0.20 mg/L, and 2.06 ± 0.15 mg/L with respect to the aluminum sulfate dosage scheme (Figure 1e). The trend of increasing F removal efficiency with increasing aluminum coagulant dosage is in agreement with previously reported results.[193,194] Aluminum sulfate dosing decreased total Fe concentration to around 0.05 ppm, but no benefit was seen when the dosage increased over 40 mg Al^{3+}/L (Figure 1f). The plateau in iron removal with increasing aluminum sulfate dosage was previously reported.[195] After sedimentation, the alkalinity of the water was determined to be 244 ± 7 mg/L as $CaCO_3$

for 0 mg Al^{3+}/L (Figure 1g); the alkalinity of the supernatant decreased to 199 ± 3 mg/L, 153 ± 11 mg/L, 106 ± 2 mg/L, 61 ± 5 mg/L, and 28 ± 8 mg/L as $CaCO_3$ with respect to the aluminum sulfate dosage scheme. The trend of decreasing alkalinity with respect to aluminum sulfate dosage is associated with the formation of aluminum hydroxide flocs, which consume hydroxide ions.[196,197] The TDS of natural groundwater decreased with respect to the aluminum sulfate dosed (Figure 1h), which is opposite to what was observed in the synthetic case (Figure S2h), with values declining from 865 ± 36 mg/L at 0 mg Al^{3+}/L s to 644 ± 7 mg/L at 50 mg Al^{3+}/L. The difference could be significantly higher alkalinity level in natural groundwater that was greatly reduced by coagulation. Aluminum sulfate coagulation was not effective at removing Cl ions (Figure 1i). Based on our findings, an optimal aluminum sulfate dosage of 30 mg Al^{3+}/L was identified, which allowed for pH to be within the acceptable range while reducing levels of total As, F, alkalinity, and TDS compared to lower aluminum sulfate dosages.

3.4.2 Media and membrane filtration

When supernatant from the coagulation/sedimentation treatment step (treating synthetic groundwater) was further treated with media filtration (QS, Grsand, or AA), TOC removal by the three filter-media was not statistically significant (Figure S3a). Effluent from QS and Grsand had similar pH and alkalinity, while AA filtration elevated effluent pH and alkalinity (Figure S3b and g). The increase in pH of AA effluent was previously reported.[198] It was speculated that the increase in pH is due to the release of hydroxide (OH^-) ions during the ion exchange with F at the surface of AA, although the amount of OH^- ions released to water was much greater than the amount of F absorbed to AA. The increase in the pH of Grsand effluent remains unclear, since the decrease in pH after Grsand filtration was observed with synthetic groundwater. No general trend was observed regarding alkalinity in media filtration effluent. All types of filter media displayed similar water effluent quality in terms of total As, turbidity, total Fe, TDS, and Cl concentrations

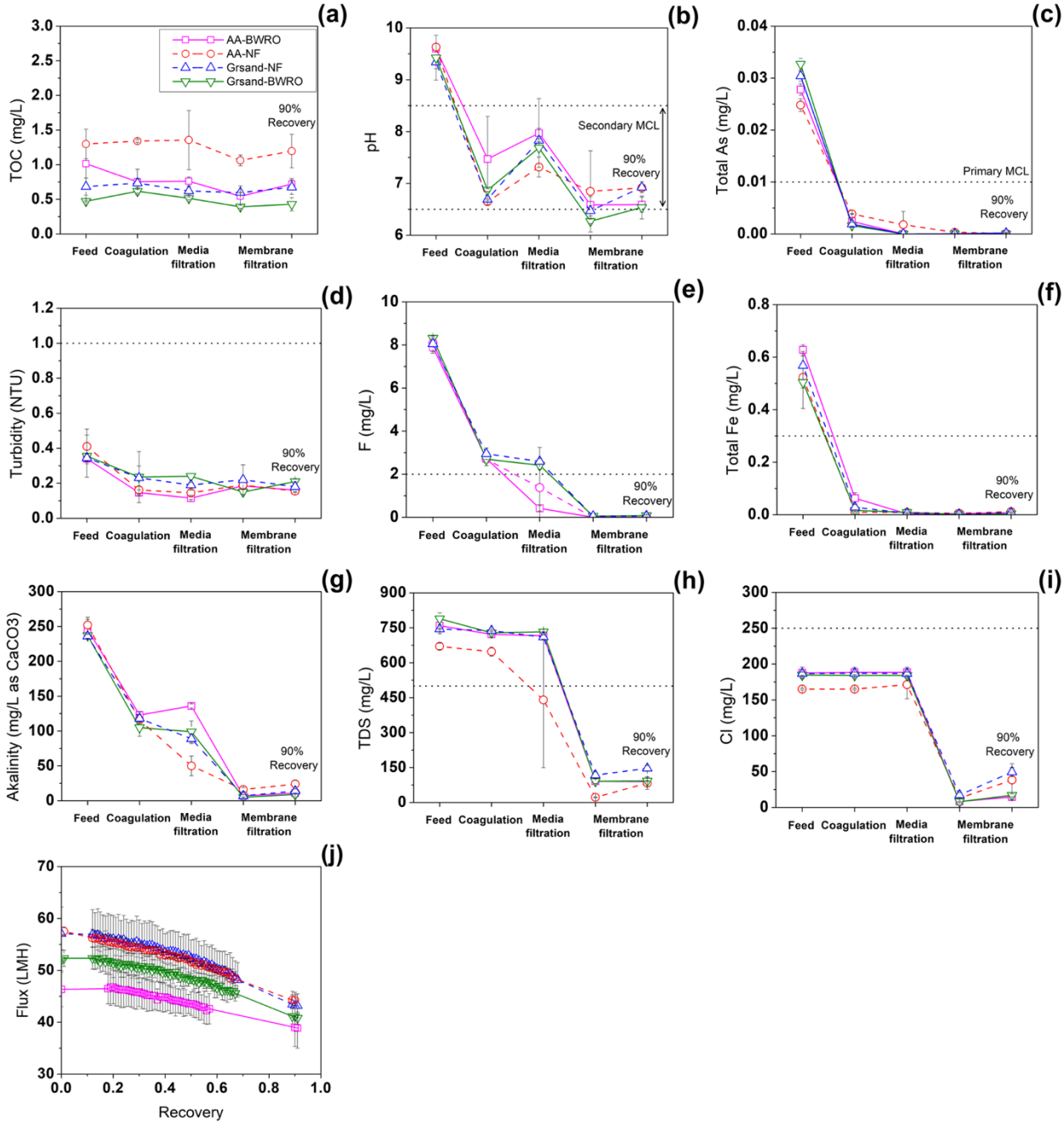

Figure 3.2. Natural groundwater quality parameters (a-h) for the feed, after coagulation, after media filtration, and after membrane filtration at 90% recovery, for combinations of AA or Grsand with NF or BWRO. Water flux of NF and BWRO membranes as a function of recovery (j). A dashed line for NF, a solid line for BWRO, a circle for AA, and a triangle for Grsand. Horizontal dotted line indicates secondary MCL for specific water quality parameters, unless otherwise noted.

(Figure S3). However, F concentrations in the media filter effluent was strongly affected by the type of

adsorbent used (Figure S3e). AA filtration completely removed F, followed by Grsand, with QS exhibiting the least F removal. The difference could be explained by the different surface charges present on filter media. AA is known to have positive charges at pH < 8, while the other media have negative surface charges, which repel negatively charge ionic species, such as fluoride.[199–201] While Grsand has negative surface charges, its removal towards As and Fe is governed by oxidation by an oxidizing reagent (i.e., NaOCl), co-precipitation of As with Fe and adsorption.[202] Since QS exhibited poor removal of F in synthetic groundwater, it was not tested for the treatment of natural groundwater.

When the media-filtration effluent (treated synthetic groundwater) that underwent the coagulation/sedimentation step was fed into a membrane filtration system (NF or BWRO), treated water at 80% recovery met water quality targets (i.e., secondary MCL), with the exception of Grsand, which produced a permeate pH of 5.5 (for both types of membranes), which is outside of the acceptable MCL range of 6.5 to 8.5 (Figure S4). Both of NF and BWRO membrane filtration hugely reduced TDS, Cl and F concentration, while slight reduction in TOC, turbidity, and alkalinity was achieved by membrane filtration. NF membrane had higher initial flux than BWRO, although they both showed flux decline along with increasing water recovery. This flux decline could be explained by higher osmotic pressures at higher recovery and scale (i.e., gypsum) formation on the membrane surface. Details can be found in the Supporting Information.

Since treated synthetic groundwater at 80% recovery met water quality targets, membrane filtration with natural groundwater conducted to 90% recovery was assessed, with the goal of reducing the volume of waste and increasing the economic viability and environmental sustainability of the process. Figure 2 shows water quality parameters after each treatment step. As observed in the previous section, coagulation did not effectively remove TOC in natural groundwater (Figure 2a). After Grsand filtration and membrane filtration, the TOC of initial NF permeate was 0.60 ± 0.00 mg/L, increasing to 0.67 ± 0.10 mg/L at 90% recovery, and the TOC of initial BWRO permeate TOC was 0.39 ± 0.02 mg/L, increasing to 0.43 ± 0.10 mg/L at 90% recovery. After AA filtration and membrane filtration, the TOC of the initial NF permeate was 1.06 ± 0.08 mg/L, increasing to 1.20 ± 0.24 mg/L at 90% recovery, and the TOC of initial BWRO

permeate was 0.54 ± 0.15 mg/L, increasing to 0.72 ± 0.08 mg/L at 90% recovery. No water treatment technology used in this study completely removed TOC from the groundwater. For natural groundwater, pH adjustment for optimum coagulation was achieved by adding aluminum sulfate. Media filtration, unlike for synthetic groundwater, slightly elevated the pH of the filtrate, although the reason is unclear (Figure 2b). After Grsand filtration and membrane filtration, the initial NF permeate pH was 6.47 ± 0.10 and the initial BWRO permeate pH was 6.27 ± 0.04. At 90% recovery, NF permeate pH increased to 6.93 ± 0.11 and BWRO permeate pH increased to 6.54 ± 0.22. After AA filtration and membrane filtration, the pH of the initial NF permeate was 6.85 ± 0.78, increasing to 6.92 ± 0.04 at 90% recovery. The pH of the BWRO permeate was barely changed during the course of the experiments and (6.59 ± 0.14 at 90% recovery).

Coagulation significantly reduced total As concentrations, media filtration further reduced As concentrations, and membrane filtration removed nearly all of the remainder As (Figure 2c). The large reduction of As concentrations by media and membrane filtration can be explained by the relatively large amount of adsorbent media with respect to the influent As concentration, and the high As removal efficiency of membranes (i.e., 71.53% for NF90 and 98.34% for BWRO30). Effective As removal by NF and BWRO membranes is in agreement with the previously reported results.[203,204] After Grsand filtrate underwent NF, initial total As concentrations in the permeate were 0.05 ± 0.07 g/L, increasing to 0.18 ± 0.07 g/L at 90% recovery. After Grsand filtrate underwent BWRO, initial total As concentrations of 0.03 ± 0.04 g/L slightly decreased to 0.02 ± 0.02 g/L at 90% recovery. After AA filtration and NF, the total As in the NF permeate was initially 0.32 ± 0.35 g/L and decreased to 0.10 ± 0.07 g/L at 90% recovery. The decrease in total As concentration in the membrane's permeate at higher recovery was not statistically significant in either case, and regardless, these concentrations are well below the MCL for As. After AA filtration and BWRO treatment, the total As in the permeate was always less than the detection limit (0.04 ppb). The majority of turbidity was removed in the coagulation step, so subsequent media filtration and member filtration had little impact of turbidity removal (Figure 2d). After Grsand filtration and membrane filtration at 90% recovery, NF permeate turbidity was 0.18 ± 0.03 NTU, and BWRO permeate turbidity was 0.21 ± 0.01 NTU. After AA filtration and membrane filtration at 90% recovery, NF permeate turbidity was 0.16 ±

0.00 NTU, and BWRO permeate turbidity was 0.16 ± 0.00 NTU. Coagulation reduced the F concentration in natural groundwater, in agreement with results from synthetic groundwater (Figures S2e and S4e). Both filter media reduced the remaining F concentrations, but AA was more effective than Grsand (Figure 2e). After Grsand filtration and NF, the initial F concentration of the NF permeate was 0.05 ± 0.00 mg/L, increasing to 0.06 ± 0.04 mg/L at 90% recovery. After Grsand filtration and BWRO, the F concentration of the BWRO permeate was initially 0.05 ± 0.01 mg/L, increasing to 0.08 ± 0.02 mg/L at 90% recovery. After AA filtration and membrane filtration, the F concentrations for both NF and BWRO permeates were always lower than the detection limit (0.02 ppm). Coagulation eliminated the majority of the total Fe, and remaining Fe ions were removed by media filtration and membrane filtration (Figure 2f). Although greensand filtration had a slightly better removal efficiency towards Fe, effluent from both media filter materials was compliant with the recommended total Fe concentrations (i.e., 0.05 ppm) in the feed stream of the membrane filtration process.[171,205] After Grsand filtration and membrane filtration at 90% recovery, the total Fe of NF permeate was 0.01 ± 0.00 mg/L, and the total Fe of BWRO permeate was at ppb levels (3 ± 2 ppb). After AA filtration and membrane filtration at 90% recovery, total Fe of NF permeate was 0.01 ± 0.01 mg/L, and total Fe of BWRO permeate was 0.01 ± 0.00 mg/L. Coagulation reduced alkalinity from feed values of around 230 mg/L as $CaCO_3$ to supernatant values of around 110 mg/L as $CaCO_3$ (Figure 2g). Media filtration had little impact on alkalinity. Since majority of carbonate ions exist as bicarbonate in the pH range of media filtration effluent (i.e., pH 7 – 8), membrane filtration that is known to have high bicarbonate removal efficiency significantly reduced the remaining alkalinity.[206,207] After Grsand filtration and NF, the permeate alkalinity was initially 7 ± 1 mg/L as $CaCO_3$ and increased to 14 ± 3 mg/L as $CaCO_3$ at 90% recovery. After Grsand filtration and BWRO, the initial permeate alkalinity of 5 ± 1 mg/L as $CaCO_3$ increased to 9 ± 4 mg/L as $CaCO_3$ at 90% recovery. After AA filtration and NF, NF permeate alkalinity was initially 16 ± 3 mg/L as $CaCO_3$, increasing to 24 ± 6 mg/L as $CaCO_3$ at 90% recovery. After AA filtration and BWRO, initial permeate alkalinity of 7 ± 1 mg/L as $CaCO_3$ increased 11 ± 1 mg/L as $CaCO_3$ at 90% recovery.

Membrane filtration removed the majority of TDS (Figure 2h). The decrease of TDS after AA filtration was associated with a large error bar and likely not statistically significant. After Grsand filtration and NF,

the initial permeate TDS of 118 ± 13 mg/L increased to 147 ± 12 mg/L at 90% recovery. After Grsand filtration and BWRO, the permeate TDS was initially 91 ± 10 mg/L, increasing to 93 ± 1 mg/L at 90% recovery. After AA filtration and NF, the initial permeate TDS of 22 ± 1 mg/L increased to 83 ± 27 mg/L at 90% recovery. After AA filtration and BWRO, the permeate TDS was initially 92 ± 4 mg/L, decreasing to 90 ± 19 mg/L at 90% recovery (not statistically significant). After Grsand filtration and NF, the initial Cl concentration in the permeate was 17.33 ± 3.46 mg/L, increasing to 49.45 ± 6.23 mg/L at 90% recovery (Figure 2i). After Grsand filtration and BWRO, the permeate Cl concentration was initially 7.89 ± 0.76 mg/L, increasing to 16.95 ± 1.99 mg/L at 90% recovery. After AA filtration and NF, the initial Cl concentration of the permeate was 12.79 ± 3.33 mg/L, increasing to 38.37 ± 22.66 mg/L at 90% recovery. After AA filtration and BWRO, the permeate Cl concentration was initially 8.31 ± 0.21 mg/L and increased to 14.62 ± 3.32 mg/L at 90% recovery. As expected, BWRO was more effective than NF in reducing Cl concentration.

For a treatment train consisting of coagulation, Grsand filtration, and membrane treatment, the initial flux was 57.05 ± 5.16 LMH and 51.98 ± 2.04 LMH, for the NF and BWRO membranes, respectively. At 90% recovery, NF flux was 43.17 ± 2.27 LMH, and BWRO flux was 40.81 ± 1.18 LMH. When the Grsand filtration was replaced by AA filtration in the treatment train, the initial NF flux was 57.54 ± 0.81 LMH, and the initial BWRO flux was 46.33 ± 3.34 LMH. At 90% recovery, the NF flux was to 44.24 ± 1.07 LMH, and the initial BWRO flux was 38.85 ± 3.84 LMH. As the recovery increased, so did the concentration of dissolved solids in the feed stream, which increased the osmotic pressure of the stream and led to flux declined. In addition, membrane fouling (e.g., scaling) likely contributed to the flux decline. SEM and EDAX analysis of fouled membrane imply the formation of $CaSO_4$ scale on the surface as a result of operation at 90% recovery (Figure S6). All treatment trains using membrane filtration at 90% recovery produced potable water that met the MCL drinking water guidelines. Given this, the selection of a particular treatment train will likely be based on its cost-effectiveness, as demonstrated in the following section.

3.4.3 Optimization of blending

Based on the identified potential treatment steps (coagulation/sedimentation, media filtration, membrane desalination), ten possible combinations of water treatment processes were identified: 1) Coagulation + NF, 2) Coagulation + BWRO, 3) AA + NF, 4) AA + BWRO, 5) Grsand + NF, 6) Grsand + BWRO, 7) Coagulation + Grsand + NF, 8) Coagulation + Grsand + BWRO, 9) Coagulation + AA + NF, and 10) Coagulation + AA + BWRO (Figure S7). Coagulation alone, media filtration alone, and membrane filtration alone options were discarded because either product water does not meet drinking water regulations (i.e., TDS and Cl) or because an unacceptable degree of membrane fouling is expected. The contaminant removal efficiency of each treatment process obtained in Section 3.2., were used in Equations

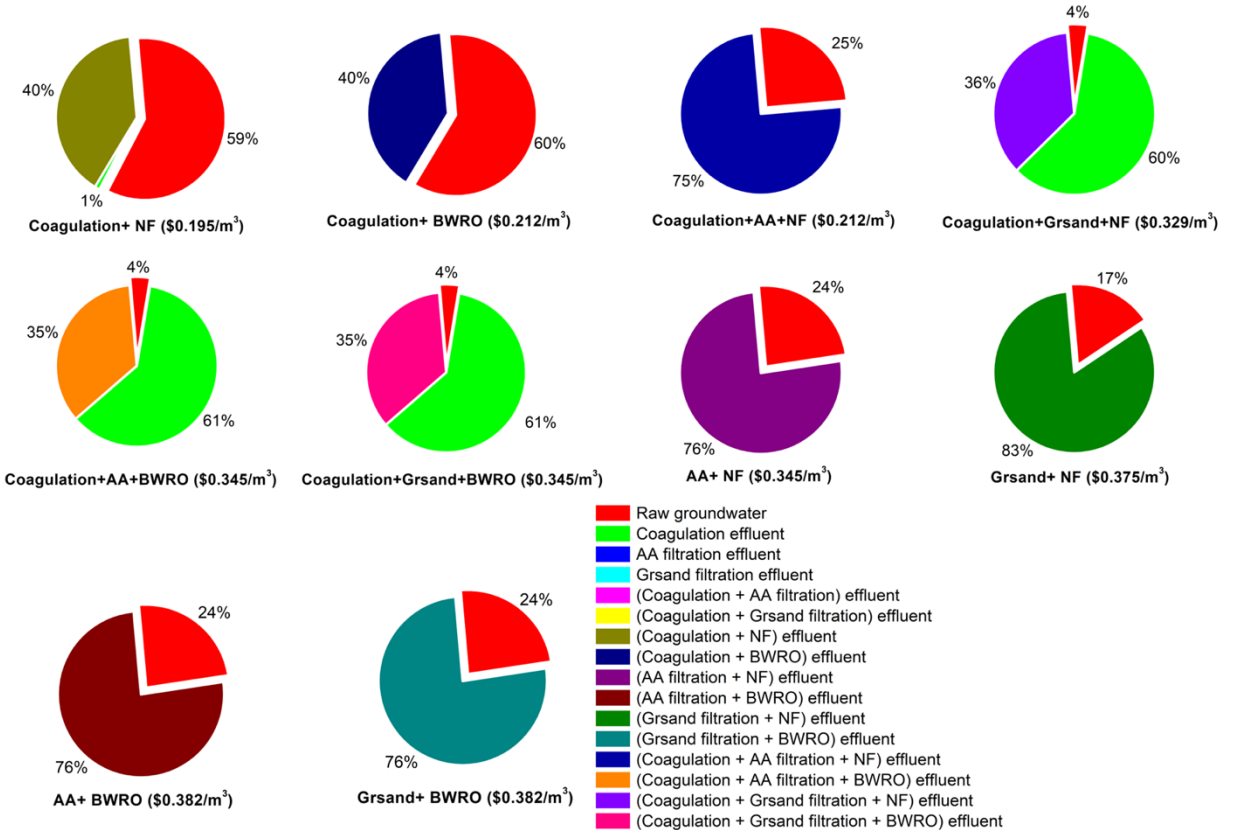

Figure 3.3. Blending ratios and water production cost for ten possible water treatment train permutation in the order from the lowest to the highest water production cost. The costs represented include chlorine disinfection.

S1 – S3 to estimate ion concentrations in the blended water, and water production cost. Details about removal efficiencies and unit water production costs of each treatment processes, as well as estimated aqueous constituent concentrations in a blended water can be found in the Supporting Information (Table S1 - S3). It should be noted that Cl concentrations in the raw groundwater were already below the secondary MCL, which excludes this parameter from the list of model constraints.

Among the ten possible treatment train combinations, the lowest water production cost of \$0.195/m^3 (including the cost of chlorine disinfection) was achieved with a train that consisted of coagulation and NF (Figure 3). However, water produced from this treatment train contains F concentration greater than the secondary MCL (Table S2). A similar issue of high F concentration occurs in a treatment train that consisted of coagulation and BWRO, where water production cost was the second lowest. Product water that met drinking water guidelines was successfully produced with a train that consisted of coagulation, AA filtration, and NF at water production cost of \$0.212/m^3. In this process, a given volume of water consisted of 25% raw groundwater and 75% of NF permeate that underwent coagulation and AA filtration, where these streams were blended together to produce a final water blend where contaminant levels are below the secondary MCL. The limiting factors of this process is F concentration that is close to secondary MCL. With the other treatment train options, it was possible to produce a blended solution meeting the drinking water regulation, albeit at a higher water production cost.

3.5 Conclusion

In this study, the performance of different water treatment processes (aluminum sulfate coagulation, QS filtration, Grsand filtration, AA filtration, NF filtration, and BWRO filtration) were evaluated for the treatment of synthetic and natural groundwater containing elevated concentrations of F, As, Fe and TDS, with respect to nine water quality parameters (TOC, pH, total As, turbidity, F, Total Fe, alkalinity, TDS, and

Cl). Then, an economic model, RWRM, was used to identify the most cost-effective treatment train that produces drinking water that meets drinking water guidelines.

For synthetic groundwater, 10 mg Al^{3+}/L of aluminum sulfate was determined to be the optimal dosage, with higher aluminum sulfate dosing not significantly reducing the level of TOC, pH, total As, turbidity, total Fe, and alkalinity. With this optimal dosage of coagulant, the level of total As, total Fe, and turbidity in the coagulation effluent met the regulatory limits; however, further treatment was required to reduce the F, TDS, and Cl concentrations. When supernatant from the coagulation/sedimentation step was treated with three different filter media (QS, Grsand, and AA), comparable levels of turbidity, and TDS remained in the treated water. However, AA and Grsand achieved the complete removal of the remaining As, while ppb levels of As remained in the QS effluent. In addition, complete removal of F was achieved with AA filtration, while QS and Grsand were less effective, likely because of their negative surface charges. Thus, it was decided to exclude QS for the rest of the study. When synthetic feed water was treated by coagulation following Grsand and NF/BWRO filtration, water produced at 80% recovery satisfied drinking water guidelines, except for pH, which was slightly acidic. With a treatment train that consisted of coagulation, AA, and NF/BWRO filtration, water that meets drinking water guideline was successfully produced at 80% recovery.

In general, the removal of the various constituents in the synthetic groundwater was similar to that observed in the natural groundwater throughout the treatment train, although elevated level of alkalinity was observed in natural groundwater. Unlike synthetic groundwater, the optimum aluminum sulfate dosing for natural groundwater was found to be 30 mg AL^{3+}/L (vs. 10 mg AL^{3+}/L for the synthetic groundwater). At this optimal aluminum sulfate dosage, coagulation/sedimentation reduced the concentration of As to acceptable levels (i.e., lower than primary MCL) and F concentration close to the secondary MCL. The removal efficiency of F by coagulation/sedimentation was higher in the natural groundwater than in the synthetic groundwater, which could be explained by the different amount of aluminum sulfate used in the coagulation. The effectiveness of As removal by aluminum sulfate coagulation corresponds to the results observed in the synthetic groundwater. However, further treatment was required to treat excess

concentrations of F, and TDS. AA filtration significantly reduced the concentration of F in the coagulation/sedimentation effluent, while Grsand filtration had little effect on F removal. Both filter media effectively removed the remaining As and total Fe in the coagulation effluent, which was also observed with synthetic groundwater. In addition, the concentration of total Fe in the media filtration effluent (either AA or Grsand) was lower than the recommended level of 0.05 ppm. With membrane filtration (either NF or BWRO), Cl and TDS levels were reduced to well below to the regulatory limit at 90% recovery. Thus, when natural groundwater was treated with a treatment train consisting of coagulation (30 mg Al^{3+}/L of aluminum sulfate dose), media filtration (Grsand or AA), and membrane filtration (NF or BWRO), the water produced at 90% recovery satisfied drinking water regulations.

When the experimental findings were used as input into the RWRM, the most cost-effective treatment train that treats groundwater having elevated concentrations of F, As, Fe, and TDS was identified to consist of coagulation, AA filtration, NF, and disinfection. The lowest production cost of \$0.212/m^3 was achieved when 25% of raw groundwater was blended with 75% of NF filtration effluent that underwent coagulation and AA filtration. Although a treatment train consisting of coagulation and membrane filtration (either NF or BWRO) was capable of producing blended water that contains concentrations of As, Fe, and TDS that met regulatory guidelines at a lower water production costs (i.e., \$0.195/m^3 with NF, and \$0.212/m^3 with BWRO), F concentration in the blended water was always higher than the regulatory limit. Thus, AA filtration was found to be an important component during the treatment of F-containing water.

3.6 Acknowledgements

Funding for this project was generously provided by the City of Lawton (OK). The authors acknowledge the use of ICP-MS core facility within the UC Center for Environmental Implications of Nanotechnology in CNSI at UCLA.

3.7 Supporting Information

3.7.1 Properties of feed water

Table S 3.1 Properties and constituents of feed water and secondary maximum concentration level

	Synthetic groundwater	**Natural groundwater**	**Secondary Maximum Concentration Level[a)]**
TOC (mg/L)	1.97 ± 0.28	0.98 ± 0.25	n.a[b)]
pH	8.50 ± 0.71	9.40 ± 0.23*	6.5 - 8.5
As (µg/L)	20.2 ± 3.8*	24.5 ± 3.2*	10[c)]
Turbidity (NTU)	2.69 ± 0.54	0.37 ± 0.07	1 - 5
F (mg/L)	7.57 ± 2.29*	7.89 ± 0.20*	2
Fe (mg/L)	2.05 ± 0.45*	0.33 ± 0.12	0.3
Alkalinity (mg/L as CaCO3)	6.71 ± 1.86	245 ± 10	n/a
TDS (mg/L)	765.56 ± 71.26*	800 ± 103*	500
Cl (mg/L)	385.55 ± 10.76*	154.55 ± 6.67	250

* indicates values exceeding the Secondary Maximum Concentration Level

a) set by U.S. Environmental Protection Agency [208]

b) n/a indicates no Secondary Maximum Concentration Level set by U.S. Environmental Protection Agency

c) this value is Primary Maximum Concentration Level. There is no Secondary Maximum Concentration Level set by U.S. Environmental Protection Agency

3.7.2 Groundwater treatment train

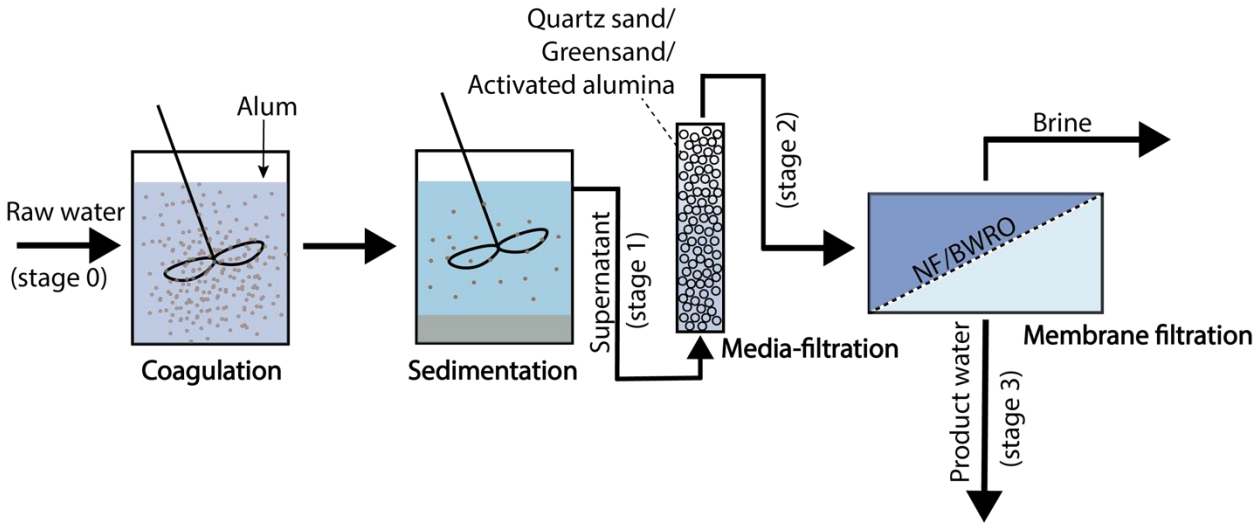

Figure S 3.1. Process diagram of the groundwater treatment train

3.7.3 Economic modeling

In this model, the cost of an individual treatment technology as part of the entire treatment process is expressed as a unit production cost, multiplied by the blending fraction of water produced by that process:

$$C_T = \sum_{j=0}^{J_T} b_T(j) \times c_T(j) \qquad (Equation\ S1)$$

where C_T is total water production cost in \$/m^3, T is a specific treatment train that consists of J_T unique processes, j is a specific stage within a treatment train T (specific location of each stages in a treatment train is described in Figure S1.), effluent quality from a particular stage considers the cumulative treatment from all prior steps (stage 0 is raw groundwater), $b_T(j)$ is blending ratios of effluent from a specific stage j within a treatment train T, and $c_T(j)$ is a unit water production cost (\$/m^3) of a unit process T. The sum of all blending fractions equals to one, mathematically express by:

$$\sum_{j=0}^{J_T} b_T(j) = 1 \qquad (Equation\ S2)$$

Concentration of each contaminants in the final product water was calculated using the equation:

$$C_i = \sum_{j=0}^{J_T} b_T(j) \times C_{i.o}(j) \times (1 - R_{T,i}(j)) \qquad (Equation\ S3)$$

Where C_i is the concentration of specific constituent i in the final blended solution, $C_{i.o}(j)$ is inlet concentration of specific constituent to the specific process j within a treatment train T, and $R_{T,i}(j)$ is constituent i removal efficiency of individual process j within a treatment train T ($R_{T,i}(0)$ equals to 0).

The blending ratio between raw groundwater and each treatment process effluent in a treatment train was iteratively adjusted using an open-source programming language, Python. For instance, when a treatment train is composed of coagulation followed by AA filtration and NF filtration, blending volumes from each stage was iteratively adjusted from 0 to 1 with a step of 0.01 under the constraints of Equation S2. During each iteration, each b_T value was entered into Equations 3 and 5 to obtain contaminant concentrations in the final product water. Then, consideration of the water quality constraints (i.e., pH, total As, F, total Fe, Cl, and TDS) was applied to determine the lowest cost blending ratio that met drinking water standards.

Table S2. represents $R_{T,i}(j)$ values obtained from Section 3.2.

Table S 3.2 Removal efficiency (%) of each contaminant by different treatment processes used in this study.

Treatment Process	pH	TDS	Turbidity	Alkalinity	TOC	Cl	F	Total Fe	Total As
Coagulation	26.86	8.43	32.50	53.50	-7.74	-0.08	65.46	91.25	88.27
Grsand filtration	-14.46	1.62	91.30	14.23	16.09	0.11	10.98	62.88	100.00
AA filtration	-8.47	16.71	82.14	23.07	-2.32	-1.91	67.53	47.26	100.00
NF filtration	22.78	93.01	30.92	88.67	27.61	90.59	97.00	-6.08	71.53
BWRO filtration	23.94	94.48	33.53	96.21	36.06	97.01	98.36	14.33	98.34

Table S 3.3 Estimated contaminant concentrations in the blended solution. (highlighted values are the limiting factors of the specific treatment train)

Treatment train	pH	TDS (mg/L)	Turbidity (NTU)	Alkalinity (mg/L as CaCO3	TOC (mg/L)	Cl (mg/L)	F (mg/L)	Fe (mg/L)	As (mg/L)
Coag-NF	7.74	500	0.29	151	0.89	98.55	4.72*	0.207	0.015
Coag-BWRO	7.73	496	0.29	149	0.86	94.58	4.75*	0.208	0.015
Coag-AA-NF	6.67	232	0.12	69	0.83	49.76	1.99	0.095	0.006
Coag-Grsand-BWRO	6.69	490	0.17	82	0.90	104.22	1.98	0.035	0.003
Coag-AA-BWRO	6.56	491	0.18	80	0.93	102.18	1.98	0.035	0.003
Coag-Grsand-BWRO	6.66	493	0.17	81	0.88	102.15	1.99	0.034	0.003
AA-NF	8.24	227	0.12	75	0.79	48.36	1.95	0.220	0.006
Grsnad-NF	8.49	182	0.08	61	0.66	38.33	1.52	0.164	0.004
AA-BWRO	8.15	220	0.12	64	0.72	40.67	1.93	0.193	0.006
Grsand-BWRO	8.48	225	0.11	65	0.63	40.60	1.98	0.159	0.006

C_i and C_T for the unique treatment train J_T are represented in Table S3 – S4.

*: values do not satisfy the secondary MCL

Table S 3.4 Water production cost for each water treatment technologies.

Treatment process	Water production cost ($/m^3)*
Coagulation	0.045 ± 0.039 [186,209,210]

Grsand filtration	0.764 ± 0.023 [211,212]
AA filtration	0.544 ± 0.115 **a),** [213,214]
NF filtration	0.424 ± 0.107 **b),** [215–219]
BWRO filtration	0.473 ± 0.132 **b),** [220,221]
Chlorination	0.023 ± 0.015 [222]

* costs from references were adjusted to the value of US dollars in 2020, using consumer price index (CPI).

a) includes water production cost from a private conversation with a company

b) water production cost may be overestimated, since the cost reported in references may result from a membrane filtration process equipped with pretreatment processes (i.e., filter cartridge, acidification, and antiscalant dosage)

3.7.4 Treatment of groundwater

3.7.4.1 Optimization of coagulation with synthetic groundwater

To explore the impact of aluminum sulfate dosing on the different water quality parameters, aluminum sulfate dosages ranging between 0 and 50 mg Al^{3+}/L, (in 10 mg Al^{3+}/L increments) were added to the synthetic groundwater (Figure S2). When sedimentation of the feed water was conducted after the coagulation/sedimentation step without aluminum sulfate, 1.80 ± 0.28 mg/L of TOC remained in the water. While the addition of aluminum sulfate led to a decline in TOC levels, no improvement in TOC removal was observed when the aluminum sulfate dosage increased beyond 10 ppm Al^{3+}, with final TOC concentrations of 1.03 ± 0.29 mg/L, 1.07 ± 0.26 mg/L, 1.12 ± 0.34 mg/L, 1.06 ± 0.30 mg/L and 1.14 ± 0.35 mg/L for aluminum sulfate concentrations of 10 mg Al^{3+}/L, 20 mg Al^{3+}/L, 30 mg Al^{3+}/L, 40 mg Al^{3+}/L, and 50 mg Al^{3+}/L, respectively (Figure S2a). Subsequent measurements will refer to the series of the five aluminum sulfate concentrations from 10 mg Al^{3+}/L to 50 mg Al^{3+}/L as the aluminum sulfate dosage scheme. In this study, TOC in the synthetic groundwater can be attributed to humic acid, and aluminum sulfate coagulation has been previously reported to be effective at removal of humic substances [188]. After sedimentation, the pH of the 0 mg Al^{3+}/L sample decreased from the feed water value of 8.50 ± 0.71 to 7.13 ± 0.69, likely from exposure to air, which allowed CO_2 to dissolve into the water. The pH of all samples dosed with aluminum sulfate decreased from approximately 6.0 after coagulation to approximately 5.7 after sedimentation (Figure S2b). Total As concentrations for the 0 mg Al^{3+}/L sample did not change post sedimentation. However, the addition of 10 mg Al^{3+}/L dramatically reduced As concentrations, with the total As concentrations reduced to 2.07 ± 0.29 ppb. As concentrations were nearly unchanged with

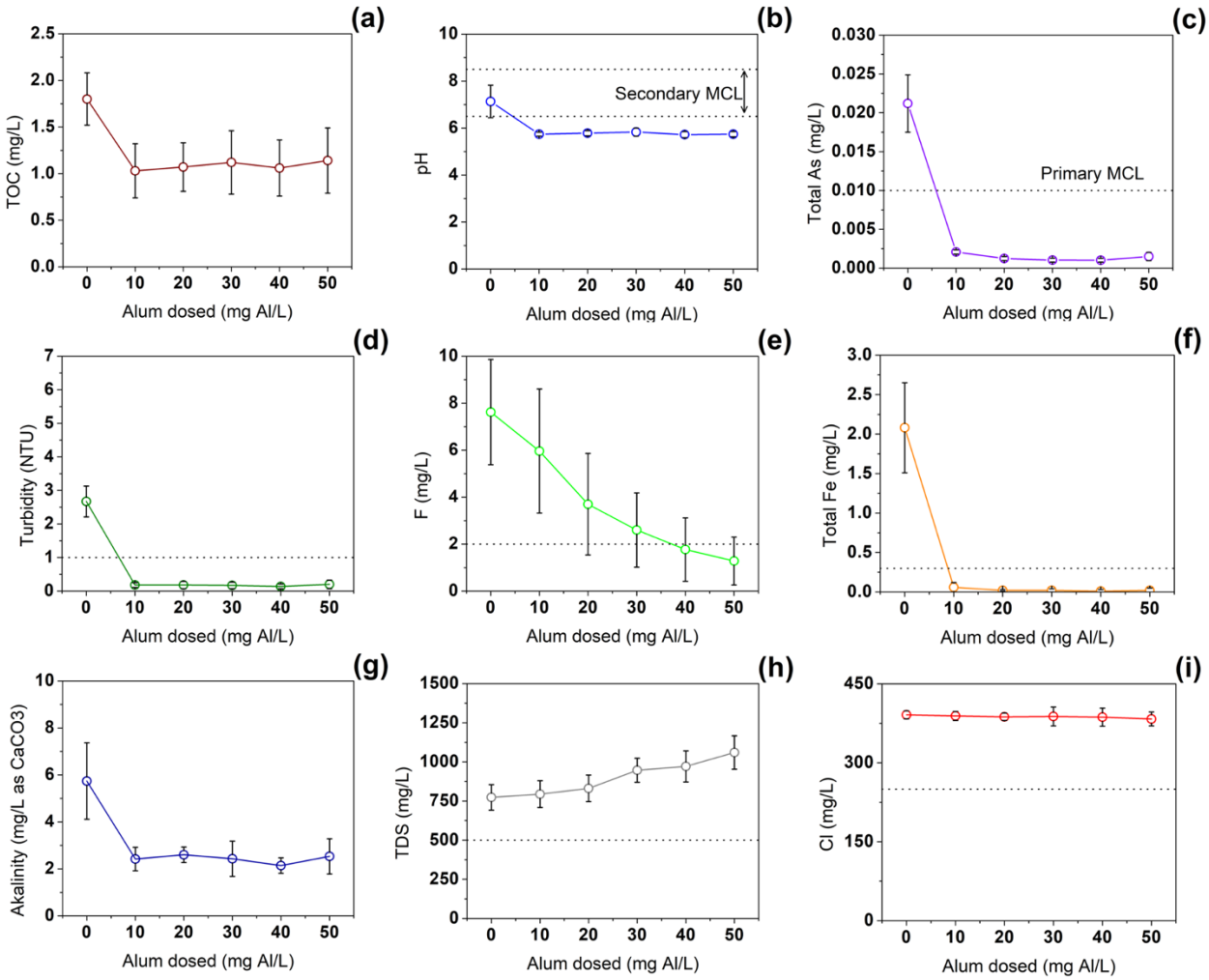

Figure S 3.2. Average concentrations of TOC (a), pH (b), total As (c), turbidity (d), F (e), total Fe (f), alkalinity (g), TDS (h), and Cl (i) in synthetic groundwater after coagulation and sedimentation steps over a range of aluminum sulfate dosage (0 – 50 mg Al^{3+}/L). Error bars indicate standard deviation of triplicate. Horizontal dotted line indicates secondary MCL for specific water quality parameters, unless otherwise noted.

increasing aluminum sulfate dosages (20 mg Al^{3+}/L to 50 mg Al^{3+}/L), likely due to diffusion limitations (Figure S2c). The addition of 10 mg Al^{3+}/L effectively reduced turbidity from 2.67 ± 0.46 NTUs (at 0 mg Al^{3+}/L) to 0.18 ± 0.07 NTU. However, increasing aluminum sulfate dosages did not reduce turbidity further (Figure S2d). F concentrations were sensitive to aluminum sulfate dosages, with decreased concentrations observed with increasing aluminum sulfate loading (5.96 ± 2.64 mg/L, 3.70 ± 2.16 mg/L, 2.60 ± 1.58 mg/L,

1.77 ± 1.35 mg/L and 1.28 ± 1.02 mg/L of F with respect to the aluminum sulfate dosage scheme) (Figure S2e). This is not surprising, as F strongly adsorbs to alumina, and F concentrations were not as low as As, [194,223]. Total Fe concentrations generally decreased with increasing aluminum sulfate dosing (0.06 ± 0.06 mg/L, 0.02 ± 0.01 mg/L, 0.02 ± 0.02 mg/L, 0.01 ± 0.02 mg/L and 0.02 ± 0.03 mg/L of total Fe concentration with respect to the aluminum sulfate dosage scheme) (Figure S2f). The alkalinity of the water was determined to be 5.74. ± 1.63 mg/L of $CaCO_3$ for the 0 mg Al^{3+}/L sample. Water alkalinity declined to 2.42 ± 0.50 mg/L upon the addition of 10 mg Al^{3+}/L, but increasing aluminum sulfate dosing did not change alkalinity values (Figure S2g). These samples shared similar values for alkalinity despite different aluminum sulfate concentrations likely because the pH of these samples was adjusted to 6.0 following aluminum sulfate dosage. The TDS of the treated water increased with increasing aluminum sulfate concentrations. The 0 mg Al^{3+}/L sample had and lowest TDS of 773.33 ± 81.24 mg/L, while the 50 mg Al^{3+}/L sample had highest TDS of 1060 ± 106.77 mg/L (Figures S2h). Higher concentrations of aluminum sulfate required larger amounts of NaOH to raise the pH to 6, resulting in higher TDS in the treated water with respect to aluminum sulfate concentrations. Cl concentrations were unaffected by aluminum sulfate coagulation, unlike other water quality parameters (Figure S2i).

Based on these measurements, we determined that the optimal aluminum sulfate dosage was 10 mg Al^{3+}/L, because it balanced sufficiently high effluent water quality while minimizing chemical dosing and TDS. Beyond the optimal aluminum sulfate dosage, there was no significant change in TOC, pH, total As, turbidity, total Fe, and alkalinity.

3.7.4.2 Optimization of media-filtration with synthetic groundwater

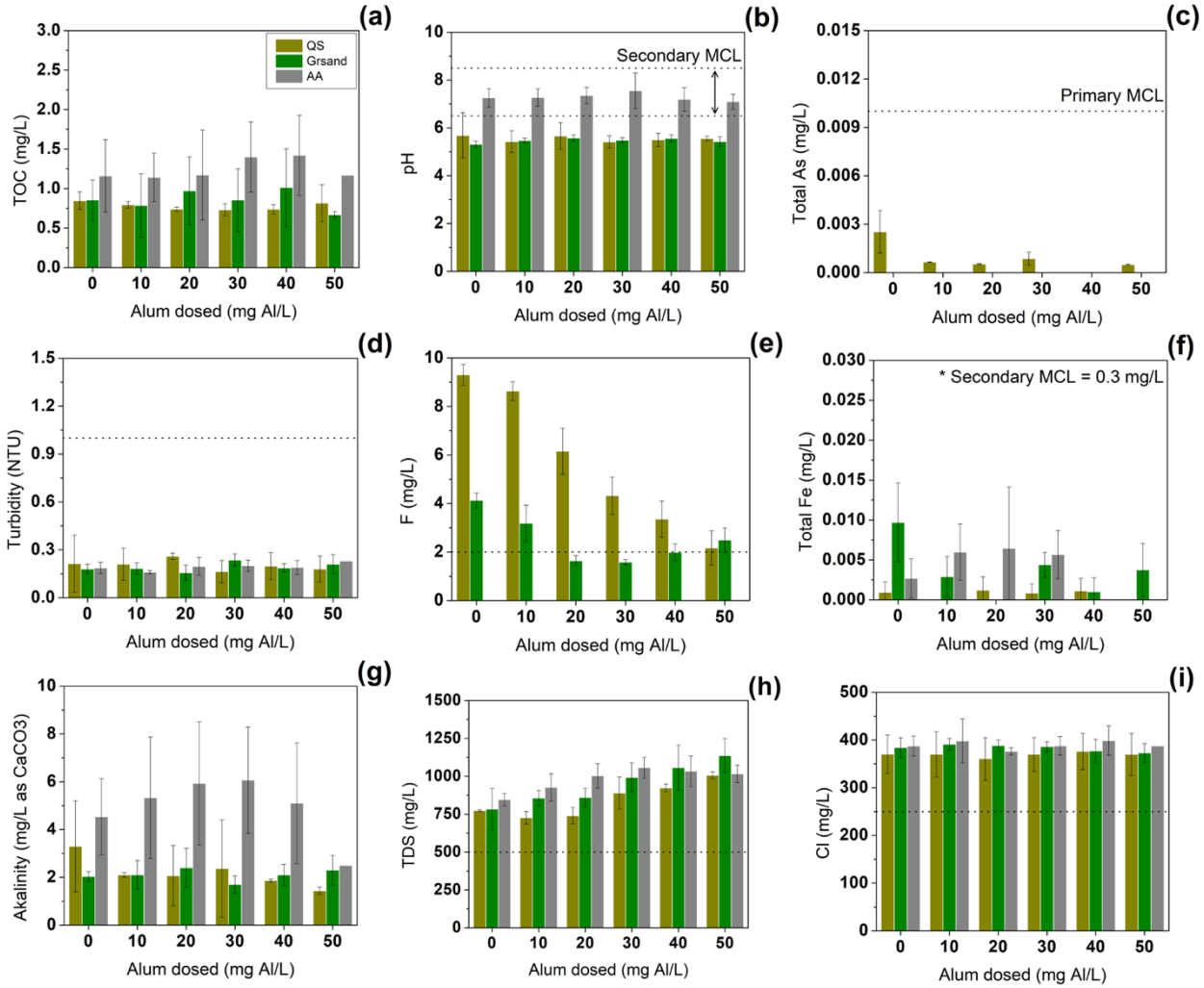

Figure S 3.3. Average concentrations of TOC (a), pH (b), total As (c), turbidity (d), F (e), total Fe (f), alkalinity (g), TDS (h), and Cl (i) in synthetic groundwater after filtration step (QS, Grsand or AA) following coagulation and sedimentation with 10 mg AL^{3+}/L of alum dosage. Error bars indicate standard deviation of triplicate. Data points indicating zero are concentrations below the limit of detection. Horizontal dotted line indicates secondary MCL for specific water quality parameters, unless otherwise noted.

After coagulation and sedimentation, the supernatant received additional treatment through packed-bed filtration with one of the three different filter media: QS, Grsand, or AA (Figure S3). When media filtration was conducted without coagulation, the TOC level was reduced from 1.80 ± 0.28 mg/L for the feed to 0.85 ± 0.11 mg/L, 0.85 ± 0.25 mg/L, and 1.16 ± 0.46 mg/L for QS, Grsand, and AA filtration, respectively. TOC

concentrations following media filtration of coagulation effluent treated with varying aluminum sulfate dosages showed some variation, but in general, the impact of changing aluminum sulfate dosage was not statistically significant (Figure S3a). However, filtration with QS and Grsand generally produced the lowest effluent TOC concentrations. For coagulation followed by QS or Grsand filtration, the resulting pH was approximately 5, but for coagulation followed by AA filtration, the resulting pH was approximately 7 (Figure S3b). The difference in pH could be explained by the contaminant removal mechanism of AA that involves not only adsorption, as is the case for QS and Grsand, but also ion-exchange [224,225]. However, the exact reason for pH increase after AA filtration remains unclear.

As concentrations following Grsand and AA filtration were lower than the detection limit (0.04 ppb), but after QS filtration, total As was detectable at ppb levels (Figure S3c). The low concentration of As prior to filtration contributed to Grsand and AA filtration in being able to reduce total As to below detection levels. When filtration was conducted without coagulation, the resulting filtrate turbidity was 0.21 ± 0.18, 0.18 ± 0.03, and 0.19 ± 0.04 NTU for QS, Grsand, and AA, respectively, with every filter media exhibiting effective turbidity removal. (Figure S3d). AA achieved the highest removal efficiency for F, followed by Grsand, and QS (Figure S3e). For AA, F concentration in the filtrate was below the detection limit (0.2 mg/L) for every aluminum sulfate dosage. For QS filtration, F concentrations decreased with increasing aluminum sulfate dosage. F concentrations following Grsand filtration reached a minimum at a 30 mg Al^{3+}/L dosage (reason unclear). All filtration media were effective in reducing total Fe concentrations to below the secondary MCL levels of 0.3 ppm (Table S1). In some cases, Fe concentrations were less than a detection limit (0.53 ppb), but no clear trends with respect to aluminum sulfate dosage were observed (Figure S3f). While QS and Grsand filtration did not significantly change alkalinity, AA filtration increased alkalinity, which can be explained by the release of hydroxide ions from AA during ion-exchange (Figure S3g). Changes in TDS and Cl concentrations after media filtration were marginal (Figures S3h-i). The TDS remained largely unchanged after filtration because no treatment processes conducted in this section effectively removed Na and Cl, which were the most abundant ions in the synthetic groundwater. When

using the optimal coagulation dosage, QS produced an effluent containing F and As concentrations that exceeded the regulatory limit. Thus, QS was excluded for the rest of study.

3.7.4.3 Optimization of membrane filtration with synthetic groundwater

NF and BWRO membranes were used to treat effluent from Grsand and AA filtration, with treatment steps are carried out sequentially as described in Figure S1, unless otherwise noted (Figure S4). The coagulation step with 10 mg Al^{3+}/L eliminated the majority of TOC from the raw groundwater, and the subsequent media and membrane filtration did not completely eliminate TOC (Figure S4a). When coagulation and Grsand filtration were followed by NF, initial NF permeate TOC of 0.59 ± 0.12 mg/L increased to 0.71 ± 0.07 mg/L at 80% recovery, although this increase is not significant. When coagulation and Grsand filtration were followed by BWRO treatment, BWRO permeate TOC was initially 0.46 ± 0.17 mg/L, remained at 0.45 ± 0.18 mg/L at 80% recovery. When coagulation and AA filtration were followed by NF, initial permeate TOC of 1.30 ± 0.44 mg/L increased to 1.56 ± 0.61 mg/L at 80% recovery (not a statistically significant change). When coagulation and AA filtration were followed by BWRO, initial permeate TOC was 0.80 ± 0.01 mg/L, increasing to 0.99 ± 0.07 mg/L at 80% recovery. Following Grsand filtration, the pH generally decreased after each treatment step (Figure S4b), with the NF permeate pH determined to be 5.57 ± 0.21, and BWRO permeate pH measured at 5.49 ± 0.05 at 80% recovery. In contrast, following coagulation, AA filtration, and membrane filtration, NF permeate pH was 7.69 ± 0.09, and BWRO permeate pH was 7.67 ± 0.10 at 80% recovery. Per the explanation in Section 3.3 in the Supporting Information, after AA filtration, the pH of the groundwater increased due to the release of hydroxide ions. Aluminum sulfate coagulation removed the majority of the total As, and Grsand and AA filtration removed the majority of any residual As. Following NF or BWRO filtration at 80% recovery, little As was detected in the permeate (Figure S4c). After Grsand filtration and membrane filtration at 80% recovery, the NF filtrate turbidity was 0.27 ± 0.09 NTU, and the BWRO filtrate turbidity was 0.24 ± 0.03 NTU (Figure S4d).

When AA filtration was followed by membrane filtration at 80% recovery, the NF filtrate turbidity was 0.16 ± 0.01 NTU and the BWRO filtrate turbidity was 0.18 ± 0.02 NTU, respectively (Figure S5d). As observed in sections (3.1 and 3.3) in the Supporting Information, a slight reduction in F concentration was achieved by aluminum sulfate coagulation (Figure S4e). Subsequent media filtration using AA greatly reduced remaining F levels, while only a negligible amount of F was removed by Grsand filtration. After Grsand filtration and NF, the initial permeate F concentration of 0.84 ± 0.20 mg/L, which increased to 1.59 ± 0.30 mg/L at 80% recovery. After Grsand filtration and BWRO, permeate F concentration was always lower than the detection limit. After AA filtration and NF or BWRO, permeate F concentration was always lower than the detection limit. Coagulation had a large impact on Fe removal, with any residual Fe removed by media filtration with Grsand or AA; NF and BWRO filtrate contained no detectable Fe ions (Figure S4f). The majority of alkalinity was reduced by aluminum sulfate coagulation. Then, alkalinity was further reduced by Grsand filtration while alkalinity was elevated after AA filtration, likely due to hydroxide release from AA (Figure S4g). After Grsand filtration and NF, the initial permeate alkalinity was 1.07 ± 0.11 mg/L as $CaCO_3$, increasing to 1.33 ± 0.31 mg/L as $CaCO_3$ at 80% recovery. After Grsand filtration and BWRO, the permeate alkalinity was initially 0.90 ± 0.10 mg/L as $CaCO_3$, increasing to 0.90 ± 0.00 mg/L as $CaCO_3$ at 80% recovery. After AA filtration and NF, initial permeate alkalinity of 2.70 ± 0.13 mg/L as $CaCO_3$ decreased to 2.55 ± 0.49 mg/L as $CaCO_3$ at 80% recovery. After AA filtration and BWRO, initial permeate alkalinity was 1.95 ± 0.07 mg/L as $CaCO_3$, increasing to 2.75 ± 0.21 mg/L as $CaCO_3$ at 80% recovery.

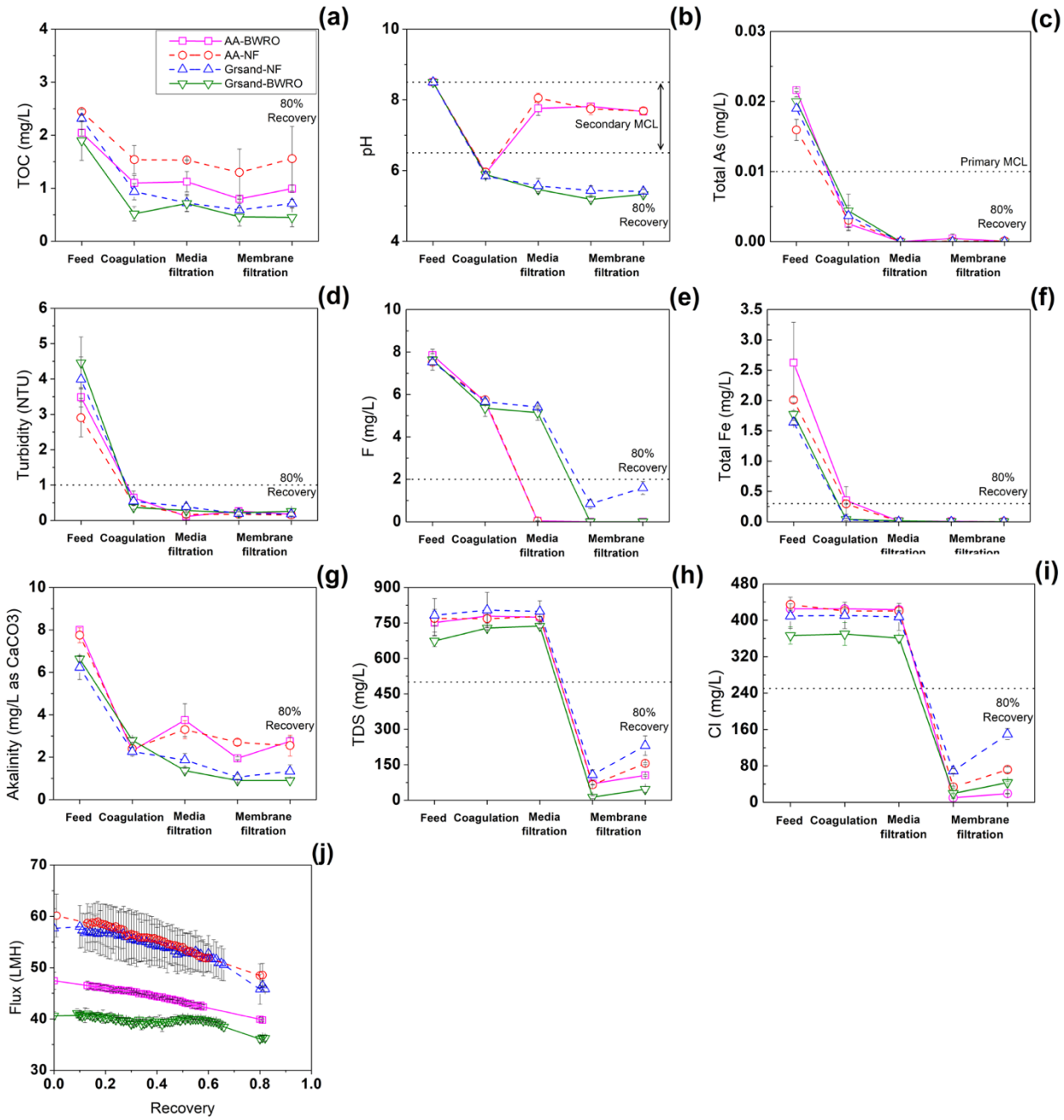

Figure S 3.4. Synthetic groundwater quality parameters (a-i) for the feed, after coagulation, after media filtration, and after membrane filtration at 80% recovery, for combinations of AA or Grsand with NF or BWRO. Water flux of NF and BWRO membranes as a function of recovery (j). A dashed line for NF, a solid line for BWRO, a circle for AA, and a triangle for Grsand. Horizontal dotted line indicates the secondary MCL for specific water quality parameters, unless otherwise noted.

After Grsand filtration and NF, initial permeate TDS of 107 ± 22 mg/L increased to 231 ± 41 mg/L at

80% recovery. After Grsand filtration and BWRO, permeate TDS was initially 13 ± 6 mg/L, increasing to 46 ± 12 mg/L at 80% recovery. After AA filtration and NF, initial permeate TDS of 66 ± 0.7 mg/L increased to 155 ± 4 mg/L at 80% recovery. After AA filtration and BWRO, permeate TDS was initially 70 ± 7 mg/L, increasing to 105 ± 3 mg/L at 80% recovery. After Grsand filtrate underwent NF, permeate concentrations of Cl increased from 68.87 ± 5.02 mg/L initially, to 74.78 ± 6.14 mg/L at 80% recovery. After Grsand filtration and BWRO, concentrations of Cl increased from 19.55 ± 0.90 mg/L initially, to 43.37 ± 2.04 mg/L at 80% recovery. After AA filtrate underwent NF, permeate concentrations of Cl increased from 33.61 ± 1.87 mg/L initially, to 71.73 ± 6.21 mg/L at 80% recovery. After AA filtration and BWRO, permeate concentrations of Cl increased from 9.95 ± 1.29 mg/L initially, to 19.10 ± 0.71 mg/L at 80% recovery.

During the NF process, the initial flux was 57.68 ± 3.80 LMH and 60.15 ± 4.20 LMH for the AA and Grsand pretreatment, respectively – not a significant difference (Figure S4j); the final flux (at 80% recovery) was 45.80 ± 0.54 LMH and 48.55 ± 2.30 LMH for the AA and Grsand pretreatment, respectively, again, not significantly different (Figure S4j). In contrast, flux from the BWRO membranes was sensitive to the type of pretreatment. For the Grsand filtration, the initial and final flux was 40.61 ± 0.74 LMH and 36.26 ± 0.55 LMH, respectively, while for AA filtration the initial and final flux was 47.44 ± 1.69 LMH and 39.79 ± 0.23, respectively (Figure S4j). However, there may be no correlation because the opposite result (i.e., higher initial flux of BWRO following Grsand filtration than that of BWRO following AA filtration) was observed when treating natural groundwater. Flux decline with increasing recovery may be a result of concentrated feed concentration and scaling formation. SEM and EDAX results imply the formation of $CaSO_4$ on membrane surface (Figure S5).

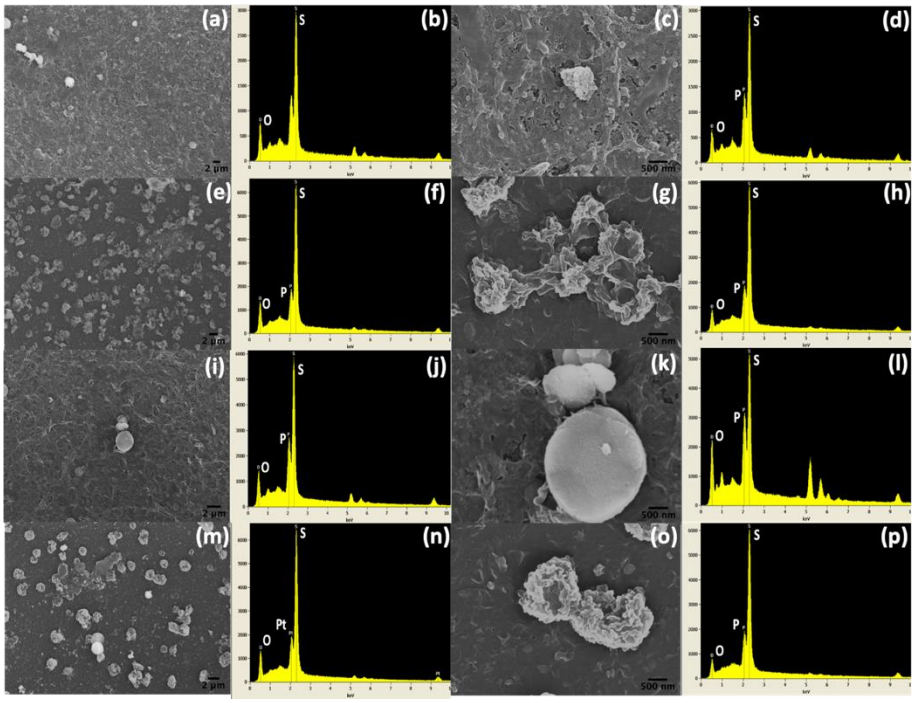

Figure S 3.5. For a synthetic groundwater treatment train consisted of coagulation, Grsand filtration, and membrane filtration (a-h); (a) SEM image of scaled NF membrane used to treat synthetic groundwater at 80% recovery; (b) EDAX results of the scaled NF membrane at 80% recovery; (c) SEM image of scaled NF membrane at higher magnitude; (d) EDAX results of scaled NF membrane at higher magnitude; (e) SEM image of scaled BWRO membrane used to treat synthetic groundwater at 80% recovery; (f) EDAX results of the scaled BWRO membrane at 80% recovery; (g) SEM image of scaled BWRO membrane at higher magnitude; (h) EDAX results of the scaled BWRO membrane at higher magnitude. For treatment train consisted of coagulation, AA filtration, and membrane filtration (i-q); (i) SEM image of scaled NF membrane used to treat synthetic groundwater at 80% recovery; (j) EDAX results of the scaled NF membrane at 80% recovery; (k) SEM image of scaled NF membrane at higher magnitude; (l) EDAX results of scaled NF membrane at higher magnitude; (m) SEM image of scaled BWRO membrane used to treat synthetic groundwater at 80% recovery; (n) EDAX results of the scaled BWRO membrane at 80% recovery; (o) SEM image of scaled BWRO membrane at higher magnitude; (p) EDAX results of the scaled BWRO membrane at higher magnitude.

3.7.5 Optimization of membrane filtration with natural groundwater

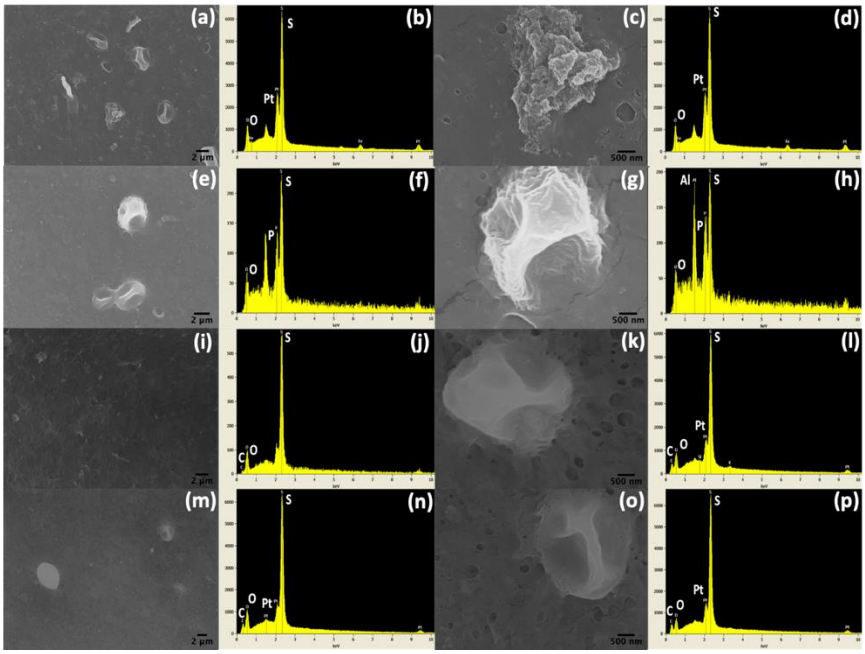

Figure S 3.6. For a natural groundwater treatment train consisted of coagulation, Grsand filtration, and membrane filtration (a-h); (a) SEM image of scaled NF membrane used to treat synthetic groundwater at 90% recovery; (b) EDAX results of the scaled NF membrane at 90% recovery; (c) SEM image of scaled NF membrane at higher magnitude; (d) EDAX results of scaled NF membrane at higher magnitude; (e) SEM image of scaled BWRO membrane used to treat synthetic groundwater at 90% recovery; (f) EDAX results of the scaled BWRO membrane at 90% recovery; (g) SEM image of scaled BWRO membrane at higher magnitude; (h) EDAX results of the scaled BWRO membrane at higher magnitude. For treatment train consisted of coagulation, AA filtration, and membrane filtration (i-q); (i) SEM image of scaled NF membrane used to treat synthetic groundwater at 90% recovery; (j) EDAX results of the scaled NF membrane at 90% recovery; (k) SEM image of scaled NF membrane at higher magnitude; (l) EDAX results of scaled NF membrane at higher magnitude; (m) SEM image of scaled BWRO membrane used to treat synthetic groundwater at 90% recovery; (n) EDAX results of the scaled BWRO membrane at 90% recovery; (o) SEM image of scaled BWRO membrane at higher magnitude; (p) EDAX results of the scaled BWRO membrane at higher magnitude.

3.7.6 Optimization of blending

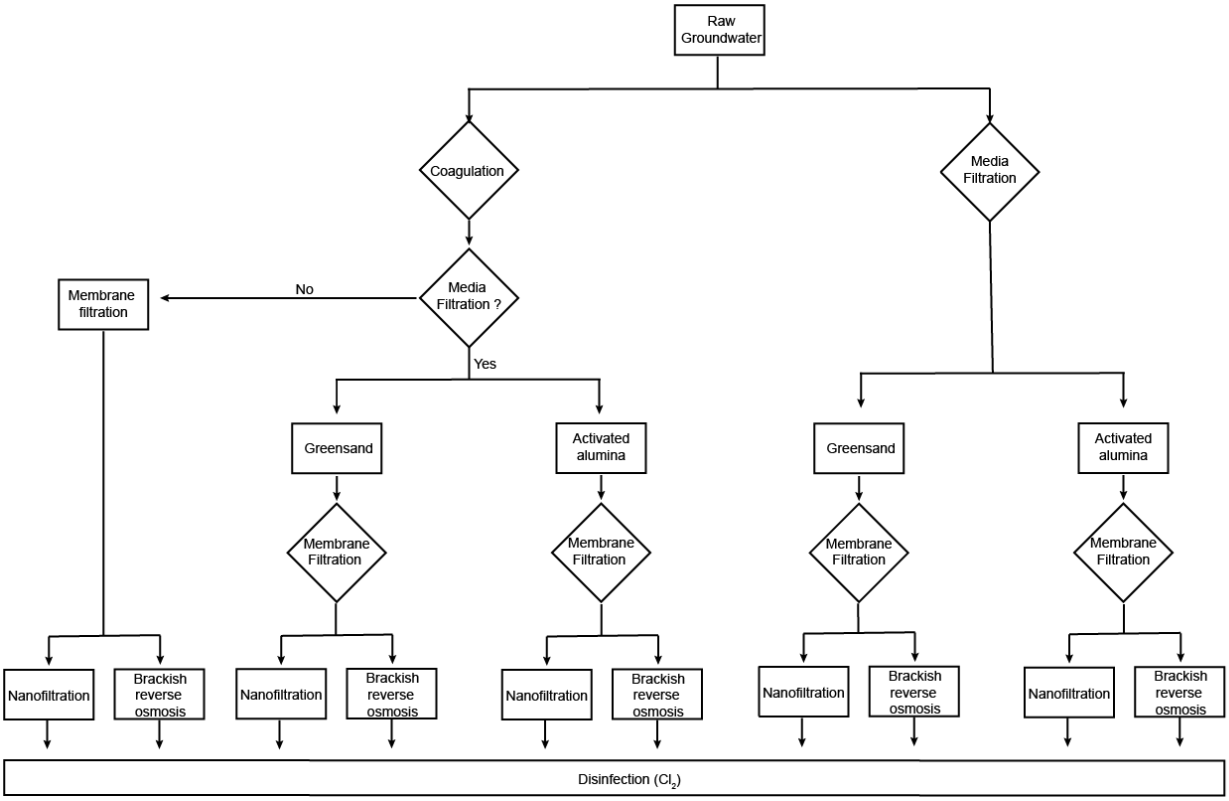

Figure S 3.7. All groundwater treatment train permutations conducted in this experiment.

Chapter 4.

Impact of Polarity Reversal Frequency on Inorganic Scaling on Carbon Nanotube-based Electrically-Conductive Nanofiltration Membranes

4.1 Summary

Inorganic salt precipitation (mineral scaling) on desalination membranes limits product water recovery, increases energy demand and pretreatment, requires harsh chemical cleaning and reduces membrane useful life. Conventional strategies employed to mitigate scale formation on membrane surface include chemical pretreatment (to remove scale forming minerals), lowering product water recovery and anti-scaling chemical addition. Anti-scaling chemicals either interfere with crystal nucleation or growth processes, and hence, increase product water recovery by preventing scale formation up to a certain level of supersaturation. While somewhat effective, anti-scaling chemicals are costly and can lead to membrane biofouling and surface water eutrophication. Lowering recovery leads to higher waste volumes and is highly undesired. Chemical pretreatment increases capital costs, plant footprint and process complexity. Therefore, a method that mitigates scale formation in an environmentally benign and affordable way is of great interest. In this study, we demonstrate how electrically conducting nanofiltration (ECNF) membranes inhibit mineral scaling during the treatment of both synthetic and natural groundwater. ECNF membranes are synthesized by cross-linking a percolating network of carbon nanotubes within a partially aromatic polyamide coating film. Without applying any potential, ECNF membranes exhibited significant flux decline, much of which was irreversible upon chemical cleaning with acid. Application of an alternating positive and negative potentials on the surface of the membrane eliminated irreversible membrane scaling, and allowed the membrane to operate at a water recovery where the concentrated feedwater was supersaturated.

4.2 Introduction

When salt concentrations in water exceed their solubility limit, mineral crystals (known as mineral scale) begin to precipitate. This precipitation is widely observed on many water handling systems such as desalination membranes, steam turbines, boilers, and heat exchangers.[226–228] Scale formation is problematic as it forms a barrier to energy (i.e., heat) and mass (i.e., water) transport, which increases operational costs, and can also damage equipment (e.g., needle-like $CaSO_4$ crystals can perforate the surface of desalination membranes, which damages their ability to reject salt). Scale formation is particularly challenging during membrane-based desalination processes.[229–231] In these processes, the passage of water through the membrane results in a layer of rejected ions at the membrane/water interface (known as the concentration polarization (CP) layer), where the concentration of retained ions is higher than the concentration in the bulk feed.[232] In the CP layer, the concentration of ions can rapidly exceed the solubility of certain sparingly soluble salts, which can lead to their precipitation and subsequent membrane scaling.[233] As a result, membrane performance is degraded (reduced flux and permeate quality), and depending on the scaling species, the membrane itself may be damaged.[234]

Many inland regions are increasingly reliant on desalinated brackish groundwater (BGW) for their potable water needs, with nanofiltration (NF) and/or reverse osmosis (RO) being the most widely employed desalination technologies. In these regions, achieving high water recovery is of particular importance as brine disposal constitutes a large portion of the treatment cost, accounting for as much as 25% of the total treatment cost.[235] In addition, inland brine disposal presents numerous ecological concerns, as brine disposal solutions (e.g., evaporation ponds) can damage the environment.[236] BGW contains elevated concentrations of dissolved divalent ions (calcium, magnesium, carbonates, and sulfate), as well as silicates.[237–239] During BGW desalination, these

ions accumulate in the CP layer where their concentrations exceed the solubility of $CaCO_3$, $CaSO_4$, and silica gels (SiO_2); importantly, the membrane/water interface facilitates heterogeneous nucleation of these solids, which is the reason for their rapid formation.[240–242]

Using $CaCO_3$ as a model scalant, it was demonstrated that the formation of mineral crystals is presaged by the appearance of pre-nucleation clusters (small and stable amorphous clusters of $CaCO_3$), which appear within seconds even under unsaturated conditions. [226,243] Cluster formation can be explained by the entropic solvent effect, where the release of water molecules from the solvated ions during cluster formation is the reason for the increased degrees of freedom in the system.[226,244] Following their formation, the clusters can aggregate and/or grow and lead to the formation of crystalline $CaCO_3$.[226] A similar mechanism has been attributed to the formation of hemihydrate $CaSO_4$.[245] When using polyamide-based NF/RO membranes, carboxylic groups in the polyamide layer can react with divalent metal cations (e.g., Ca^{2+}) and form complexes over the membrane surface. These specific interactions result in increased Ca^{2+} concentrations that initiate pre-nucleation and subsequent amorphous nanostructure formation over the surface.[246] Later, these amorphous nanostructures serve as a template and grow by adding additional ions from the solution to form the crystalline structure over the membrane surface.[246]

Several approaches are used to prevent mineral scaling at the industrial scale: i) Feed stream acidification, which is effective at minimizing $CaCO_3$ formation, but is not effective at preventing sulfate scaling (e.g., $CaSO_4$), whose formation is not sensitive to pH;[226,247] in addition, low pH can worsen SiO_2 scaling, due to increased polymerization rates (the dehydration of non-ionic SiO_2 i.e. monosilicic acid ($pH \leq 7$) may result in polysilicic acid formation *via* silica-oxygen bonding).[248] ii) The addition of anti-scalant chemicals (often phosphate-based) to the feed stream that chelate scaling ions and/or absorb onto the growing crystal surface which blocks growth sites.[235] However,

anti-scalants have several shortcomings, including their high cost (~10% of the total treatment), potential to promote biofouling, and eutrophication of water bodies receiving the spent brine.[249–251] iii) Limiting water recovery during desalination can keep the feed stream below supersaturation and prevent scaling. However, this decreases the volume of desalinated water, increases the volume of brine requiring disposal, and can dramatically increase the cost of desalination.[252–254] iv) feed stream softening using ion exchange or lime softening, which can be effective at controlling scaling, but incurs a heavy price tag.[255,256] Another approach involves the periodic reversal of flow through the system, which can dissolve crystals that form on a membrane surface.[257–259] More experimental approaches towards scaling control include the minimization of ionic pairing and nucleation by inducing ion migration, sequestration nuclei, and limiting pairing by creating a stoichiometric ion imbalance in the feed. [105,142]

Electrically conducting membranes, which enable the application of electrical potentials with varying magnitude and frequency to the membrane surface, have shown excellent anti-fouling performance.[260–265] The transport properties of carbon nanotube (CNT)-based membranes can be readily tuned through the cross-linking of the CNTs with different polymers, where the choice of polymer controls the pore size, rejection properties, surface roughness, and hydrophobicity of the composite material.[266,267] Critically, by cross-linking the CNTs with polyamide, the composite takes on the transport properties of nanofiltration or reverse osmosis membranes (the two most common desalination membranes).[142,268] In a previous study, we reported that the application of DC conditions to the surface of a conducting RO membrane slowed down, but did not eliminate, the formation of $CaSO_4$ scale.[142] It was speculated that the constant anodic conditions at the membrane surface repelled Ca^{2+} ions, creating a zone along the membrane where the concentrations of anions and cations were not at the optimal stoichiometric ratio for nucleation

and crystal growth. A more recent study demonstrated that AC conditions applied to the surface of an electrically conducting membrane distillation material prevented the formation of $CaSO_4$ and silicate scale.[105] Here, it was speculated that the periodic motion of ions in response to the applied potential (i.e., electrophoretic mixing) led to efficient mixing that minimized the co-location of the ions and prevented the formation of the pre-nucleation clusters. However, the application of electrically conducting membranes for the purpose of scale mitigation has been limited to synthetic solutions with simple water chemistry. Unlike synthetic solutions, natural water has the potential for the simultaneous formation of multiple scale species (e.g., $CaCO_3$, $CaSO_4$, $BaSO_4$, silicates, etc.) during membrane filtration processes.[254,269,270] In addition, the performance of electrically conducting membranes at high water recovery has not yet been explored. Operating electrically conducting membranes at high water recoveries leads to highly challenging conditions (i.e., high saturation of sparingly soluble salts) at the membrane/water interface, which needs to be evaluated for potential applications of the process. In this study, we fabricate and characterize CNT-based electrically conducting nanofiltration (ECNF) membranes, and use them to treat both synthetic and real BGW. We show that the application of AC conditions to the membrane surface successfully controlled the formation of mineral crystals and membrane fouling. In addition, we show that the technique can be applied to other conducting surfaces: by immersing two titanium plates into a super-saturated $CaSO_4$ solution and applying AC conditions to the plates we show that homogeneous nucleation can be dramatically slowed.

4.3 Material and Methods

4.3.1 Feed solutions

Ion composition of model gypsum scaling solution, no-scaling solution, and natural groundwater is listed in Table 1.

Table 4.1 Concentrations of ions in gypsum scale, no-scaling solutions, and natural groundwater.

Constituent	Concentration (mM)		
	Synthetic BGW	**No-scaling solution**	**Natural BGW**
Na	21.00	21	3.13
Ca	16.40	0	1.60
Mg	14.50	30.91	2.29
Cl	32.81	65.61	3.63
SO_4	25.01	25.01	3.25
HCO_3	0	0	2.13
Si	0	0	0.32
pH	5.61	5.82	8.47
Conductivity (mS/cm)	6.3613	6.3113	1.2023
Total dissolved solids (mg/L)	5,058	4,799	1,024

Calcium chloride ($CaCl_2 \cdot H_2O$), magnesium sulphate ($MgSO_4 \cdot 6H_2O$), sodium chloride (NaCl), were purchased from Fisher scientific, and used as received. All synthetic solutions were prepared with DIW. Natural groundwater sample was provided by Santa Monica Water Treatment Plant (Santa Monica, CA) and pretreated with a filter cartridge to remove suspended solids.

The extent of scale tendency of solutions was quantified in terms of SI_g, defined as:

$$SI_g = \frac{(\alpha_a)(C_a) \times (\alpha_b)(C_b)}{K_{SP}}$$

where α is activity of scalant, C is molar concentration of scalant, and K_{SP} is solubility product. Model gypsum scale solution has a SI_g of 0.96 in terms of gypsum, while natural groundwater has SI_g of 1.94 in terms of $CaCO_3$, and SI_g of 0.05 in terms of gypsum. The SI_g was calculated using OLI software.

4.3.2 ECNF fabrication

Procedures to fabricate ECNF membranes followed previously reported method except piperazine (PIP, Alfa Aesar) was used to cast polyamide instead of m-phenylenediamine.[142] In brief, carboxyl-functionalized carbon nanotubes (CNT, Cheaptubes Inc.) suspension solution was prepared by sonicating a mixture of CNT and surfactant (sodium dedocylbenzensulfonate, Sigma Aldrich). Afterwards, certain volume of the suspension solution was pressure-deposited on PSf membrane support (PS35, Solatec). Then, the fabricated CNT-membrane was immersed in a 2 wt% PIP aqueous solution for one hour. Plastic roller was used to remove excessive amount of PIP on the membrane surface, followed by soaking the membrane in 0.15 wt% 1,3,5-benzenetricarboxylic acid chloride (TMC, Sigma-Aldrich) in hexane (Fisher Scientific) for 2 minutes. Finally, the membrane was cured at 80 ℃ for 5 minutes.

4.3.3 System design and operation

Schematic diagram of membrane filtration system can be found in our previous study.[271]

A membrane coupon (effective area of 0.004 m^2) was placed into a custom-built crossflow membrane cell and conditioned with DIW overnight until stable permeate flux is obtained. Pure water permeate flux of membranes was measured at the end of conditioning. Then, feed solution was fed into the feed tank, and pressure in the system was adjusted to achieve initial permeate flux of 40 LMH for gypsum scale solution and no-scaling solution, and 50 LMH for natural groundwater. Then, constant pressure was applied over the course of experiment. Higher initial flux for natural groundwater was applied to facilitate concentration polarization, which enhances the nucleation of scale on membrane surface. The filtration system was operated at cross flow velocity of 4.66 cm/s (corresponding to Reynolds number of 158) and operated in concentration mode where permeate stream is constantly disposed while brine stream is recycled until water recovery reaches at a desired point. For testing gypsum scale solution, a filter cartridge (0.45 μm) was placed in brine stream to avoid bulk crystallization of gypsum in the feed tank. For testing natural groundwater, 1 μm filter cartridge was employed to minimize the hold-up volume of cartridge to achieve a high recovery (i.e., 85%) with a given feed volume (3L). Samples from feed and permeate were periodically collected to monitor observed salt rejection, defined as $R_{obs} = (1 - \gamma_p/\gamma_f)$, where γ_p and γ_f are conductivity in permeate and feed, respectively.

Once water recovery reached to the target recovery (55% for synthetic solution and 85% for natural water), membrane cleaning practice was conducted to test reversibility of membrane performance (i.e., water flux and salt rejection) using deionized water (DIW) for synthetic solution, and hydrochloric acid (HCl, Fisher Scientific) for natural groundwater. Scaled membrane with synthetic solution was rinsed by DIW for 30 minutes, and membrane scaled with natural groundwater was soaked in a HCl solution (pH 2) for 1 hour. Then, a new solution was fed as a feed to test reversibility of membrane performance.

4.3.4 Water quality analysis

Water quality (pH, conductivity, anion and cation concentrations) of feed and permeate samples was monitored to compare the performance of ECNF membranes over the course of experiment.

pH and conductivity of samples were immediately measured after the sample collection using portable pH (Thermo Scientific, Orion 720A) and conductivity meter (Orion A321). Turbidity was measured using a turbidity meter (Hach, 2100P).

Anion (Cl^- and SO_4^{2-}) concentrations were measured by ion-chromatography (IC, Thermo Fisher, Dionex Integrion HPIC). Cation (Na^+, Ca^{2+}, and Mg^{2+}) and silicon concentration were measured by induced-couple plasma (ICP-OES, Shimadzu, ICPE9000). Inorganic carbon concentration was measured using a total organic carbon (TOC) analyzer (Shimadzu, TOC-L) by measuring inorganic carbon content.

4.3.5 Characterization of membrane surface

The surface of bare and scaled membrane was characterized using field-emission scanning electron microscopy (FESEM, Zeiss, Supra 40VP) equipped with energy-dispersive X-ray spectroscopy. EDAX provides an information about atomic composition of the surface being taken. Contact angle measurement was conducted using a contact angle goniometer (Rame-hart, model 250) to compare the degree of hydrophobicity/hydrophilicity of the membrane surface in different fabrication steps. DIW was used for contact angle measurement, and at least 10 different area of each membrane piece were taken. The sheet resistance of fabricated ECNF membrane was

measured using 4-poing probe (Mitsubishi, MCP-T610). At least, 5 different points of the membrane surface were measured.

4.4 Results and Discussion

4.4.1 Characterization of ECNF membranes

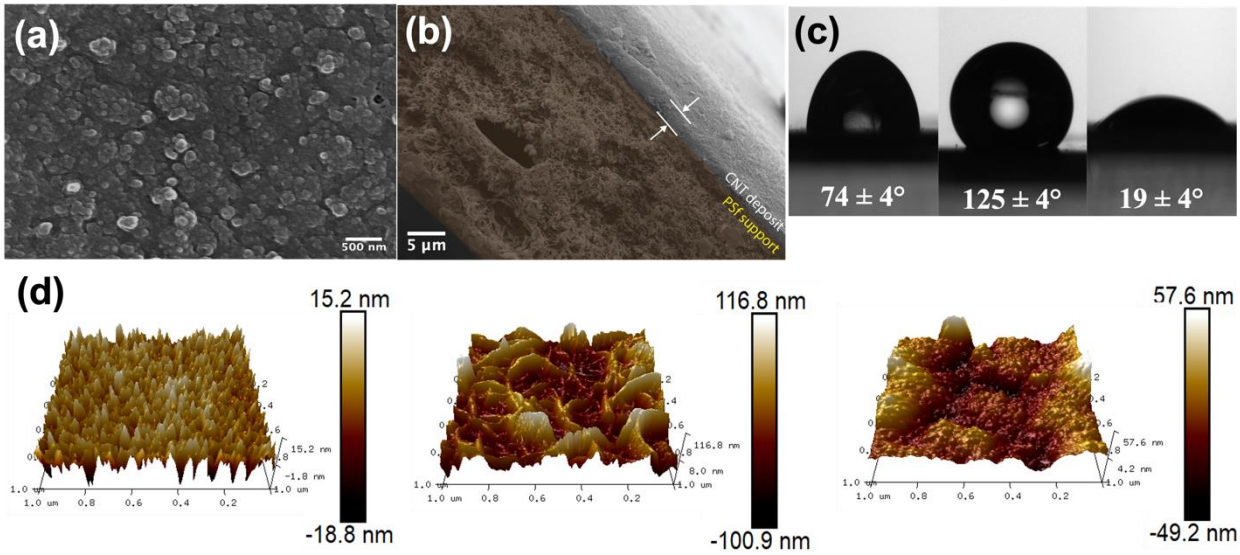

Figure 4.1. Characterization of ECNF membranes. (a) top-view FESEM image of nodular structure of ECNF membrane. (b) Cross-sectional SEM image of ECNF membrane having 2 thick CNT-layer on top of PSf support. (c) Contact angle measurement of PSf support (left), CNT-deposited PSf support (middle), and ECNF (right). (d) AFM images (scan area of 2 µm by 2 µm) of PSf support (left), CNT-deposited PSf support (middle), and ECNF (right).

ECNF membranes were fabricated by pressure-depositing a CNT suspension onto a porous polysulfone (PSf) support, followed by cross-linking the CNTs using a piperazine-based polyamide. Field emission scanning electron microscope (FESEM) imaging of the surface of the ECNF show a nodular surface morphology, which is typical of piperazine-based polyamide materials used in NF membranes; cross-sectional analysis of the ECNF material shows that the thickness of the CNT layer deposited on the PSf support was approximately 2 µm (Figure 1a and

b).[272–274] While the contact angle of the PSf support was 74 ± 4°, the addition of the CNT coating increased the contact angle to 125 ± 4°; when the polyamide layer was used to cross-link the CNTs, the resulting contact angle of the final composite was a very hydrophilic 19 ± 4° (Figure 1c). AFM measurements show that the PSf support has a surface root mean square (RMS) roughness of 4.59 nm, while the CNT-deposited PSf support and ECNF have a surface RMS roughness of 30.8 nm and 14.4 nm, respectively. The sheet resistance of the ECNF membrane was 135.57 ± 11.52 Ω/sq, which translates into an electrical conductivity of 3707 ± 284 S/m. The ECNF membranes were evaluated for their ability to reject NaCl and $MgSO_4$ solutions, with salt rejection values of 58.51 ± 4.65% and 93.75 ± 1.00%, respectively.

4.4.2 Performance of ECNF treating synthetic solutions

Figure 2 shows the water permeation flux and salt rejection of the ECNF membrane over the course of the experiment with a synthetic BGW solution (super-saturated with respect to $CaSO_4$) and a no-scaling solution, where Ca was replaced with an equimolar amount of Mg ($MgSO_4$ is highly soluble, and does not precipitate under the conditions tested). The no-scaling solution was used to separate the impact of increasing osmotic pressure from that of membrane scaling when considering the flux decline experienced by the system over time. Under all experimental conditions, permeate flux decreased as water recovery increased due to the increase in osmotic pressure. At 55% water recovery, the flux of the no-scaling solution reached to 19.23 ± 1.46 LMH from 29.83 ± 0.15 LMH (i.e., a 36% decline), while the flux of the synthetic BGW without applied potential reached to 15.08 ± 1.97 LMH from 29.83 ± 0.27 LMH (i.e., a 49% decline) at the same recovery (Figure 2a). The higher flux decline suggests that $CaSO_4$ crystals did indeed form on the membrane, which obstructed the flow of water.[275,276] When 4 V_{pp}, 1 Hz conditions were applied

to the membrane surface, the ECNF exhibited 17.16 ± 1.77 LMH at 55% recovery (a 42% decline) (Figure 2a). The higher water flux measured at 55% recovery under the 4 V_{pp}, 1 Hz conditions suggest less $CaSO_4$ crystal formation on the membrane surface, resulting in a reduced flux decline.

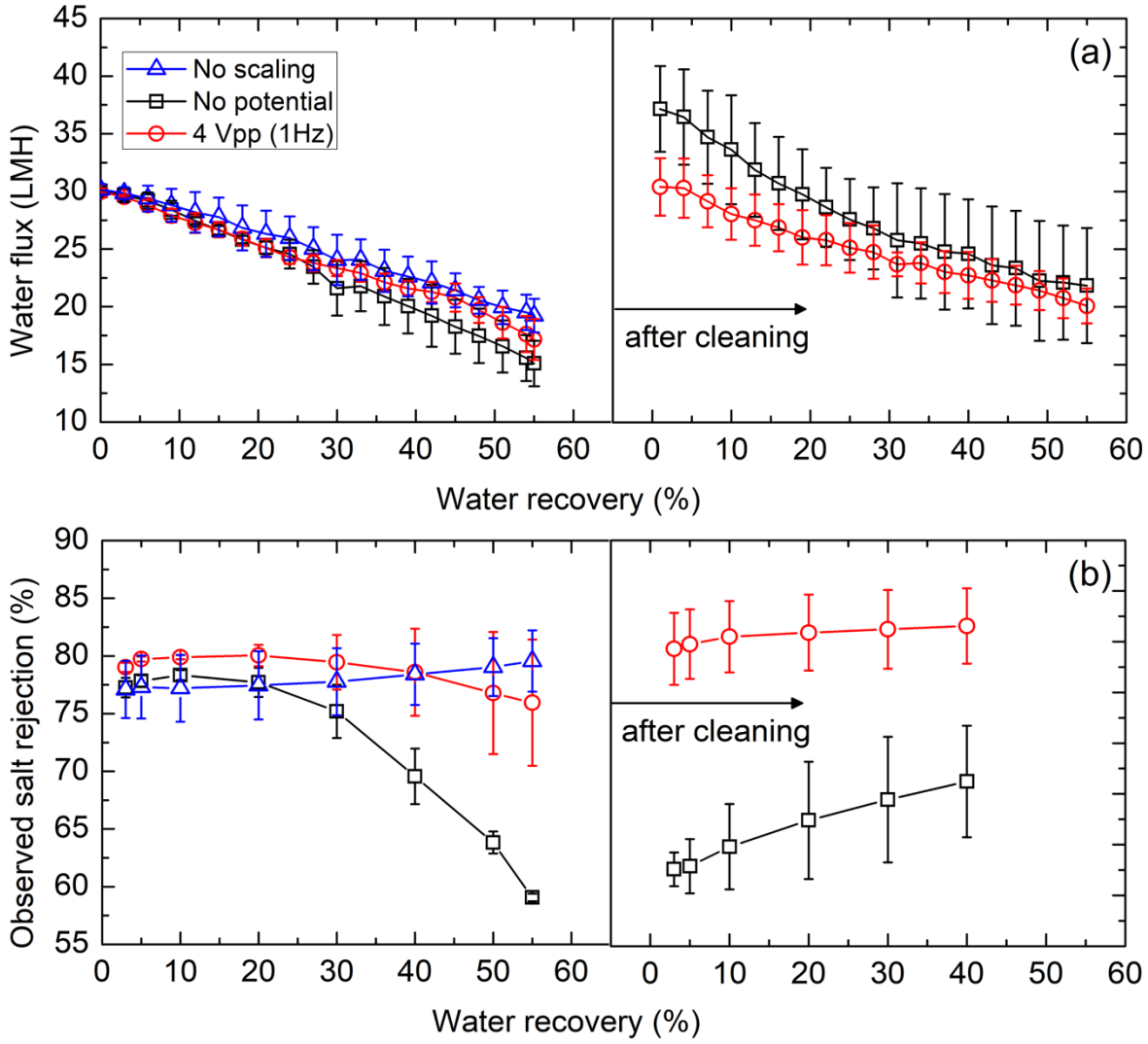

Figure 4.2. Performance of ECNF treating synthetic BGW: (a) water flux of ECNF membranes over water recovery under no potential, 4 V_{pp}, and no-scaling (with no potential) condition. (b) observed salt rejection of ECNF over water recovery under no potential, 4 V_{pp}, and no-scaling (with no potential) condition. Each figure shares the legend – no potential (black square), 4 V_{pp} (red circle), and no-scaling (blue triangle).

The characteristic morphology of $CaSO_4$ crystals (long and needle-like) can result in damage to the membrane surface.[277,278] This damage is manifested as an observed decline in salt rejection. When the no-scaling solution was used, the observed salt rejection increased with water recovery (the salt rejection increased to 79.56 ± 2.65% from 77.10 ± 2.48% at 55% water recovery) (Figure 2b). The increase in salt rejection with increasing recovery can be attributed to changes in the ion composition of the feed solution as it is concentrated throughout the experiment. Since the ECNF membranes have a lower rejection (~58%) of monovalent ions compared to the rejection of divalent ions (~93%), and because the membrane permeate was not returned back to the feed, the molar ratio of monovalent ions to divalent ions in the feed solution decreased with increasing water recovery. At 3% recovery, the molar ratio of monovalent to divalent ions in the feed was 1.00, while the ratio was 0.74 at 55% recovery. As this ratio decreases, the membrane appears to have higher rejection; a similar observation has been previously reported.[279] When no potential was applied, the observed salt rejection increased until ~10% recovery, but decreased afterwards. At 55% recovery, the rejection reached 59.07 ± 0.32% (76% of its initial value), implying that the membrane was damaged. However, when AC conditions were applied, salt rejection increased until 20% recovery, with the final rejection reached at 55% being 75.94 ± 5.47% (96% of its initial rejection) - not statistically different from the no-scaling solution case. This further suggests that scale formation was suppressed in the presence of the applied electrical conditions.

In addition to the measured salt rejection (determined by measuring the difference in conductivity between the feed and permeate), the rejection of specific cations and anions by the ECNF under all experimental conditions was monitored (Figure S1 and S2). When treating the no-scaling solution, rejection of both of cations (i.e., Mg^{2+}) and anions (i.e., Cl^- and SO_4^{2-}) increased with increasing water recovery, while the rejection of Na^+ fluctuated. When treating the synthetic

BGW with no potentials applied, a significant drop in cation (i.e., Ca^{2+}, Mg^{2+}, and Na^{+}) and anion (i.e., SO_4^{2-}, and Cl^{-}) rejection was observed, while the drop in rejection was less significant when potentials were applied. Specifically, in the absence of applied potential, the respective rejection of Ca^{2+}, Mg^{2+}, Na^{+}, SO_4^{2-}, and Cl^{-} decreased to 80.41 ± 5.62%, 69.78 ± 3.66%, 52.53 ± 8.87%, 79.76 ± 1.85%, and 50.39 ± 2.38% (83%, 73%, 82%, 83%, and 70% of their initial rejections, respectively), at 55% water recovery. In contrast, when AC conditions were applied, the respective rejection of Ca^{2+}, Mg^{2+}, Na^{+}, SO_4^{2-}, and Cl^{-} were 95.29 ± 3.40%, 93.09 + 4.70%, 66.14 + 5.38%, 94.46 ± 4.62%, and 69.92 ± 8.41% (97%, 95%, 95%, 97%, and 97% of their initial rejection, respectively), at 55% water recovery.

Once water recovery reached 55%, the experiment was stopped, and the membrane surface was rinsed, without removing the membrane from the module, for 15 minutes with deionized water (DIW). Following the DIW rinse, a fresh solution was introduced, and the experiment repeated (Figure 2). Since $CaSO_4$ scale is known to be pH-insensitive, the DIW rinse was expected to dislodge loosely-attached particles and remove the CP layer, but not significantly dissolve any scale that grew as a result of heterogenous nucleation and crystal growth.[280,281] After the rinse, the ECNF tested with fresh synthetic BGW under the applied AC conditions completely recovered its water flux of 30.4 ± 2.49 LMH (102% of initial flux), while the flux of the ECNF tested with fresh synthetic BGW in the absence of the applied potential was 37.16 ± 3.72 LMH (124% of its initial value) (Figure 2a). This increased flux corresponds with the significant drop in salt rejection, indicating that the membrane was damaged from the deposited $CaSO_4$ scale. In contrast, when the AC conditions were applied, only a modest drop was observed: the rinsed ECNF maintained 68.58 ± 7.08% (87% of its initial rejection), and the rejection reached 73.09 ± 7.42% (92% of initial rejection) at 40% recovery with new feed solution. Similarly, in the absence of the applied potential,

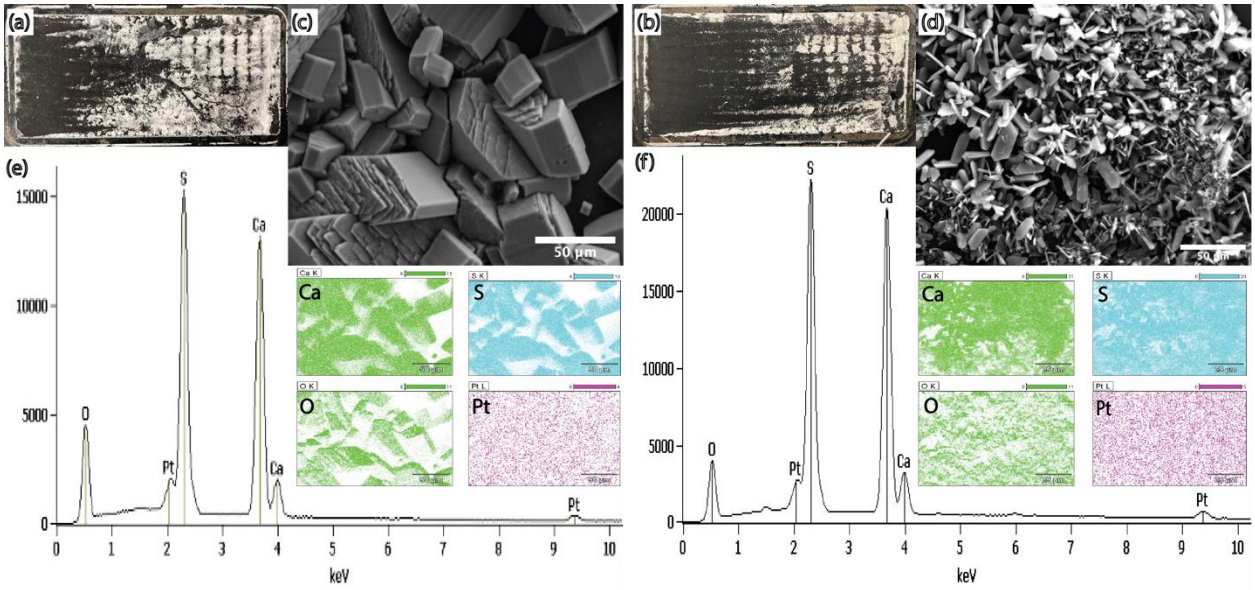

Figure 4.3. Surface characterization of scaled membrane that treated synthetic BGW: (a) image of scaled membrane after two rounds of treatment under the no potential condition; (b) image of scaled membrane after two rounds of treatment under 4 V_{pp} conditions (c) FESEM image of scaled membrane under no potential conditions (d) FESEM image of scaled membrane under 4 V_{pp} conditions (e) EDAX spectrum of membrane under no potential condition (f) EDAX spectrum of membrane under 4 V_{pp} condition.

significant rejection drop of cations and anions was observed when testing the new feed solution, while the drop in rejection was less pronounced when potentials were applied (Figure S1 and S2). In the absence of the applied potentials, the respective rejection of Ca^{2+}, Mg^{2+}, Na^{+}, SO_4^{2-}, and Cl^{-} decreased to 44.02 ± 3.74%, 32.20 ± 3.55%, 45.37 ± 2.39%, 40.36 ± 4.02%, and 21.25 ± 5.39% (47%, 33%, 71%, 42%, and 30% of their initial rejections, respectively, in the first run of the experiment). However, when AC conditions were applied, the rejection of Ca^{2+}, Mg^{2+}, Na^{+}, SO_4^{2-}, and Cl^{-} was 86.13 ± 9.42%, 85.01 ± 9.76%, 67.10 ± 3.11%, 88.78 ± 10.60%, and 57.17 ± 9.05% (88%, 87 %, 97 %, 91%, and 79% of their initial rejection in the first run of the experiment, respectively). The difference in the salt rejection drop after cleaning further strengthens our

speculation that membranes without potentials suffered from more severe gypsum scale formation, which damaged the surface.

The surface of the ECNF membranes after two rounds of treatment were imaged using a digital camera, FESEM, and energy-dispersive X-ray spectroscopy (EDAX). Membrane images clearly show that less scale was formed on the membrane when AC conditions were applied, compared to the no potential condition. (Figure 3a and b). FESEM images of the $CaSO_4$ scale did not show the distinct rosette structure typically associated with heterogeneous gypsum crystals (Figure 3c and d).[282,283] At low water recovery, the estimated gypsum saturation index (SI_g) in the bulk feed was 0.96, such that no bulk precipitation is expected to occur (precipitation occurs when SI_g>1). However, the SI_g of gypsum near the membrane surface (in the CP layer) was estimated to be 2.42, and heterogeneous nucleation near the membrane is expected; detailed calculations used to obtain the SI_g near the membrane surface can be found in the Supporting Information. At high water recovery (55%), gypsum's SI_g in the bulk feed and near membrane surface increased to 2.00 and 3.04. Therefore, at high water recovery, both homogeneous and heterogeneous nucleation likely contribute to gypsum crystal formation, possibly leading to the observed crystal structures – a result of homogeneously-formed gypsum crystals depositing on the membrane surface. $CaSO_4$ scale formation was confirmed using EDAX analysis, which showed that the dominant atomic species on the scaled membrane surface were Ca, S, and O (Figure 3e and f).

4.4.3 Performance of ECNF treating natural groundwater

The same experimental approach was applied towards the treatment of natural BGW extracted from an aquifer in Santa Monica, CA, with the % recovery extended to 85% to simulate a desirable

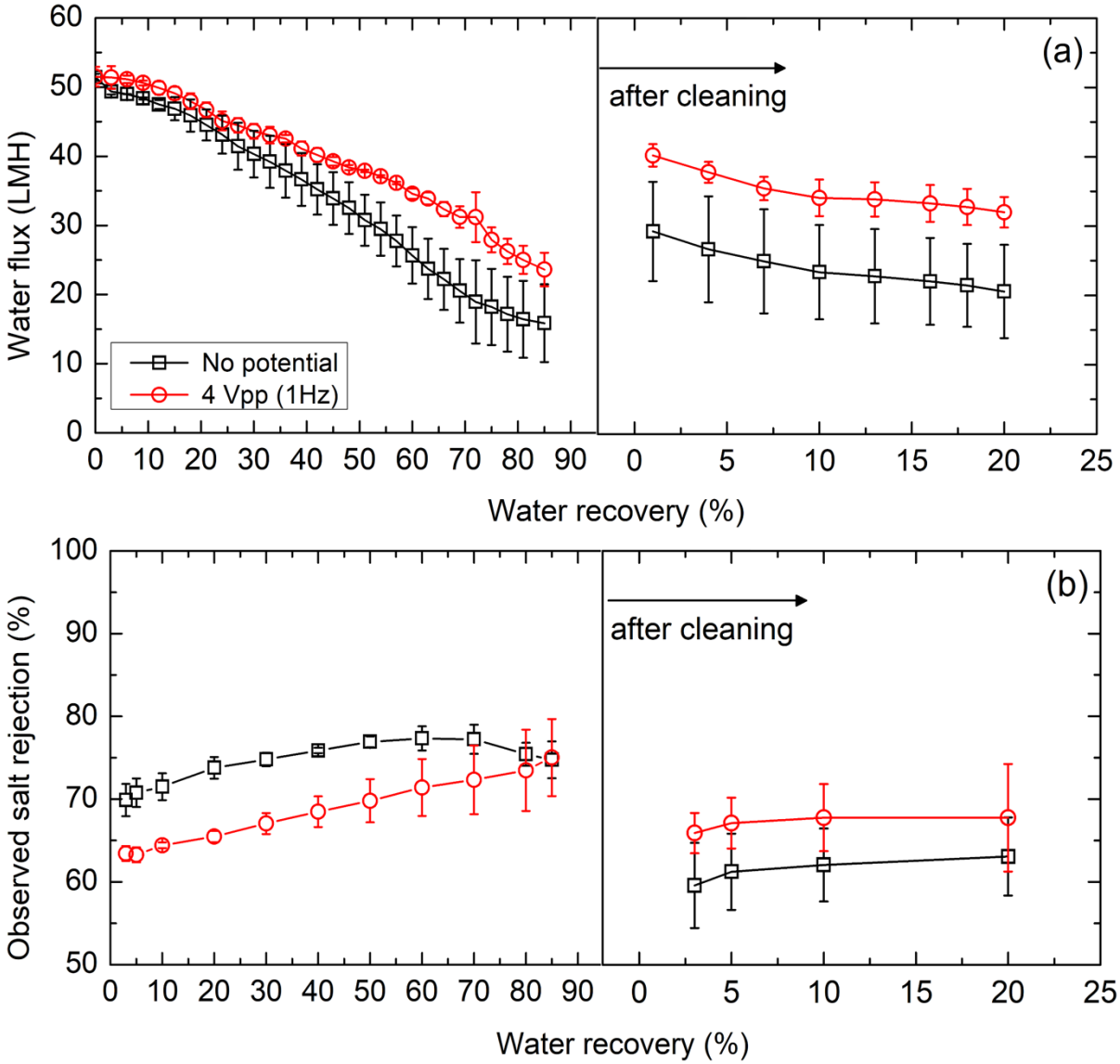

Figure 4.4. Performance of ECNF treating natural BGW: (a) water flux of ECNF membranes over water recovery under no potential. and 4 V_{pp}. (b) observed salt rejection of ECNF over water recovery under no potential, and 4 V_{pp} condition. Each figure shares the legend – no potential (black square), and 4 V_{pp} (red circle).

treatment outcome that minimizes the volume of brine; the ionic composition of this BGW can be

seen in Table 1. Changes in the water flux and salt rejection with and without the applied electrical

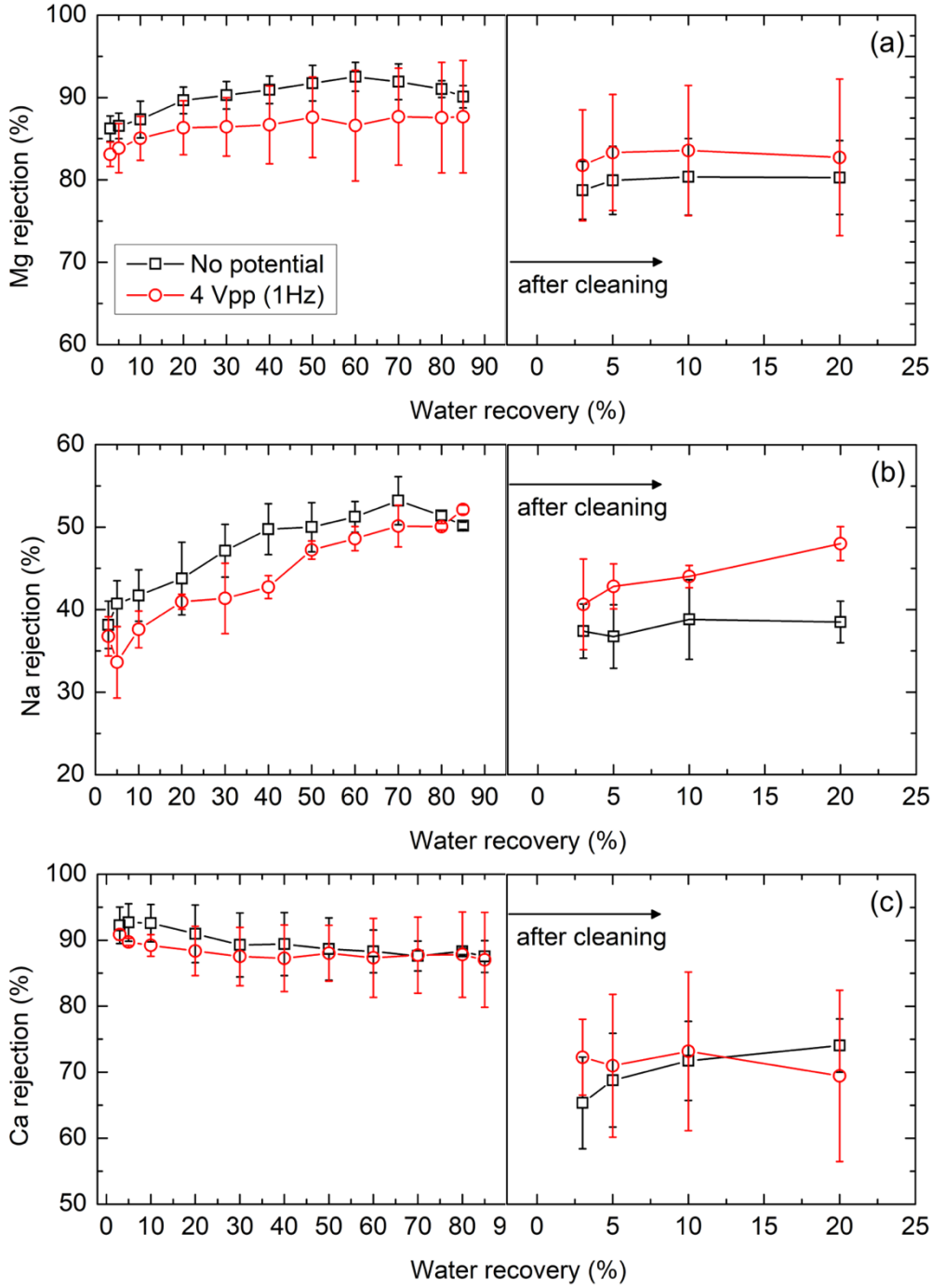

Figure 4.5. Cation rejections of ECNT treating natural BGW over water recovery under no potential and 4 V_{pp}, 1 Hz conditions: (a) Mg^{2+} rejection. (b) Na^{+} rejection. (c) Ca^{2+} rejection. Each figure shares the legend – no potential (black square), and 4 V_{pp} (red circle).

conditions can be seen in Fig. 4a and b. Similarly to the results generated with synthetic BGW,

water flux decreased with increasing water recovery under all experimental conditions. The flux of ECNF without potentials

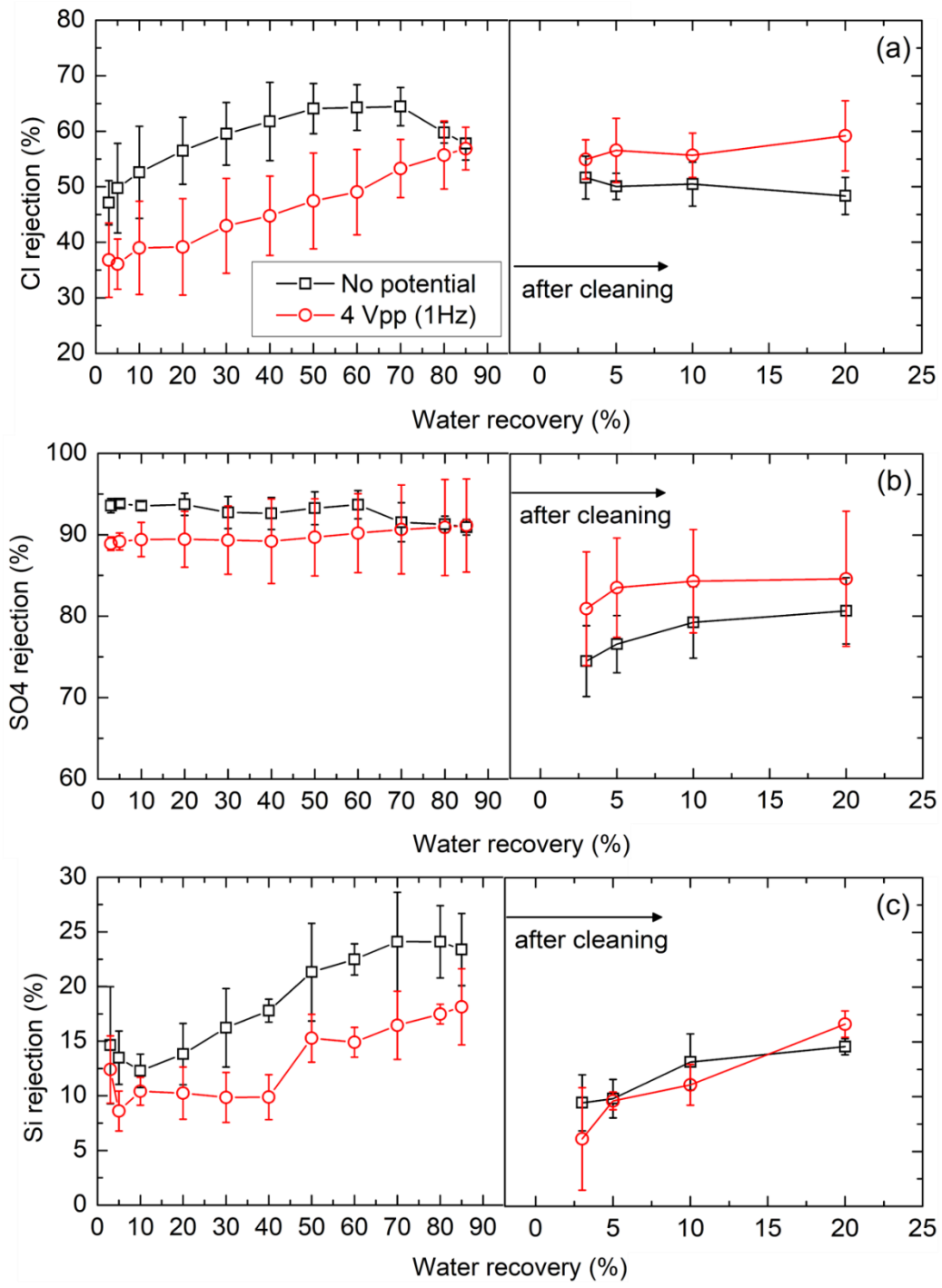

Figure 4.6. Anion rejections of ECNT treating natural BGW over water recovery under no potential and 4 V_{pp}, 1 Hz conditions: (a) Cl^- rejection. (b) SO_4^{2-} rejection. (c) Si rejection. Each figure shares the legend – no potential (black square), and 4 V_{pp} (red circle).

decreased to 15.86 ± 5.62 LMH from 50.80 ± 0.72 LH (69% decline) at 85% recovery, while the flux of ECNF with the applied potential only decreased to 23.62 ± 2.44 LMH from 51.51 ± 1.54 LMH (54% decline) at the same recovery (Figure 4a). For salt rejection, when AC conditions were applied, the ECNF exhibited increasing salt rejection over the course of the experiment, with salt rejection increasing from 63.42 ± 0.90% to 75.02 ± 4.65% (18% increase) at 85% recovery. However, in the absence of applied potential, the ECNF exhibited an increasing salt rejection only up to 70% recovery (from 69.01 ± 1.73% to 78.11 ± 1.28%), at which point the rejection declined (to 74.74 ± 3.15% at 85%) (Figure 4b). While not statistically significant, the trend suggests that the membrane may have been damaged as a result of crystal growth. Furthermore, the larger flux decline observed in the absence of AC conditions further strengthens the case that AC conditions, when applied to the surface of ECNF membranes, minimize the formation of scale, even with the complex chemistry of natural BGW.

The rejection of cations (Ca^{2+}, Mg^{2+}, and Na^{+}) and anions (SO_4^{2-}, Cl^{-}, and Si) by the ECNF was monitored throughout the experiments (Figure 5 and 6). In the absence of applied potentials, a notable decrease in Na^{+} and Mg^{2+} rejection was observed when recovery reached ~70 % (Figure 5a and b). In contrast, under the applied AC conditions, no drop in rejection was observed throughout the experiment. For anions, in the absence of the applied potentials, a decrease in Cl^{-} and SO_4^{2-} rejection at high recovery, and no change in Si rejection was observed (Figure 6a – c). When AC conditions were applied, Cl^{-} and SO_4^{2-} rejection increased with increasing water recovery. However, Si rejection decreased at low water recovery, and began to increase at 50% recovery; although the reason is unclear, Si is expected to be uncharged (i.e., $Si(OH)_4$) in the pH range of groundwater (8 – 8.5), which should minimize the impact of the applied potential.

Once 85% recovery was achieved, the membranes were soaked in an HCl solution (pH 2) for 1 hour, and the performance of the cleaned membrane was tested with fresh feed. After the cleaning, the ECNF membranes without the applied AC conditions recovered to 29.23 ± 7.17 LMH (57% of their initial flux) while ECNF membrane with the applied AC conditions recovered to 40.20 ± 1.62 LMH (79% of their initial flux) (Figure 4a). Unlike in the synthetic BGW case, cleaning (i.e., acid soaking) was less effective in restoring flux, which is likely due to the different composition of the scale. Natural BGW not only has a potential for gypsum scale formation, but also has a potential of calcium carbonate and silicate scale. In the bulk feed solution at 85% recovery, natural BGW had SI_g values of 4.59, 0.17, and 0.24 in terms of $CaCO_3$, $CaSO_4{\cdot}2H_2O$, and SiO_2, respectively, while the respective SI_g values of $CaCO_3$, $CaSO_4{\cdot}2H_2O$, and SiO_2 in the CP layer were estimated to be 8.11, 0.34, and 0.41. Although SI_g values for $CaSO_4{\cdot}2H_2O$ and SiO_2 were both <1, indicating no scale formation should occur at these conditions, EDAX data shows both S and Si peaks, indicating possible crystal formation from these species (Figure 7). For complex scale, a combination of cleaning steps (e.g., acid cleaning followed by base cleaning) is typically employed in groundwater treatment plants. [284,285] Interestingly, the ECNF membrane without the applied AC conditions experienced a significant drop (i.e., 15% decrease) in salt rejection after the cleaning. In contrast, the ECNF membranes with the applied AC conditions fully recovered their salt rejection (104% of their initial value). In line with the overall decrease in salt rejection, a significant decrease in divalent ion (Mg^{2+}, Ca^{2+}, and SO_4^{2-}) rejection after the cleaning was observed in the absence of the AC potentials; monovalent ion rejections (Na^+ and Cl^-) remained relatively unchanged (Figure 5 and 6). Similarly, in the presence of AC potentials, a significant decrease in Ca^{2+} and SO_4^{2-} rejection was observed after the cleaning step. However, no significant decrease in Mg^{2+} rejection was observed, and monovalent ion rejection was higher than the initial

rejection values measured in the 1st round of the experiment (Figure 5 and 6). Thus, it is suspected that the cleaning step (i.e., soaking in a HCl solution (pH 2)) altered the properties of the polyamide salt rejecting layer. To investigate this hypothesis, the performance (i.e., salt rejection and water flux) of a fresh ECNF membrane before and after the acid soaking was compared using a synthetic groundwater solution that had a similar composition to the natural BGW (Table S1). Condition of the cleaning practice (i.e., cleaning duration, procedures, and concentration of the cleaning agent) were identical to those used during the natural BGW treatment. Acid soaking did not significantly change the water flux and salt rejection, increasing slightly from 28.25 ± 0.06 LMH to 30.43 ± 1.76 LMH and from 55.29 ± 5.61% to 60.72 ± 5.08%, respectively (not a statistically significant increase) (Figure S3). Ca^{2+} rejection did not change significantly, either (from 90.13 ± 6.31 to 89.06 ± 7.42%), while the rejection of other ions (Mg^{2+}, SO_4^{2-}, Na^+, and Cl^-) were enhanced by the acid soaking, but the increase was not statistically significant (Figure S3). Although it was previously reported that acid soaking can result in enhanced water flux with a lower salt rejection due to polyamide hydrolysis, we did not observe a dramatic change in salt rejection after soaking the membrane in acid. [286–289] Therefore, we speculate that the decrease in Ca^{2+} rejection observed after the acid cleaning is a result of the elevated Ca concentrations at the membrane/water interface, which were potentially caused by dissolution of Ca-dominant minerals that accumulated on the membrane (Figure 4a).

Once 20% water recovery was achieved in the second round of treatment, the surface of ECNF membranes was analyzed using FESEM and EDAX. In general, less scale was observed on the surface of ECNF membrane when AC conditions were applied (Figure 7). Specifically, scale was formed throughout the membrane surface when no potentials were applied (Figure 7a), while under the AC conditions the membrane was scale-free in the entrance region (left side of membrane in

Figure 7b), with some scale visible at the exit region. FESEM images showed a non-specific crystal structure, likely due to its mixed nature (i.e., $CaSO_4$, $CaCO_3$, silicate, etc.) (Figure 7c and d). EDAX results showed that the dominant atoms in the scale were Ca, S, and O (Figure 7e and f).

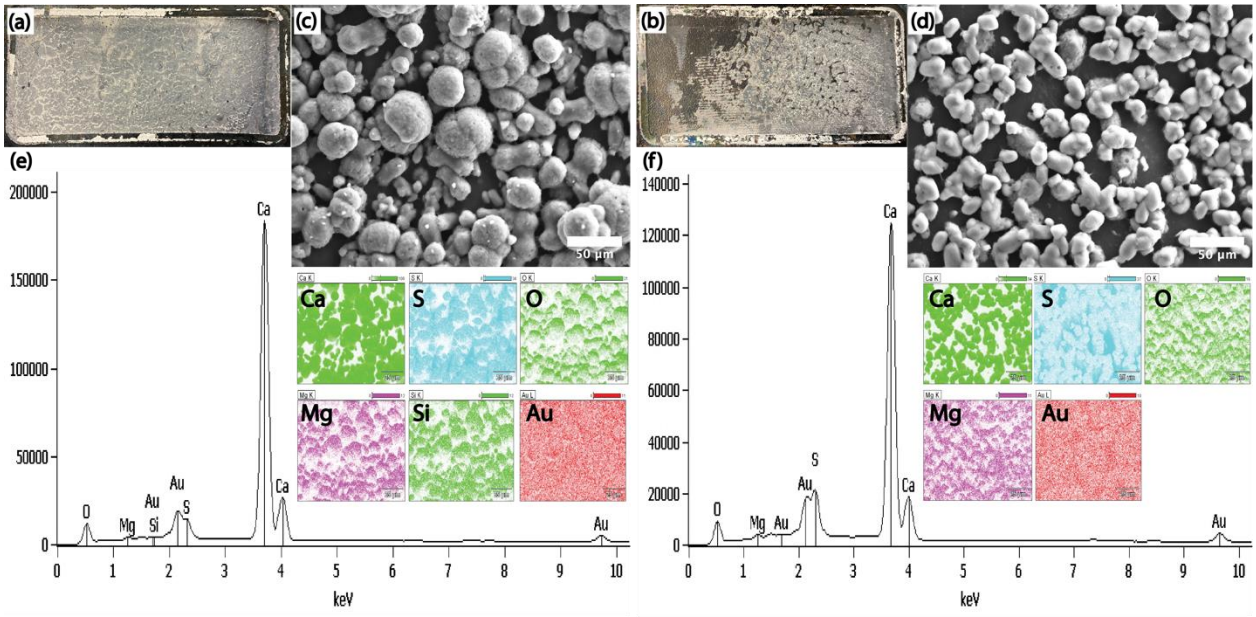

Figure 4.7. Surface characterization of scaled membrane that treated natural BGW solution: (a) image of scaled membrane after twice running of experiments under no potential condition. (b) image of scaled membrane after twice running of experiments under 4 V_{pp} condition. (c) FESEM images of scaled membrane under no potential condition. (d) FESEM image of scaled membrane under 4 V_{pp} condition. (e) EDAX results of scaled membrane under no potential condition. (f) EDAX results of scaled membrane under 4 V_{pp} condition.

The reduced/delayed scaling on the membrane surface is likely a result of the electrophoretic mixing induced by the polarity reversal (Figure 2). As the potential is alternated between positive and negative signs, cations (i.e., Ca^{2+}, Mg^{2+}, and Na^{+}) and anions (i.e., Cl^{-} and SO_4^{2-}) move in opposite directions, with the change in direction occurring at the frequency of the AC signal (1 Hz in our work).[105] We speculate that this constant change in ion migration direction prevents their co-location for sufficient periods of time, which minimizes the formation of pre-nucleation clusters,

and slows the overall crystallization reaction. In addition, even when nucleation does occur, the enhanced surface charge provided by the externally applied voltage leads to the formation of a thick electrical double layer (which is a function of the surface charge) that moves the nucleation zone away from the membrane surface where only one ion species exists. Then, nuclei that are formed away from the membrane surface can be easily carried away by the feed cross-flow.[142]

4.5 Conclusions

In this study, the effect of AC potentials (4 V_{pp}, 1 Hz, square form) on gypsum scale formation was investigated. An ECNF membrane treating a synthetic BGW (prone to gypsum scaling) and natural BGW was employed to investigate membrane scaling, while an electrolytic cell was used to investigate the impact of the alternating potentials on homogeneous nucleation and crystal growth in a solution. In all cases, the application of AC potentials effectively mitigated scale formation both on the surface of ECNF membranes (simultaneous homogenous and heterogeneous nucleation) and titanium plates in a stirred electrolytic cell (homogeneous nucleation dominant).

With AC potentials applied, the ECNF membrane treating synthetic BGW experienced less severe flux decline, and almost no salt rejection drop over the course of the experiments. In contrast, in the absence of applied potentials, a significant flux decline and large salt rejection drop was observed. In addition, after a cleaning step (using a DIW rinse), it was observed that membrane performance (i.e., flux and salt rejection) deteriorated under the no-potential condition due to irreversible scale formation, while the performance was nearly fully recovered with AC potentials. Similarly, when the ECNF membrane was used to treat natural BGW, the application of AC potentials resulted in less severe flux decline, no decrease in salt rejection, and excellent reversibility of membrane performance (flux and salt rejection) after a cleaning step. However, in

the absence of the applied potentials, the membrane suffered from significant flux decline, salt rejection drop, and severe irreversibility of membrane performance after cleaning. These findings imply that employing ECNF membranes with applied AC potentials could be a chemical-free and environmentally benign way to minimize brine production and increase the availability of potable water, by increasing water recovery during BGW desalination. Importantly, ECNF could be more cost-effective than the use of antiscalants, which also pose a threat to the water quality of receiving waters (where brines are disposed of) and membrane performance. The additional cost associated with the fabrication of the ECNF membranes (above the standard cost of NF membranes) is only \$0.10/m^2 (the cost of the CNTs). The application of AC potentials (i.e., 4 V_{pp}, 1 Hz) costs only \$0.02/m^3 of treated water as reported previously. [36] In contrast, the cost of antiscalant with optimal pH adjustment adds between \$0.02/m^3 – \$0.04/m^3, and the addition of antiscalants adds an environmental cost that is hard to estimate (it should be noted that the additional price for the dose of antiscalant and acid depends on the quality of chemicals and feed water).[65]

4.6 Supporting information

4.6.1 Calculation of saturation index

With an assumption of one-dimensional flow and full development of boundary layer, film model provides a following differential equation:

$$J_s = C \times J_v \times (-D\frac{dC}{dy}) \qquad \text{Equation (1)}$$

where J_s is solute flux, C is solute concentration in the boundary layer, J_v is water flux, and C is the diffusion coefficient of solute in water. For a boundary layer having a thickness of δ, integration of Equation. (1) gives

$$\frac{C_m - C_p}{C_b - C_p} = \exp(\frac{J_v \times \delta}{D}) \qquad \text{Equation (2)}$$

where C_m is solute concentration near the membrane surface, $C_p$is solute concentration in the permeate, and C_b is solute concentration in the bulk feed. The term, $\frac{\delta}{D}$, can be expressed as k, a mass transfer coefficient. By rearranging Equation (2),

$$C_m = (C_b - C_p) \times \exp(\frac{J_v}{k}) + C_p \quad \text{Equation (3)}$$

Mass transfer coefficient, k, can be expressed with Sherwood number (Sh):

$$k = \frac{Sh \times D}{dh} \quad \text{Equation (4)}$$

where dh is hydraulic diameter of the flow channel. Then, Sherwood number has an empirical correlation with Schmidt number (Sc) and Reynold's number (Re):

$$Sh = 0.6 \times Sc^{\frac{1}{3}} \times Re^{\frac{1}{2}} \quad \text{Equation (5)}$$

Thus, mass transfer coefficient was obtained using Equation (4) and (5). Diffusion coefficient was obtained from the OLI software. Then, ion concentrations near the membrane surface (i.e., in the CP layer) was obtained from Equation (3). Finally, using the ion concentrations in the CP layer, saturation index was predicted through OLI software.

4.6.2 ECNF treating synthetic BGW solutions

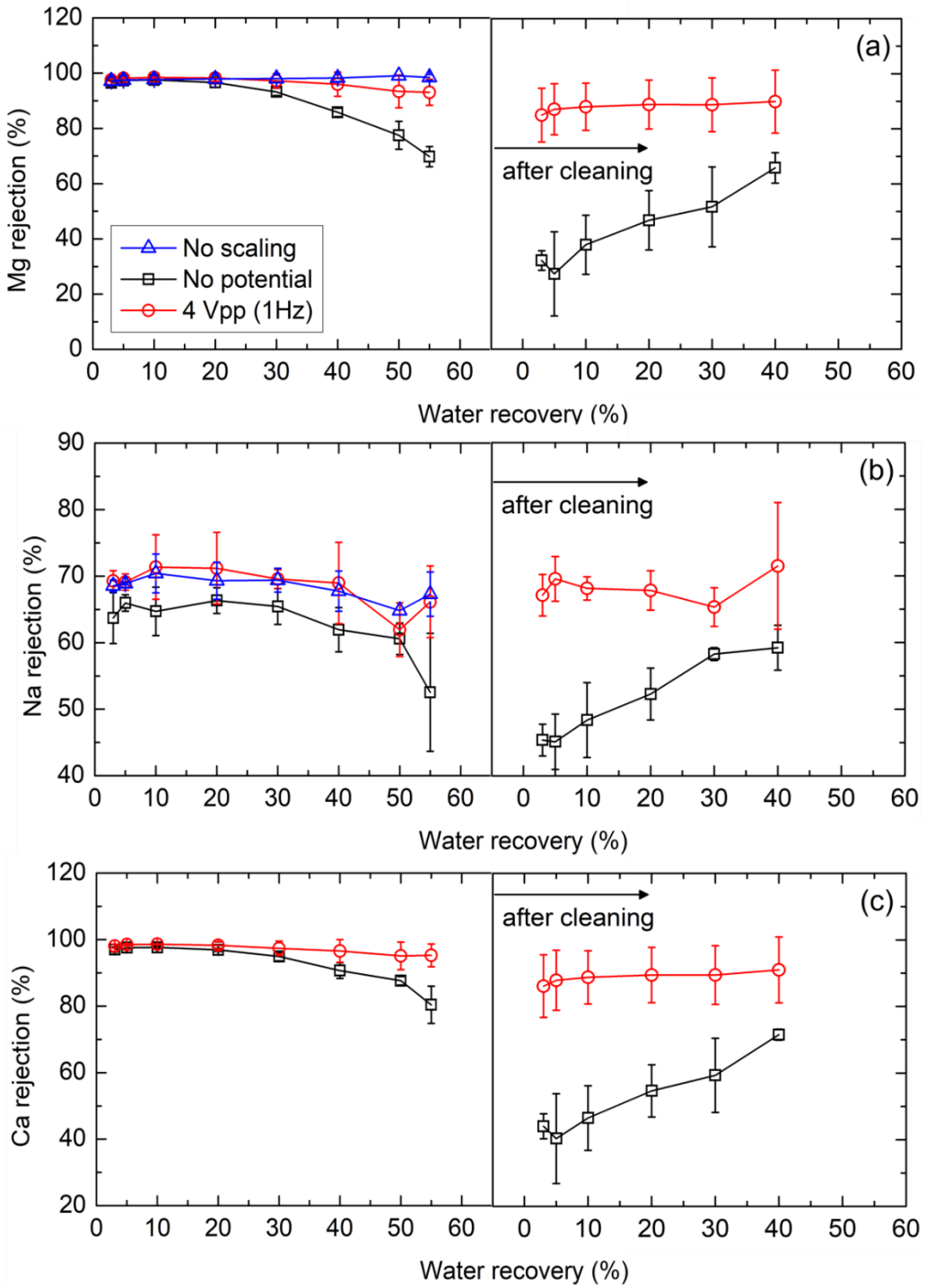

Figure S 4.1. Cation rejections of ECNT treating synthetic BGW over water recovery under no potential and 4 V_{pp}, 1 Hz conditions: (a) Mg^{2+} rejection. (b) Na^{+} rejection. (c) Ca^{2+} rejection. Each figure shares the legend – no potential (black square), 4 V_{pp} (red circle), and no scaling (blue triangle).

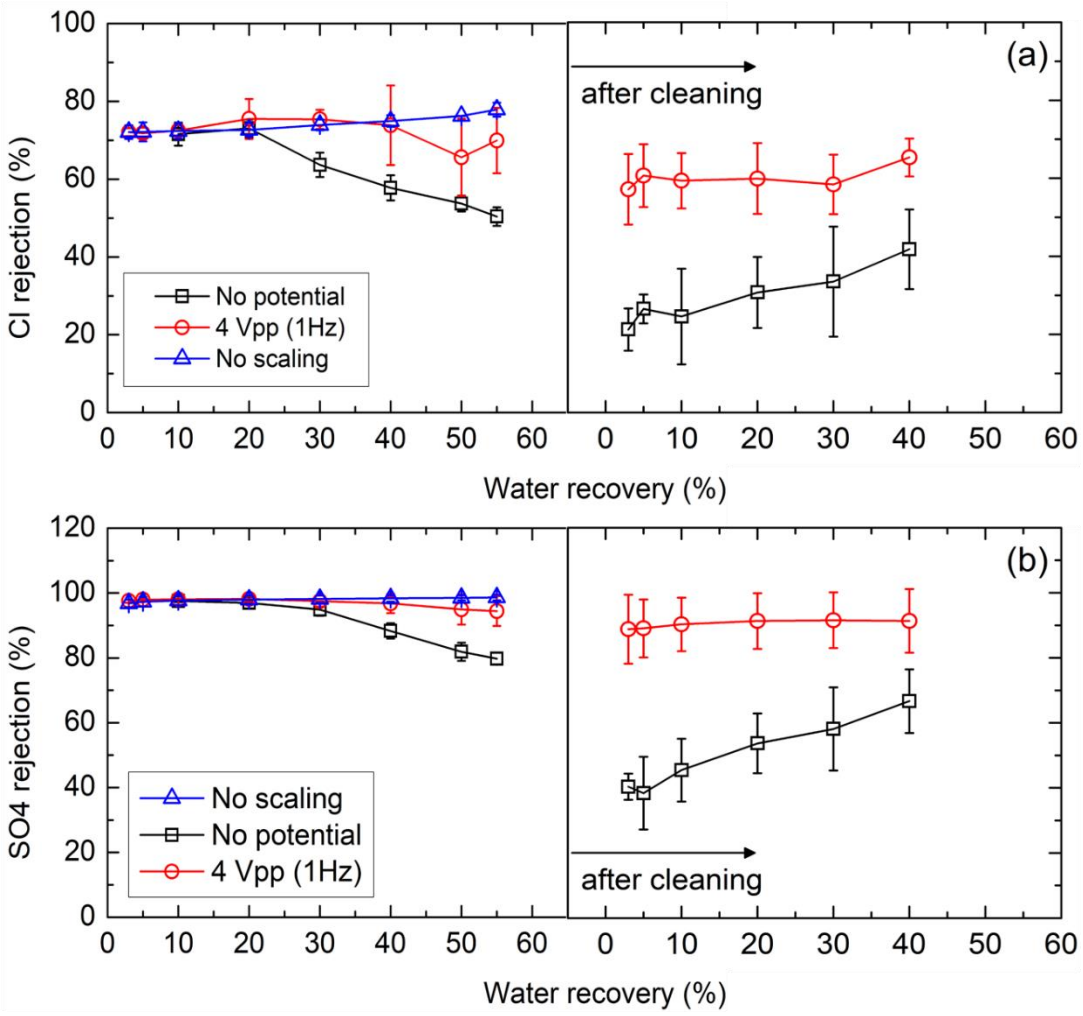

Figure S 4.2. Anion rejections of ECNF treating natural BGW over water recovery under no potential and 4 V_{pp}, 1 Hz conditions: (a) Cl^- rejection. (b) SO_4^{2-} rejection. Each figure shares the legend – no potential (black square), 4 V_{pp} (red circle), and no scaling (blue triangle).

Table S 4.1. Concentration of ions for acid soaking test

Constituents	Concentration (mM)
Na	8.70
Cl	11.28
Mg	8.23
SO4	2.08
Ca	4.99
HCO3	3.28

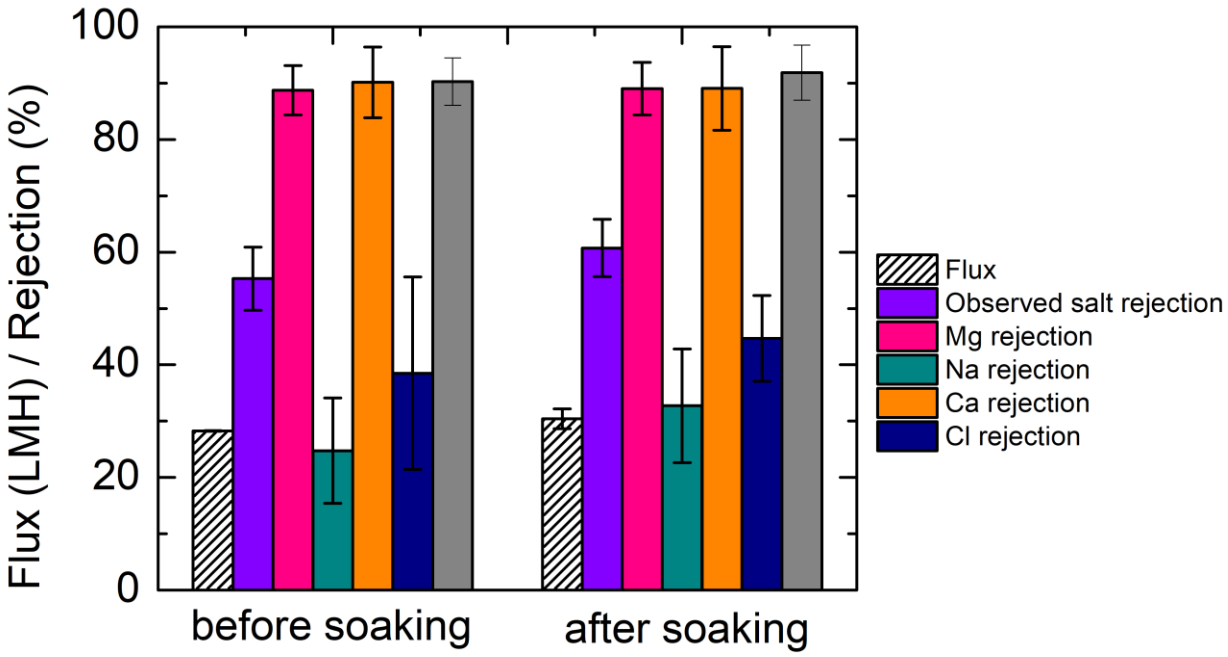

Figure S 4.3. Comparison of water flux, observed salt rejection, Mg rejection, Na rejection, Ca rejection, and Cl rejection of ECNF before and after acid soaking

Chapter 5.

Conclusion

The dissertation presented optimization of groundwater desalination treatment trains, as well as improved performance of desalination with electrically-conducting membranes.

In Chapter 1, we briefly discussed the necessity of membrane filtration to solve the problem of water scarcity. Then, brief history of each membrane types (i.e., MF, UF, NF, and RO) was addressed with their characteristics, industrial application, and removal mechanisms. Then, *pros and cons* of membrane filtration was briefly discussed, followed by in-depth discussion of the most challenging problem that membrane filtration has, membrane fouling. Finally, we review different approaches to overcome the disadvantages of membrane filtration.

In Chapter 2, we briefly addressed relative ineffectiveness of RO membrane for remove boron removal during sweater desalination, possible outcomes when desalinated water that contains high boron concentration is consumed by boron-sensitive plants, and conventional strategy to enhance boron removal efficiency by RO. Since the conventional strategy comes with a huge price tag (i.e., capital and operational cost), we presented an application of cathodic potentials on electrically conducting RO membranes that facilitated water electrolysis, resulting in enhanced boron removal efficiency without any chemical assist or post-treatment. Lastly, an economic analysis suggested using electrically conducting RO membranes for boron treatment could be more economical when it is compared to conventional method.

In Chapter 3, we briefly compared different water treatment technologies, and stated possible outcomes when product water contains high contaminants level, justifying the necessity of optimization of water treatment train. Then, possible candidates of technologies for groundwater desalination were chosen based on the water quality that would be used as feed. By treating synthetic groundwater, it was found that quartz sand filtration is relatively less effective on contaminant removal compared to greensand and activated alumina. By treating natural

groundwater, it was found that with a combination of selected technologies can produce potable water that meets drinking water standard set by USEPA. Finally, an economical model predicted the best combination of treatment train that produces potable water at the lowest possible water production cost while water quality meets the drinking water standard.

Chapter 4 elaborated the impact of frequent polarity reversal on mineral scale formation on electrically conducting nanofiltration membranes. By applying alternating current (4 Vpp, 1 Hz) on the surface of ECNF membrane, gypsum scaling formation was significantly delayed, resulting in less flux decline as well as less salt rejection drop. Without any voltages applied, ECNF membrane significantly suffered from the formation of scale. This approach was applied to both synthetic brackish groundwater and natural groundwater. Under both conditions, ECNF successfully delayed the formation of mineral scale on the surface, which could be a promising method to mitigate membrane scaling without any chemical dosage.

References

(1) Wallace, J. S. Increasing Agricultural Water Use Efficiency to Meet Future Food Production. *Agric. Ecosyst. Environ.* **2000**, *82* (1–3), 105–119. https://doi.org/10.1016/S0167-8809(00)00220-6.

(2) Dinar, A.; Tieu, A.; Huynh, H. Water Scarcity Impacts on Global Food Production. *Glob. Food Sec.* **2019**, *23* (May), 212–226. https://doi.org/10.1016/j.gfs.2019.07.007.

(3) Mancosu, N.; Snyder, R. L.; Kyriakakis, G.; Spano, D. Water Scarcity and Future Challenges for Food Production. *Water* **2015**, *7* (3), 975–992. https://doi.org/10.3390/w7030975.

(4) Mekonnen, M. M.; Gerbens-Leenes, W. The Water Footprint of Food. *Water* **2020**, *12* (10), 2696.

(5) Gopakumar, A.; Ren, P.; Chen, J.; Manzolli Rodrigues, B. V.; Vincent Ching, H. Y.; Jaworski, A.; Doorslaer, S. Van; Rokicińska, A.; Kuśtrowski, P.; Barcaro, G.; Monti, S.; Slabon, A.; Das, S. Lignin-Supported Heterogeneous Photocatalyst for the Direct Generation of H2O2from Seawater. *J. Am. Chem. Soc.* **2022**, *144* (6), 2603–2613. https://doi.org/10.1021/jacs.1c10786.

(6) Liu, G.; Wang, M.; Xu, Y.; Wang, X.; Li, X.; Liu, J.; Cui, X.; Jiang, L. Porous CoP/Co2P Heterostructure for Efficient Hydrogen Evolution and Application in Magnesium/Seawater Battery. *J. Power Sources* **2021**, *486* (December 2020), 229351. https://doi.org/10.1016/j.jpowsour.2020.229351.

(7) Dingenen, F.; Verbruggen, S. W. Tapping Hydrogen Fuel from the Ocean: A Review on Photocatalytic, Photoelectrochemical and Electrolytic Splitting of Seawater. *Renew. Sustain. Energy Rev.* **2021**, *142* (October 2020), 110866. https://doi.org/10.1016/j.rser.2021.110866.

(8) Awaad, H. A.; Mansour, E.; Akrami, M.; Fath, H. E. S.; Javadi, A. A.; Negm, A. Availability and Feasibility Ofwater Desalination as a Non-Conventional Resource for Agricultural Irrigation in the MENA Region: A Review. *Sustain.* **2020**, *12* (18), 1–14. https://doi.org/10.3390/su12187592.

(9) Ma, T.; Sun, S.; Fu, G.; Hall, J. W.; Ni, Y.; He, L.; Yi, J.; Zhao, N.; Du, Y.; Pei, T.; Cheng, W.; Song, C.; Fang, C.; Zhou, C. Pollution Exacerbates China's Water Scarcity and Its Regional

Inequality. *Nat. Commun.* **2020**, *11* (1), 1–9. https://doi.org/10.1038/s41467-020-14532-5.

(10) Gleick, P. H.; Palaniappan, M. Peak Water Limits to Freshwater Withdrawal and Use. *Proc. Natl. Acad. Sci. U. S. A.* **2010**, *107* (25), 11155–11162. https://doi.org/10.1073/pnas.1004812107.

(11) Bozorg-Haddad, O.; Zolghadr-Asli, B.; Sarzaeim, P.; Aboutalebi, M.; Chu, X.; Loáiciga, H. A. Evaluation of Water Shortage Crisis in the Middle East and Possible Remedies. *J. Water Supply Res. Technol. - AQUA* **2020**, *69* (1), 85–98. https://doi.org/10.2166/aqua.2019.049.

(12) Wan, L.; Cai, W.; Jiang, Y.; Wang, C. Impacts on Quality-Induced Water Scarcity: Drivers of Nitrogen-Related Water Pollution Transfer under Globalization from 1995 to 2009. *Environ. Res. Lett.* **2016**, *11* (7). https://doi.org/10.1088/1748-9326/11/7/074017.

(13) Hoekstra, A. Y. Water Scarcity Challenges to Business. *Nat. Clim. Chang.* **2014**, *4* (5), 318–320. https://doi.org/10.1038/nclimate2214.

(14) Mukherjee, S.; Shah, Z.; Kumar, M. D. Sustaining Urban Water Supplies in India: Increasing Role of Large Reservoirs. *Water Resour. Manag.* **2010**, *24* (10), 2035–2055. https://doi.org/10.1007/s11269-009-9537-8.

(15) Distefano, T.; Kelly, S. Are We in Deep Water? Water Scarcity and Its Limits to Economic Growth. *Ecol. Econ.* **2017**, *142*, 130–147. https://doi.org/10.1016/j.ecolecon.2017.06.019.

(16) Mitchell, V. G.; Mein, R. G.; McMahon, T. A. Utilising Stormwater and Wastewater Resources in Urban Areas. *Australas. J. Water Resour.* **2002**, *6* (1), 31–43. https://doi.org/10.1080/13241583.2002.11465208.

(17) Cisternas, L. A.; Gálvez, E. D. The Use of Seawater in Mining. *Miner. Process. Extr. Metall. Rev.* **2018**, *39* (1), 18–33. https://doi.org/10.1080/08827508.2017.1389729.

(18) Asano, T. Reusing Urban Wastewater—an Alternative and a Reliable Water Resource. *Water Int.* **1994**, *19* (1), 36–42. https://doi.org/10.1080/02508069408686194.

(19) Toro, N.; Gálvez, E.; Robles, P.; Castillo, J.; Villca, G.; Salinas-Rodríguez, E. Use of Alternative Water Resources in Copper Leaching Processes in Chilean Mining Industry—A Review. *Metals (Basel).* **2022**, *12* (3), 1–17. https://doi.org/10.3390/met12030445.

(20) Leung, R. W. K.; Li, D. C. H.; Yu, W. K.; Chui, H. K.; Lee, T. O.; Van Loosdrecht, M. C. M.; Chen, G. H. Integration of Seawater and Grey Water Reuse to Maximize Alternative Water Resource for Coastal Areas: The Case of the Hong Kong International Airport. *Water Sci. Technol.* **2012**, *65* (3), 410–417. https://doi.org/10.2166/wst.2012.768.

(21) Lu, X.; Liu, L.; Liu, R.; Chen, J. Textile Wastewater Reuse as an Alternative Water Source for Dyeing and Finishing Processes: A Case Study. *Desalination* **2010**, *258* (1–3), 229–232. https://doi.org/10.1016/j.desal.2010.04.002.

(22) Papaiacovou, I. Case Study - Wastewater Reuse in Limassol as an Alternative Water Source. *Desalination* **2001**, *138* (1–3), 55–59. https://doi.org/10.1016/S0011-9164(01)00244-2.

(23) Jose, A. J.; Kappen, J.; Alagar, M. *Polymeric Membranes: Classification, Preparation, Structure Physiochemical, and Transport Mechanisms*; Elsevier Ltd., 2018. https://doi.org/10.1016/B978-0-08-102194-1.00002-5.

(24) Pouliot, Y. Membrane Processes in Dairy Technology-From a Simple Idea to Worldwide Panacea. *Int. Dairy J.* **2008**, *18* (7), 735–740. https://doi.org/10.1016/j.idairyj.2008.03.005.

(25) Villacorte, L. O.; Ekowati, Y.; Winters, H.; Amy, G.; Schippers, J. C.; Kennedy, M. D. MF/UF Rejection and Fouling Potential of Algal Organic Matter from Bloom-Forming Marine and Freshwater Algae. *Desalination* **2015**, *367*, 1–10. https://doi.org/10.1016/j.desal.2015.03.027.

(26) Zhang, L.; Hamelers, H. V. M.; Biesheuvel, P. M. Modeling Permeate PH in RO Membranes by the Extended Donnan Steric Partitioning Pore Model. *J. Memb. Sci.* **2020**, *613* (February). https://doi.org/10.1016/j.memsci.2020.118511.

(27) Bason, S.; Oren, Y.; Freger, V. Characterization of Ion Transport in Thin Films Using Electrochemical Impedance Spectroscopy. II: Examination of the Polyamide Layer of RO Membranes. *J. Memb. Sci.* **2007**, *302* (1–2), 10–19. https://doi.org/10.1016/j.memsci.2007.05.007.

(28) Xu, P.; Drewes, J. E.; Kim, T. U.; Bellona, C.; Amy, G. Effect of Membrane Fouling on Transport of Organic Contaminants in NF/RO Membrane Applications. *J. Memb. Sci.* **2006**, *279* (1–2), 165–175. https://doi.org/10.1016/j.memsci.2005.12.001.

(29) Dlamini, D. S.; Levchenko, S.; Bass, M.; Mamba, B. B.; Hoek, E. M. V.; Thwala, J. M.; Freger, V. Solute Hindrance in Non-Porous Membranes: An ATR-FTIR Study. *Desalination* **2015**, *368*, 60–68. https://doi.org/10.1016/j.desal.2015.03.009.

(30) Dolar, D.; Košutić, K.; Vučić, B. RO/NF Treatment of Wastewater from Fertilizer Factory - Removal of Fluoride and Phosphate. *Desalination* **2011**, *265* (1–3), 237–241. https://doi.org/10.1016/j.desal.2010.07.057.

(31) Gul, A.; Hruza, J.; Yalcinkaya, F. Fouling and Chemical Cleaning of Microfiltration Membranes: A Mini-Review. *Polymers (Basel).* **2021**, *13* (6). https://doi.org/10.3390/polym13060846.

(32) Cui, Z. F.; Muralidhara, H. S. *Membrane Technology*; 2010. https://doi.org/10.1016/C2009-0-19129-8.

(33) Ramaswamy, S.; Greenberg, A. R.; Peterson, M. L. Non-Invasive Measurement of Membrane Morphology via UFDR: Pore-Size Characterization. *J. Memb. Sci.* **2004**, *239* (1), 143–154. https://doi.org/10.1016/j.memsci.2003.08.030.

(34) An, S.; Lee, J.; Sim, J.; Park, C.; Lee, J.; Rho, H.; Park, K.; Kim, H.; Woo, Y. C. Evaluation of the Advanced Oxidation Process Integrated with Microfiltration for Reverse Osmosis to Treat Semiconductor Wastewater. *Process Saf. Environ. Prot.* **2022**, *162*, 1057–1066. https://doi.org/10.1016/j.psep.2022.05.010.

(35) Huang, C. J.; Yang, B. M.; Chen, K. S.; Chang, C. C.; Kao, C. M. Application of Membrane Technology on Semiconductor Wastewater Reclamation: A Pilot-Scale Study. *Desalination* **2011**, *278* (1–3), 203–210. https://doi.org/10.1016/j.desal.2011.05.032.

(36) Van Reis, R.; Zydney, A. Membrane Separations in Biotechnology. *Curr. Opin. Biotechnol.* **2001**, *12* (2), 208–211. https://doi.org/10.1016/S0958-1669(00)00201-9.

(37) Thiam, B. G.; El Magri, A.; Vanaei, H. R.; Vaudreuil, S. 3D Printed and Conventional Membranes—A Review. *Polymers (Basel).* **2022**, *14* (5), 1–16. https://doi.org/10.3390/polym14051023.

(38) Remanan, S.; Sharma, M.; Bose, S.; Das, N. C. Recent Advances in Preparation of Porous

Polymeric Membranes by Unique Techniques and Mitigation of Fouling through Surface Modification. *ChemistrySelect* **2018**, *3* (2), 609–633. https://doi.org/10.1002/slct.201702503.

(39) Glater, J. Early History of Reverse Osmosis Membrane Development. *Water Supply* **1999**, *17* (1), 103–115.

(40) Schlichter, B.; Mavrov, V.; Chmiel, H. Comparative Characterisation of Different Commercial UF Membranes for Drinking Water Production. *J. Water Supply Res. Technol. - AQUA* **2000**, *49* (6), 321–328. https://doi.org/10.2166/aqua.2000.0027.

(41) Taniguchi, M.; Kilduff, J. E.; Belfort, G. Modes of Natural Organic Matter Fouling during Ultrafiltration. *Environ. Sci. Technol.* **2003**, *37* (8), 1676–1683. https://doi.org/10.1021/es020555p.

(42) Hu, X.; Bekassy-Molnar, E.; Koris, A. Study of Modelling Transmembrane Pressure and Gel Resistance in Ultrafiltration of Oily Emulsion. *Desalination* **2004**, *163* (1–3), 355–360. https://doi.org/10.1016/S0011-9164(04)90208-1.

(43) Al Aani, S.; Mustafa, T. N.; Hilal, N. Ultrafiltration Membranes for Wastewater and Water Process Engineering: A Comprehensive Statistical Review over the Past Decade. *J. Water Process Eng.* **2020**, *35* (March 2020), 101241. https://doi.org/10.1016/j.jwpe.2020.101241.

(44) Ćurić, I.; Dolar, D.; Karadakić, K. Textile Wastewater Reusability in Knitted Fabric Washing Process Using UF Membrane Technology. *J. Clean. Prod.* **2021**, *299*. https://doi.org/10.1016/j.jclepro.2021.126899.

(45) Tang, X.; Flint, S. H.; Bennett, R. J.; Brooks, J. D. The Efficacy of Different Cleaners and Sanitisers in Cleaning Biofilms on UF Membranes Used in the Dairy Industry. *J. Memb. Sci.* **2010**, *352* (1–2), 71–75. https://doi.org/10.1016/j.memsci.2010.01.063.

(46) Cassano, A.; Molinari, R.; Romano, M.; Drioli, E. Treatment of Aqueous Effluents of the Leather Industry by Membrane Processes: A Review. *J. Memb. Sci.* **2001**, *181* (1), 111–126. https://doi.org/10.1016/S0376-7388(00)00399-9.

(47) Luján-Facundo, M. J.; Mendoza-Roca, J. A.; Cuartas-Uribe, B.; Álvarez-Blanco, S. Cleaning

Efficiency Enhancement by Ultrasounds for Membranes Used in Dairy Industries. *Ultrason. Sonochem.* **2016**, *33*, 18–25. https://doi.org/10.1016/j.ultsonch.2016.04.018.

(48) Ahmad, N. A.; Leo, C. P.; Ahmad, A. L.; Ramli, W. K. W. Membranes with Great Hydrophobicity: A Review on Preparation and Characterization. *Sep. Purif. Rev.* **2015**, *44* (2), 109–134. https://doi.org/10.1080/15422119.2013.848816.

(49) Tweddle, T. A.; Kutowy, O.; Thayer, W. L.; Sourlrajan, S. Polysulfone Membranes. **1983**, No. 1977, 320–326.

(50) Ghaemi, N.; Madaeni, S. S.; Alizadeh, A.; Daraei, P.; Zinatizadeh, A. A.; Rahimpour, F. Separation of Nitrophenols Using Cellulose Acetate Nanofiltration Membrane: Influence of Surfactant Additives. *Sep. Purif. Technol.* **2012**, *85*, 147–156. https://doi.org/10.1016/j.seppur.2011.10.003.

(51) Puls, J.; Wilson, S. A.; Hölter, D. Degradation of Cellulose Acetate-Based Materials: A Review. *J. Polym. Environ.* **2011**, *19* (1), 152–165. https://doi.org/10.1007/s10924-010-0258-0.

(52) Murphy, A. P.; Moody, C. D.; Riley, R. L.; Lin, S. W.; Murugaverl, B.; Rusin, P. Microbiological Damage of Cellulose Acetate RO Membranes. *J. Memb. Sci.* **2001**, *193* (1), 111–121. https://doi.org/10.1016/S0376-7388(01)00506-3.

(53) Diawara, C. K. Nanofiltration Process Efficiency in Water Desalination. *Sep. Purif. Rev.* **2008**, *37* (3), 302–324. https://doi.org/10.1080/15422110802228770.

(54) Lee, S.; Lee, C. H. Effect of Operating Conditions on CaSO4 Scale Formation Mechanism in Nanofiltration for Water Softening. *Water Res.* **2000**, *34* (15), 3854–3866. https://doi.org/10.1016/S0043-1354(00)00142-1.

(55) Hilal, N.; Al-Zoubi, H.; Darwish, N. A.; Mohammad, A. W.; Abu Arabi, M. A Comprehensive Review of Nanofiltration Membranes: Treatment, Pretreatment, Modelling, and Atomic Force Microscopy. *Desalination* **2004**, *170* (3), 281–308. https://doi.org/10.1016/j.desal.2004.01.007.

(56) Suhalim, N. S.; Kasim, N.; Mahmoudi, E.; Shamsudin, I. J.; Mohammad, A. W.; Zuki, F. M.; Jamari, N. L. A. Rejection Mechanism of Ionic Solute Removal by Nanofiltration Membranes: An

Overview. *Nanomaterials* **2022**, *12* (3). https://doi.org/10.3390/nano12030437.

(57) Nghiem, L. D.; Schäfer, A. I.; Elimelech, M. Role of Electrostatic Interactions in the Retention of Pharmaceutically Active Contaminants by a Loose Nanofiltration Membrane. *J. Memb. Sci.* **2006**, *286* (1–2), 52–59. https://doi.org/10.1016/j.memsci.2006.09.011.

(58) Yoon, J.; Amy, G.; Chung, J.; Sohn, J.; Yoon, Y. Removal of Toxic Ions (Chromate, Arsenate, and Perchlorate) Using Reverse Osmosis, Nanofiltration, and Ultrafiltration Membranes. *Chemosphere* **2009**, *77* (2), 228–235. https://doi.org/10.1016/j.chemosphere.2009.07.028.

(59) Ibrahim, G. P. S.; Isloor, A. M.; Farnood, R. *Fundamentals and Basics of Reverse Osmosis*; Elsevier Inc., 2019. https://doi.org/10.1016/B978-0-12-816777-9.00006-X.

(60) Swapnil, P.; Meena, M. *The Industrial Development of Polymeric Membranes and Membrane Modules for Reverse Osmosis and Ultrafiltration*; INC, 2021. https://doi.org/10.1016/B978-0-12-823804-2.00009-4.

(61) Vatanpour, V.; Pasaoglu, M. E.; Barzegar, H.; Teber, O. O.; Kaya, R.; Bastug, M.; Khataee, A.; Koyuncu, I. Cellulose Acetate in Fabrication of Polymeric Membranes: A Review. *Chemosphere* **2022**, *295* (January). https://doi.org/10.1016/j.chemosphere.2022.133914.

(62) Al Mayyahi, A. Important Approaches to Enhance Reverse Osmosis (RO) Thin Film Composite (TFC) Membranes Performance. *Membranes (Basel).* **2018**, *8* (3). https://doi.org/10.3390/membranes8030068.

(63) Fei, P.; Liao, L.; Meng, J.; Cheng, B.; Hu, X.; Song, J. Synthesis, Characterization and Antibacterial Properties of Reverse Osmosis Membranes from Cellulose Bromoacetate. *Cellulose* **2018**, *25* (10), 5967–5984. https://doi.org/10.1007/s10570-018-1990-1.

(64) Nakao, T.; Miura, Y.; Furuichi, K.; Yasukawa, M. Cellulose Triacetate (Cta) Hollow-Fiber (Hf) Membranes for Sustainable Seawater Desalination: A Review. *Membranes (Basel).* **2021**, *11* (3). https://doi.org/10.3390/membranes11030183.

(65) Xu, R.; Xu, G.; Wang, J.; Chen, J.; Yang, F.; Kang, J.; Xiang, M. Influence of L-Lysine on the Permeation and Antifouling Performance of Polyamide Thin Film Composite Reverse Osmosis

Membranes. *RSC Adv.* **2018**, *8* (44), 25236–25247. https://doi.org/10.1039/c8ra02234h.

(66) Bian, X.; Zhang, Y.; Gong, L.; Zhu, Y.; Jin, J. Calcium Ion Coordinated Polyamide Nanofiltration Membrane for Ultrahigh Perm-Selectivity Desalination. *Chem. Res. Chinese Univ.* **2021**, *37* (5), 1101–1109. https://doi.org/10.1007/s40242-021-1270-8.

(67) Bilad, M. R.; Mat Nawi, N. I.; Subramaniam, D. D.; Shamsuddin, N.; Khan, A. L.; Jaafar, J.; Nandiyanto, A. B. D. Low-Pressure Submerged Membrane Filtration for Potential Reuse of Detergent and Water from Laundry Wastewater. *J. Water Process Eng.* **2020**, *36* (March), 101264. https://doi.org/10.1016/j.jwpe.2020.101264.

(68) Tang, X.; Ding, A.; Pronk, W.; Ziemba, C.; Cheng, X.; Wang, J.; Xing, J.; Xie, B.; Li, G.; Liang, H. Biological Pre-Treatments Enhance Gravity-Driven Membrane Filtration for the Decentralized Water Supply: Linking Extracellular Polymeric Substances Formation to Flux Stabilization. *J. Clean. Prod.* **2018**, *197*, 721–731. https://doi.org/10.1016/j.jclepro.2018.06.155.

(69) Hube, S.; Eskafi, M.; Hrafnkelsdóttir, K. F.; Bjarnadóttir, B.; Bjarnadóttir, M. Á.; Axelsdóttir, S.; Wu, B. Direct Membrane Filtration for Wastewater Treatment and Resource Recovery: A Review. *Sci. Total Environ.* **2020**, *710*. https://doi.org/10.1016/j.scitotenv.2019.136375.

(70) Gao, W.; Liang, H.; Ma, J.; Han, M.; Chen, Z. lin; Han, Z. shuang; Li, G. bai. Membrane Fouling Control in Ultrafiltration Technology for Drinking Water Production: A Review. *Desalination* **2011**, *272* (1–3), 1–8. https://doi.org/10.1016/j.desal.2011.01.051.

(71) Laîné, J. M.; Campos, C.; Baudin, I.; Janex, M. L. Understanding Membrane Fouling: A Review of over a Decade of Research. *Water Sci. Technol. Water Supply* **2003**, *3* (5–6), 155–164. https://doi.org/10.2166/ws.2003.0162.

(72) Nguyen, T. T.; Kook, S.; Lee, C.; Field, R. W.; Kim, I. S. Critical Flux-Based Membrane Fouling Control of Forward Osmosis: Behavior, Sustainability, and Reversibility. *J. Memb. Sci.* **2019**, *570–571* (June 2018), 380–393. https://doi.org/10.1016/j.memsci.2018.10.062.

(73) Kanani, D. M.; Sun, X.; Ghosh, R. Reversible and Irreversible Membrane Fouling during In-Line Microfiltration of Concentrated Protein Solutions. *J. Memb. Sci.* **2008**, *315* (1–2), 1–10.

https://doi.org/10.1016/j.memsci.2008.01.053.

(74) Fan, X.; Zhao, H.; Quan, X.; Liu, Y.; Chen, S. Nanocarbon-Based Membrane Filtration Integrated with Electric Field Driving for Effective Membrane Fouling Mitigation. *Water Res.* **2016**, *88*, 285–292. https://doi.org/10.1016/j.watres.2015.10.043.

(75) Kimura, K.; Hane, Y.; Watanabe, Y.; Amy, G.; Ohkuma, N. Irreversible Membrane Fouling during Ultrafiltration of Surface Water. *Water Res.* **2004**, *38* (14–15), 3431–3441. https://doi.org/10.1016/j.watres.2004.05.007.

(76) Heidari, S.; Amirinejad, M.; Mirzadeh, S. S.; Wood, D. A. Insights into Colloidal Membrane Fouling Mechanisms for Nanofiltration of Surface Water Using Single and Hybrid Membrane Processes. *Polym. Adv. Technol.* **2021**, *32* (6), 2517–2530. https://doi.org/10.1002/pat.5282.

(77) Ben-Sasson, M.; Lin, Y. M.; Adin, A. Electrocoagulation-Membrane Filtration Hybrid System for Colloidal Fouling Mitigation of Secondary-Effluent. *Sep. Purif. Technol.* **2011**, *82* (1), 63–70. https://doi.org/10.1016/j.seppur.2011.08.020.

(78) Zheng, X.; Khan, M. T.; Croué, J. P. Contribution of Effluent Organic Matter (EfOM) to Ultrafiltration (UF) Membrane Fouling: Isolation, Characterization, and Fouling Effect of EfOM Fractions. *Water Res.* **2014**, *65*, 414–424. https://doi.org/10.1016/j.watres.2014.07.039.

(79) Liu, J.; Zhao, Y.; Fan, Y.; Yang, H.; Wang, Z.; Chen, Y.; Tang, C. Y. Dissect the Role of Particle Size through Collision-Attachment Simulations for Colloidal Fouling of RO/NF Membranes. *J. Memb. Sci.* **2021**, *638* (April), 119679. https://doi.org/10.1016/j.memsci.2021.119679.

(80) Song, L.; Elimelech, M. Particle Deposition onto a Permeable Surface in Laminar Flow. *Journal of Colloid And Interface Science*. 1995, pp 165–180. https://doi.org/10.1006/jcis.1995.1310.

(81) Guo, W.; Ngo, H. H.; Li, J. A Mini-Review on Membrane Fouling. *Bioresour. Technol.* **2012**, *122*, 27–34. https://doi.org/10.1016/j.biortech.2012.04.089.

(82) Costa, A. R.; de Pinho, M. N.; Elimelech, M. Mechanisms of Colloidal Natural Organic Matter Fouling in Ultrafiltration. *J. Memb. Sci.* **2006**, *281* (1–2), 716–725. https://doi.org/10.1016/j.memsci.2006.04.044.

(83) Kim, J.; Park, M. J.; Park, M.; Shon, H. K.; Kim, S. H.; Kim, J. H. Influence of Colloidal Fouling on Pressure Retarded Osmosis. *Desalination* **2016**, *389*, 207–214. https://doi.org/10.1016/j.desal.2016.01.036.

(84) Tian, J. Y.; Ernst, M.; Cui, F.; Jekel, M. Effect of Different Cations on UF Membrane Fouling by NOM Fractions. *Chem. Eng. J.* **2013**, *223*, 547–555. https://doi.org/10.1016/j.cej.2013.03.043.

(85) Kim, H. C.; Dempsey, B. A. Membrane Fouling Due to Alginate, SMP, EfOM, Humic Acid, and NOM. *J. Memb. Sci.* **2013**, *428*, 190–197. https://doi.org/10.1016/j.memsci.2012.11.004.

(86) Tong, T.; Wallace, A. F.; Zhao, S.; Wang, Z. Mineral Scaling in Membrane Desalination: Mechanisms, Mitigation Strategies, and Feasibility of Scaling-Resistant Membranes. *J. Memb. Sci.* **2019**, *579* (February), 52–69. https://doi.org/10.1016/j.memsci.2019.02.049.

(87) Yu, W.; Song, D.; Chen, W.; Yang, H. Antiscalants in RO Membrane Scaling Control. *Water Res.* **2020**, *183*, 115985. https://doi.org/10.1016/j.watres.2020.115985.

(88) Matin, A.; Rahman, F.; Shafi, H. Z.; Zubair, S. M. Scaling of Reverse Osmosis Membranes Used in Water Desalination: Phenomena, Impact, and Control; Future Directions. *Desalination* **2019**, *455* (December 2018), 135–157. https://doi.org/10.1016/j.desal.2018.12.009.

(89) Warsinger, D. M.; Swaminathan, J.; Guillen-Burrieza, E.; Arafat, H. A.; Lienhard V, J. H. Scaling and Fouling in Membrane Distillation for Desalination Applications: A Review. *Desalination* **2015**, *356*, 294–313. https://doi.org/10.1016/j.desal.2014.06.031.

(90) Weber, S. C.; Brangwynne, C. P. Inverse Size Scaling of the Nucleolus by a Concentration-Dependent Phase Transition. *Curr. Biol.* **2015**, *25* (5), 641–646. https://doi.org/10.1016/j.cub.2015.01.012.

(91) Christie, K. S. S.; Yin, Y.; Lin, S.; Tong, T. Distinct Behaviors between Gypsum and Silica Scaling in Membrane Distillation. *Environ. Sci. Technol.* **2020**. https://doi.org/10.1021/acs.est.9b06023.

(92) Yin, Y.; Jeong, N.; Minjarez, R.; Robbins, C. A.; Carlson, K. H.; Tong, T. Contrasting Behaviors between Gypsum and Silica Scaling in the Presence of Antiscalants during Membrane Distillation.

Environ. Sci. Technol. **2021**, *55* (8), 5335–5346. https://doi.org/10.1021/acs.est.0c07190.

(93) Kochkodan, V.; Hilal, N. A Comprehensive Review on Surface Modified Polymer Membranes for Biofouling Mitigation. *Desalination* **2015**, *356*, 187–207. https://doi.org/10.1016/j.desal.2014.09.015.

(94) Kim, C. Y.; Zhu, X.; Herzberg, M.; Walker, S.; Jassby, D. Impact of Physical and Chemical Cleaning Agents on Specific Biofilm Components and the Implications for Membrane Biofouling Management. *Ind. Eng. Chem. Res.* **2018**, *57* (9), 3359–3370. https://doi.org/10.1021/acs.iecr.7b05156.

(95) Matin, A.; Khan, Z.; Zaidi, S. M. J.; Boyce, M. C. Biofouling in Reverse Osmosis Membranes for Seawater Desalination: Phenomena and Prevention. *Desalination* **2011**, *281* (1), 1–16. https://doi.org/10.1016/j.desal.2011.06.063.

(96) Jang, E. S.; Mickols, W.; Sujanani, R.; Helenic, A.; Dilenschneider, T. J.; Kamcev, J.; Paul, D. R.; Freeman, B. D. Influence of Concentration Polarization and Thermodynamic Non-Ideality on Salt Transport in Reverse Osmosis Membranes. *J. Memb. Sci.* **2019**, *572* (August 2018), 668–675. https://doi.org/10.1016/j.memsci.2018.11.006.

(97) Li, W.; Su, X.; Palazzolo, A.; Ahmed, S. Numerical Modeling of Concentration Polarization and Inorganic Fouling Growth in the Pressure-Driven Membrane Filtration Process. *J. Memb. Sci.* **2019**, *569* (July 2017), 71–82. https://doi.org/10.1016/j.memsci.2018.10.007.

(98) Su, X.; Li, W.; Palazzolo, A.; Ahmed, S. Concentration Polarization and Permeate Flux Variation in a Vibration Enhanced Reverse Osmosis Membrane Module. *Desalination* **2018**, *433* (September 2017), 75–88. https://doi.org/10.1016/j.desal.2018.01.001.

(99) Jiang, S.; Li, Y.; Ladewig, B. P. A Review of Reverse Osmosis Membrane Fouling and Control Strategies. *Sci. Total Environ.* **2017**, *595*, 567–583. https://doi.org/10.1016/j.scitotenv.2017.03.235.

(100) Sun, M.; Wang, X.; Winter, L. R.; Zhao, Y.; Ma, W.; Hedtke, T.; Kim, J.-H.; Elimelech, M. Electrified Membranes for Water Treatment Applications. *ACS ES&T Eng.* **2021**, *1* (4), 725–752.

https://doi.org/10.1021/acsestengg.1c00015.

(101) Zheng, J.; Wang, Z.; Ma, J.; Xu, S.; Wu, Z. Development of an Electrochemical Ceramic Membrane Filtration System for Efficient Contaminant Removal from Waters. *Environ. Sci. Technol.* **2018**, *52* (7), 4117–4126. https://doi.org/10.1021/acs.est.7b06407.

(102) Sun, J.; Wang, Q.; Zhang, J.; Wang, Z.; Wu, Z. Degradation of Sulfadiazine in Drinking Water by a Cathodic Electrochemical Membrane Filtration Process. *Electrochim. Acta* **2018**, *277*, 77–87. https://doi.org/10.1016/j.electacta.2018.05.005.

(103) Tang, L.; Iddya, A.; Zhu, X.; Dudchenko, A. V.; Duan, W.; Turchi, C.; Vanneste, J.; Cath, T. Y.; Jassby, D. Enhanced Flux and Electrochemical Cleaning of Silicate Scaling on Carbon Nanotube-Coated Membrane Distillation Membranes Treating Geothermal Brines. *ACS Appl. Mater. Interfaces* **2017**, *9* (44), 38594–38605. https://doi.org/10.1021/acsami.7b12615.

(104) Duan, W.; Dudchenko, A.; Mende, E.; Flyer, C.; Zhu, X.; Jassby, D. Electrochemical Mineral Scale Prevention and Removal on Electrically Conducting Carbon Nanotube-Polyamide Reverse Osmosis Membranes. *Environ. Sci. Process. Impacts* **2014**, *16* (6), 1300–1308. https://doi.org/10.1039/c3em00635b.

(105) Rao, U.; Iddya, A.; Jung, B.; Khor, C. M.; Hendren, Z.; Turchi, C.; Cath, T.; Hoek, E. M. V.; Ramon, G. Z.; Jassby, D. Mineral Scale Prevention on Electrically Conducting Membrane Distillation Membranes Using Induced Electrophoretic Mixing. *Environ. Sci. Technol.* **2020**, *54* (6), 3678–3690. https://doi.org/10.1021/acs.est.9b07806.

(106) Güler, E.; Kaya, C.; Kabay, N.; Arda, M. Boron Removal from Seawater: State-of-the-Art Review. *Desalination* **2015**, *356*, 85–93. https://doi.org/10.1016/j.desal.2014.10.009.

(107) Dolnicar, S.; Schäfer, A. I. Desalinated versus Recycled Water: Public Perceptions and Profiles of the Accepters. *J. Environ. Manage.* **2009**, *90* (2), 888–900. https://doi.org/10.1016/j.jenvman.2008.02.003.

(108) Tran, Q. K.; Schwabe, K. A.; Jassby, D. Wastewater Reuse for Agriculture: Development of a Regional Water Reuse Decision-Support Model (RWRM) for Cost-Effective Irrigation Sources.

Environ. Sci. Technol. **2016**, *50* (17), 9390–9399. https://doi.org/10.1021/acs.est.6b02073.

(109) Tagliabue, M.; Reverberi, A. P.; Bagatin, R. Boron Removal from Water: Needs, Challenges and Perspectives. *J. Clean. Prod.* **2014**, *77*, 56–64. https://doi.org/10.1016/j.jclepro.2013.11.040.

(110) Meindersma, G. W.; Guijt, C. M.; de Haan, A. B. Desalination and Water Recycling by Air Gap Membrane Distillation. *Desalination* **2006**, *187* (1–3), 291–301. https://doi.org/10.1016/j.desal.2005.04.088.

(111) Werber, J. R.; Deshmukh, A.; Elimelech, M. The Critical Need for Increased Selectivity, Not Increased Water Permeability, for Desalination Membranes. *Environ. Sci. Technol. Lett.* **2016**, *3* (4), 112–120. https://doi.org/10.1021/acs.estlett.6b00050.

(112) Malaeb, L.; Ayoub, G. M. Reverse Osmosis Technology for Water Treatment: State of the Art Review. *Desalination* **2011**, *267* (1), 1–8. https://doi.org/10.1016/j.desal.2010.09.001.

(113) Tran, Q. K.; Jassby, D.; Schwabe, K. A. The Implications of Drought and Water Conservation on the Reuse of Municipal Wastewater: Recognizing Impacts and Identifying Mitigation Possibilities. *Water Res.* **2017**, *124*, 472–481. https://doi.org/10.1016/j.watres.2017.07.069.

(114) Finkelshtain, I.; Huber-Lee, A.; Feinerman, E.; Reznik, A.; Fisher, F.; Joyce, B.; Kan, I. Economic Implications of Agricultural Reuse of Treated Wastewater in Israel: A Statewide Long-Term Perspective. *Ecol. Econ.* **2017**, *135*, 222–233. https://doi.org/10.1016/j.ecolecon.2017.01.013.

(115) Quist-Jensen, C. A.; Macedonio, F.; Drioli, E. Membrane Technology for Water Production in Agriculture: Desalination and Wastewater Reuse. *Desalination* **2015**, *364*, 17–32. https://doi.org/10.1016/j.desal.2015.03.001.

(116) Salgot, M.; Brissaud, F.; Lazarova, V.; Icekson, N.; Cirelli, G.; Jeffrey, P. Enhancement of Integrated Water Management and Water Reuse in Europe and the Middle East. *Water Sci. Technol.* **2018**, *42* (1–2), 193–202. https://doi.org/10.2166/wst.2000.0313.

(117) Safar, M.; Jafar, M.; Abdel-Jawad, M.; Bou-Hamad, S. Standardization of RO Membrane Performance. *Desalination* **1998**, *118* (1–3), 13–21. https://doi.org/10.1016/S0011-9164(98)00070-8.

(118) Bellona, C.; Drewes, J. E.; Xu, P.; Amy, G. Factors Affecting the Rejection of Organic Solutes during NF/RO Treatment - A Literature Review. *Water Res.* **2004**, *38* (12), 2795–2809. https://doi.org/10.1016/j.watres.2004.03.034.

(119) Koseoglu, H.; Kabay, N.; Yüksel, M.; Kitis, M. The Removal of Boron from Model Solutions and Seawater Using Reverse Osmosis Membranes. *Desalination* **2008**, *223* (1–3), 126–133. https://doi.org/10.1016/j.desal.2007.01.189.

(120) Sagiv, A.; Semiat, R. Analysis of Parameters Affecting Boron Permeation through Reverse Osmosis Membranes. *J. Memb. Sci.* **2004**, *243* (1–2), 79–87. https://doi.org/10.1016/j.memsci.2004.05.029.

(121) Taniguchi, M.; Fusaoka, Y.; Nishikawa, T.; Kurihara, M. Boron Removal in RO Seawater Desalination. *Desalination* **2004**, *167* (1–3), 419–426. https://doi.org/10.1016/j.desal.2004.06.157.

(122) Ofir, E.; Brenner, A.; Muuler, K.; Gitis, V. Boron Removal from Seawater by Electro-Chemical Treatment as Part of Water Desalination. *Desalin. Water Treat.* **2011**, *31* (1–3), 102–106. https://doi.org/10.5004/dwt.2011.2334.

(123) Oo, M. H.; Song, L. Effect of PH and Ionic Strength on Boron Removal by RO Membranes. *Desalination* **2009**, *246* (1–3), 605–612. https://doi.org/10.1016/j.desal.2008.06.025.

(124) Hilal, N.; Kim, G. J.; Somerfield, C. Boron Removal from Saline Water: A Comprehensive Review. *Desalination* **2011**, *273* (1), 23–35. https://doi.org/10.1016/j.desal.2010.05.012.

(125) Burn, S.; Hoang, M.; Zarzo, D.; Olewniak, F.; Campos, E.; Bolto, B.; Barron, O. Desalination Techniques - A Review of the Opportunities for Desalination in Agriculture. *Desalination* **2015**, *364*, 2–16. https://doi.org/10.1016/j.desal.2015.01.041.

(126) Sato, T.; Qadir, M.; Yamamoto, S.; Endo, T.; Zahoor, A. Global, Regional, and Country Level Need for Data on Wastewater Generation, Treatment, and Use. *Agric. Water Manag.* **2013**, *130*, 1–13. https://doi.org/10.1016/j.agwat.2013.08.007.

(127) Grant, S. B.; Feldman, D. L.; Marusic, I.; Fletcher, T. D.; Cook, P. L. M.; Hamilton, A. J.; Levin, L. A.; Ambrose, R. F.; Saphores, J.-D.; Sanders, B. F.; Cooper, W. J.; Stewardson, M.; Rosso, D.;

Brown, R.; Jiang, S. C.; Deletic, A. Taking the “Waste” Out of “Wastewater” for Human Water Security and Ecosystem Sustainability. *Science (80-.).* **2012**, *337* (6095), 681–686. https://doi.org/10.1126/science.1216852.

(128) Bodzek, M. The Removal of Boron from the Aquatic Environment—State of the Art. *Desalin. Water Treat.* **2016**, *57* (3), 1107–1131. https://doi.org/10.1080/19443994.2014.1002281.

(129) Chong, M. F.; Lee, K. P.; Chieng, H. J.; Syazwani Binti Ramli, I. I. Removal of Boron from Ceramic Industry Wastewater by Adsorption-Flocculation Mechanism Using Palm Oil Mill Boiler (POMB) Bottom Ash and Polymer. *Water Res.* **2009**, *43* (13), 3326–3334. https://doi.org/10.1016/j.watres.2009.04.044.

(130) Ravenscroft, P.; McArthur, J. M. Mechanism of Regional Enrichment of Groundwater by Boron: The Examples of Bangladesh and Michigan, USA. *Appl. Geochemistry* **2004**, *19* (9), 1413–1430. https://doi.org/10.1016/j.apgeochem.2003.10.014.

(131) Rahmawati, K.; Ghaffour, N.; Aubry, C.; Amy, G. L. Boron Removal Efficiency from Red Sea Water Using Different SWRO/BWRO Membranes. *J. Memb. Sci.* **2012**, *423–424* (5), 522–529. https://doi.org/10.1016/j.memsci.2012.09.004.

(132) Hasson, D.; Shemer, H.; Brook, I.; Zaslavschi, I.; Semiat, R.; Bartels, C.; Wilf, M. Scaling Propensity of Seawater in RO Boron Removal Processes. *J. Memb. Sci.* **2011**, *384* (1–2), 198–204. https://doi.org/10.1016/j.memsci.2011.09.027.

(133) Tu, K. L.; Nghiem, L. D.; Chivas, A. R. Coupling Effects of Feed Solution PH and Ionic Strength on the Rejection of Boron by NF/RO Membranes. *Chem. Eng. J.* **2011**, *168* (2), 700–706. https://doi.org/10.1016/j.cej.2011.01.101.

(134) Cengeloglu, Y.; Arslan, G.; Tor, A.; Kocak, I.; Dursun, N. Removal of Boron from Water by Using Reverse Osmosis. *Sep. Purif. Technol.* **2008**, *64* (2), 141–146. https://doi.org/10.1016/j.seppur.2008.09.006.

(135) Park, P. K.; Lee, S.; Cho, J. S.; Kim, J. H. Full-Scale Simulation of Seawater Reverse Osmosis Desalination Processes for Boron Removal: Effect of Membrane Fouling. *Water Res.* **2012**, *46*

(12), 3796–3804. https://doi.org/10.1016/j.watres.2012.04.021.

(136) Andrews, B.; Davé, B.; López-Serrano, P.; Tsai, S. P.; Frank, R.; Wilf, M.; Koutsakos, E. Effective Scale Control for Seawater RO Operating with High Feed Water PH and Temperature. *Desalination* **2008**, *220* (1–3), 295–304. https://doi.org/10.1016/j.desal.2007.02.041.

(137) Karoui, H.; Riffault, B.; Jeannin, M.; Kahoul, A.; Gil, O.; Ben Amor, M.; Tlili, M. M. Electrochemical Scaling of Stainless Steel in Artificial Seawater: Role of Experimental Conditions on CaCO3 and Mg(OH)2 Formation. *Desalination* **2013**, *311*, 234–240. https://doi.org/10.1016/j.desal.2012.07.011.

(138) Faigon, M.; Hefer, D. Boron Rejection in SWRO at High PH Conditions versus Cascade Design. *Desalination* **2008**, *223* (1–3), 10–16. https://doi.org/10.1016/j.desal.2007.02.070.

(139) Park, C.; Park, P. K.; Mane, P. P.; Hyung, H.; Gandhi, V.; Kim, S. H.; Kim, J. H. Stochastic Cost Estimation Approach for Full-Scale Reverse Osmosis Desalination Plants. *J. Memb. Sci.* **2010**, *364* (1–2), 52–64. https://doi.org/10.1016/j.memsci.2010.07.055.

(140) Chillón Arias, M. F.; Valero i Bru, L.; Prats Rico, D.; Varó Galvañ, P. Approximate Cost of the Elimination of Boron in Desalinated Water by Reverse Osmosis and Ion Exchange Resins. *Desalination* **2011**, *273* (2–3), 421–427. https://doi.org/10.1016/j.desal.2011.01.072.

(141) Dudchenko, A. V.; Rolf, J.; Russell, K.; Duan, W.; Jassby, D. Organic Fouling Inhibition on Electrically Conducting Carbon Nanotube-Polyvinyl Alcohol Composite Ultrafiltration Membranes. *J. Memb. Sci.* **2014**, *468*, 1–10. https://doi.org/10.1016/j.memsci.2014.05.041.

(142) Duan, W.; Dudchenko, A.; Mende, E.; Flyer, C.; Zhu, X.; Jassby, D. Electrochemical Mineral Scale Prevention and Removal on Electrically Conducting Carbon Nanotube – Polyamide Reverse Osmosis Membranes. *Environ. Sci. Process. Impacts* **2014**, *16* (6), 1300. https://doi.org/10.1039/c3em00635b.

(143) Duan, W.; Ronen, A.; Walker, S.; Jassby, D. Polyaniline-Coated Carbon Nanotube Ultrafiltration Membranes: Enhanced Anodic Stability for in Situ Cleaning and Electro-Oxidation Processes. *ACS Appl. Mater. Interfaces* **2016**, *8* (34), 22574–22584. https://doi.org/10.1021/acsami.6b07196.

(144) Zhu, X.; Dudchenko, A.; Gu, X.; Jassby, D. Surfactant-Stabilized Oil Separation from Water Using Ultrafiltration and Nanofiltration. *J. Memb. Sci.* **2017**, *529* (February), 159–169. https://doi.org/10.1016/j.memsci.2017.02.004.

(145) Tang, L.; Iddya, A.; Zhu, X.; Dudchenko, A. V.; Duan, W.; Turchi, C.; Vanneste, J.; Cath, T. Y.; Jassby, D. Enhanced Flux and Electrochemical Cleaning of Silicate Scaling on Carbon Nanotube-Coated Membrane Distillation Membranes Treating Geothermal Brines. *ACS Appl. Mater. Interfaces* **2017**, *9* (44), 38594–38605. https://doi.org/10.1021/acsami.7b12615.

(146) Lopez, F. J.; Gimenez, E.; Hernandez, F. Analytical Study on the Determination of Boron in Environmental Water Samples. *Fresenius J. Anal. Chem.* **1993**, *346* (10–11), 984–987. https://doi.org/10.1007/BF00322763.

(147) Green, G. H.; Blincoe, C.; Weeth, H. J. Boron Contamination from Borosilicate Glass. *J. Agric. Food Chem.* **1976**, *24* (6), 1245–1246. https://doi.org/10.1021/jf60208a016.

(148) Slade, A.; Jassby, D. Affordable, Flexible, and Modular: A Guide to Open-Source Membrane-Based Water Treatment Systems. *Environ. Sci. Water Res. Technol.* **2016**, *2* (6), 965–974. https://doi.org/10.1039/c6ew00194g.

(149) Kezia, K.; Lee, J.; Ogieglo, W.; Hill, A.; Benes, N. E.; Kentish, S. E. The Transport of Hydronium and Hydroxide Ions through Reverse Osmosis Membranes. *J. Memb. Sci.* **2014**, *459*, 197–206. https://doi.org/10.1016/j.memsci.2014.02.018.

(150) Karagiannis, I. C.; Soldatos, P. G. Water Desalination Cost Literature: Review and Assessment. *Desalination* **2008**, *223* (1–3), 448–456. https://doi.org/10.1016/j.desal.2007.02.071.

(151) Fritzmann, C.; Löwenberg, J.; Wintgens, T.; Melin, T. State-of-the-Art of Reverse Osmosis Desalination. *Desalination* **2007**, *216* (1–3), 1–76. https://doi.org/10.1016/j.desal.2006.12.009.

(152) Redondo, J.; Busch, M.; Witte, J.-P. De. Boron Removal from Seawater Using FILMTECTM High Rejection S WRO Membranes. *Desalination* **2003**, *156* (May), 229–238.

(153) Halim, M. A.; Majumder, R. K.; Nessa, S. A.; Hiroshiro, Y.; Uddin, M. J.; Shimada, J.; Jinno, K. Hydrogeochemistry and Arsenic Contamination of Groundwater in the Ganges Delta Plain,

Bangladesh. *J. Hazard. Mater.* **2009**, *164* (2–3), 1335–1345. https://doi.org/10.1016/j.jhazmat.2008.09.046.

(154) Sarath Prasanth, S. V.; Magesh, N. S.; Jitheshlal, K. V.; Chandrasekar, N.; Gangadhar, K. Evaluation of Groundwater Quality and Its Suitability for Drinking and Agricultural Use in the Coastal Stretch of Alappuzha District, Kerala, India. *Appl. Water Sci.* **2012**, *2* (3), 165–175. https://doi.org/10.1007/s13201-012-0042-5.

(155) Salehi, S.; Chizari, M.; Sadighi, H.; Bijani, M. Evaluation Des Utilisateurs Des Eaux Souterraines Pour l'agriculture En Iran: Un Biais Environnemental Culturel. *Hydrogeol. J.* **2018**, *26* (1), 285–295. https://doi.org/10.1007/s10040-017-1634-9.

(156) Sandoval, M. A.; Fuentes, R.; Thiam, A.; Salazar, R. Arsenic and Fluoride Removal by Electrocoagulation Process: A General Review. *Sci. Total Environ.* **2021**, *753*, 142108. https://doi.org/10.1016/j.scitotenv.2020.142108.

(157) Bibi, S.; Kamran, M. A.; Sultana, J.; Farooqi, A. Occurrence and Methods to Remove Arsenic and Fluoride Contamination in Water. *Environ. Chem. Lett.* **2017**, *15* (1), 125–149. https://doi.org/10.1007/s10311-016-0590-2.

(158) Dugan, H. A.; Summers, J. C.; Skaff, N. K.; Krivak-Tetley, F. E.; Doubek, J. P.; Burke, S. M.; Bartlett, S. L.; Arvola, L.; Jarjanazi, H.; Korponai, J.; Kleeberg, A.; Monet, G.; Monteith, D.; Moore, K.; Rogora, M.; Hanson, P. C.; Weathers, K. C. Long-Term Chloride Concentrations in North American and European Freshwater Lakes. *Sci. Data* **2017**, *4*, 1–11. https://doi.org/10.1038/sdata.2017.101.

(159) Niazi, A.; Bentley, L. R.; Hayashi, M. Estimation of Spatial Distribution of Groundwater Recharge from Stream Baseflow and Groundwater Chloride. *J. Hydrol.* **2017**, *546*, 380–392. https://doi.org/10.1016/j.jhydrol.2017.01.032.

(160) Marin, P.; Monte-Blanco, S. P. D.; Módenes, A. N.; Bergamasco, R.; Yamaguchi, N. U.; Coldebella, P. F.; Ribeiro, R. M.; Paraiso, P. R. Equilibrium and Kinetic Mechanisms of Fluoride Ions Adsorption onto Activated Alumina. *Chem. Eng. Trans.* **2017**, *57* (2012), 607–612.

https://doi.org/10.3303/CET1757102.

(161) Ghorai, S.; Pant, K. K. Equilibrium, Kinetics and Breakthrough Studies for Adsorption of Fluoride on Activated Alumina. *Sep. Purif. Technol.* **2005**, *42* (3), 265–271. https://doi.org/10.1016/j.seppur.2004.09.001.

(162) Guzmán, A.; Nava, J. L.; Coreño, O.; Rodríguez, I.; Gutiérrez, S. Arsenic and Fluoride Removal from Groundwater by Electrocoagulation Using a Continuous Filter-Press Reactor. *Chemosphere* **2016**, *144*, 2113–2120. https://doi.org/10.1016/j.chemosphere.2015.10.108.

(163) World Health Organization. *Guidelines for Drinking-Water Quality*; 2017.

(164) Gregor, J. Arsenic Removal during Conventional Aluminium-Based Drinking-Water Treatment. *Water Res.* **2001**, *35* (7), 1659–1664. https://doi.org/10.1016/S0043-1354(00)00424-3.

(165) Stackelberg, P. E.; Gibs, J.; Furlong, E. T.; Meyer, M. T.; Zaugg, S. D.; Lippincott, R. L. Efficiency of Conventional Drinking-Water-Treatment Processes in Removal of Pharmaceuticals and Other Organic Compounds. *Sci. Total Environ.* **2007**, *377* (2–3), 255–272. https://doi.org/10.1016/j.scitotenv.2007.01.095.

(166) Kim, H. C.; Yu, M. J. Characterization of Aquatic Humic Substances to DBPs Formation in Advanced Treatment Processes for Conventionally Treated Water. *J. Hazard. Mater.* **2007**, *143* (1–2), 486–493. https://doi.org/10.1016/j.jhazmat.2006.09.063.

(167) Ahdab, Y. D.; Lienhard, J. H. *Desalination of Brackish Groundwater to Improve Water Quality and Water Supply*; INC, 2021. https://doi.org/10.1016/b978-0-12-818172-0.00041-4.

(168) Kim, H. A.; Choi, J. H.; Takizawa, S. Comparison of Initial Filtration Resistance by Pretreatment Processes in the Nanofiltration for Drinking Water Treatment. *Sep. Purif. Technol.* **2007**, *56* (3), 354–362. https://doi.org/10.1016/j.seppur.2007.02.016.

(169) Ayoub, G. M.; Korban, L.; Al-Hindi, M.; Zayyat, R. Brackish Water Desalination: An Effective Pretreatment Process for Reverse Osmosis Systems. *Water. Air. Soil Pollut.* **2019**, *230* (10). https://doi.org/10.1007/s11270-019-4299-2.

(170) Jamaly, S.; Darwish, N. N.; Ahmed, I.; Hasan, S. W. A Short Review on Reverse Osmosis

Pretreatment Technologies. *Desalination* **2014**, *354*, 30–38. https://doi.org/10.1016/j.desal.2014.09.017.

(171) Yiantsios, S. G.; Karabelas, A. J. An Assessment of the Silt Density Index Based on RO Membrane Colloidal Fouling Experiments with Iron Oxide Particles. *Desalination* **2003**, *151* (3), 229–238. https://doi.org/10.1016/S0011-9164(02)01015-9.

(172) Aoudj, S.; Drouiche, N.; Hecini, M.; Ouslimane, T.; Palaouane, B. Coagulation as a Post-Treatment Method for the Defluoridation of Photovoltaic Cell Manufacturing Wastewater. *Procedia Eng.* **2012**, *33*, 111–120. https://doi.org/10.1016/j.proeng.2012.01.1183.

(173) Hamamoto, S.; Kishimoto, N. Characteristics of Fluoride Adsorption onto Aluminium(III) and Iron(III) Hydroxide Flocs. *Sep. Sci. Technol.* **2017**, *52* (1), 42–50. https://doi.org/10.1080/01496395.2016.1242628.

(174) Khan, M. M. T.; Yamamoto, K.; Ahmed, M. F. A Low Cost Technique of Arsenic Removal from Drinking Water by Coagulation Using Ferric Chloride Salt and Alum. *Water Sci. Technol. Water Supply* **2002**, *2* (2), 281–288. https://doi.org/10.2166/ws.2002.0074.

(175) Ge, J.; Guha, B.; Lippincott, L.; Cach, S.; Wei, J.; Su, T. L.; Meng, X. Challenges of Arsenic Removal from Municipal Wastewater by Coagulation with Ferric Chloride and Alum. *Sci. Total Environ.* **2020**, *725*, 138351. https://doi.org/10.1016/j.scitotenv.2020.138351.

(176) Outram, J. G.; Couperthwaite, S. J.; Millar, G. J. Comparitve Analysis of the Physical, Chemical and Structural Characteristics and Performance of Manganese Greensands. *J. Water Process Eng.* **2016**, *13*, 16–26. https://doi.org/10.1016/j.jwpe.2016.07.006.

(177) Wong, J. M. Chlorination-Filtration for Iron and Manganese Removal. *J. / Am. Water Work. Assoc.* **1984**, *76* (1), 76–79. https://doi.org/10.1002/j.1551-8833.1984.tb05265.x.

(178) Alling, S. F. Continuously Regenerated Greensand for Iron and Manganese Removal. *J. Am. Water Works Assoc.* **1963**, *55* (6), 749–752. https://doi.org/10.1002/j.1551-8833.1963.tb01084.x.

(179) Kempic, J. B. Arsenic Removal Technologies: An Evaluation of Cost and Performance. *Arsenic* **1997**, 393–405. https://doi.org/10.1007/978-94-011-5864-0_31.

(180) Su, T.; Guan, X.; Gu, G.; Wang, J. Adsorption Characteristics of As(V), Se(IV), and V(V) onto Activated Alumina: Effects of PH, Surface Loading, and Ionic Strength. *J. Colloid Interface Sci.* **2008**, *326* (2), 347–353. https://doi.org/10.1016/j.jcis.2008.07.026.

(181) Kennedy, A. M.; Arias-Paic, M. Fixed-Bed Adsorption Comparisons of Bone Char and Activated Alumina for the Removal of Fluoride from Drinking Water. *J. Environ. Eng. (United States)* **2020**, *146* (1), 1–11. https://doi.org/10.1061/(ASCE)EE.1943-7870.0001625.

(182) Tran, Q. K.; Schwabe, K. A.; Jassby, D. Wastewater Reuse for Agriculture: Development of a Regional Water Reuse Decision-Support Model (RWRM) for Cost-Effective Irrigation Sources. *Environ. Sci. Technol.* **2016**, *50* (17), 9390–9399. https://doi.org/10.1021/acs.est.6b02073.

(183) Havens, J. S. *Reconnaissance of Ground Water in Vincinity of Wichita Mountains Southwestern Okalahoma*; 1983.

(184) 2540 SOLIDS (2017). In *Standard Methods For the Examination of Water and Wastewater*. https://doi.org/10.2105/SMWW.2882.030.

(185) Babcock, D. B.; Singer, P. C. Chlorination and Coagulation of Humic and Fulvic Acids. *J Am Water Work. Assoc* **1979**, *71* (3), 149–152. https://doi.org/10.1002/j.1551-8833.1979.tb04318.x.

(186) Bratby, J. *Coagulation and Flocculation in Water and Wastewater Treatment*; 2006. https://doi.org/10.2166/9781780407500.

(187) Jiao, R.; Fabris, R.; Chow, C. W. K.; Drikas, M.; van Leeuwen, J.; Wang, D.; Xu, Z. Influence of Coagulation Mechanisms and Floc Formation on Filterability. *J. Environ. Sci. (China)* **2017**, *57*, 338–345. https://doi.org/10.1016/j.jes.2017.01.006.

(188) Huang, C.; Shiu, H. Interactions between Alum and Organics in Coagulation. *Colloids Surfaces A Physicochem. Eng. Asp.* **1996**, *113* (1–2), 155–163. https://doi.org/10.1016/0927-7757(96)03543-1.

(189) Amirtharajah, A.; Mills, K. M. Rapid-Mix Design for Mechanisms of Alum Coagulation. *J. / Am. Water Work. Assoc.* **1982**, *74* (4), 210–216. https://doi.org/10.1002/j.1551-8833.1982.tb04890.x.

(190) Benschoten, J. E. V.; Edzwald, J. K. Chemical Aspects of Coagulation Using Aluminum Salts-

I.Hydrolytic Reactions of Alum and Polyaluminum Chloride. *Water Res.* **1990**, *24* (12), 1519–1526.

(191) EH, K.; THJ, M.; N, M. Use of Natural Coagulants for Removal of COD, Oil and Turbidity from Produced Waters in the Petroleum Industry. *J. Pet. Environ. Biotechnol.* **2018**, *09* (03). https://doi.org/10.4172/2157-7463.1000374.

(192) Prakash, K. L.; Somashekar, R. K. Groundwater Quality - Assessment on Anekal Taluk, Bangalore Urban District, India. *J. Environ. Biol.* **2006**, *27* (4), 633–637.

(193) Aoudj, S.; Khelifa, A.; Drouiche, N.; Hecini, M. Removal of Fluoride and Turbidity from Semiconductor Industry Wastewater by Combined Coagulation and Electroflotation. *Desalin. Water Treat.* **2016**, *57* (39), 18398–18405. https://doi.org/10.1080/19443994.2015.1095120.

(194) He, Z.; Liu, R.; Xu, J.; Liu, H.; Qu, J. Defluoridation by Al-Based Coagulation and Adsorption: Species Transformation of Aluminum and Fluoride. *Sep. Purif. Technol.* **2015**, *148*, 68–75. https://doi.org/10.1016/j.seppur.2015.05.005.

(195) Pramanik, B. K.; Pramanik, S. K.; Suja, F. Removal of Arsenic and Iron Removal from Drinking Water Using Coagulation and Biological Treatment. *J. Water Health* **2016**, *14* (1), 90–96. https://doi.org/10.2166/wh.2015.159.

(196) Zhang, J.; Brutus, T. E.; Cheng, J.; Meng, X. Fluoride Removal by Al, Ti, and Fe Hydroxides and Coexisting Ion Effect. *J. Environ. Sci. (China)* **2017**, *57* (Mcl), 190–195. https://doi.org/10.1016/j.jes.2017.03.015.

(197) Letterman, R. D.; Tabatabaie, M.; Ames, R. S. Effect of the Bicarbonate Ion Concentration on Flocculation With Aluminum Sulfate. *J. / Am. Water Work. Assoc.* **1979**, *71* (8), 467–472. https://doi.org/10.1002/j.1551-8833.1979.tb04395.x.

(198) Millar, G. J.; Couperthwaite, S. J.; Dawes, L. A.; Thompson, S.; Spencer, J. Activated Alumina for the Removal of Fluoride Ions from High Alkalinity Groundwater: New Insights from Equilibrium and Column Studies with Multicomponent Solutions. *Sep. Purif. Technol.* **2017**, *187*, 14–24. https://doi.org/10.1016/j.seppur.2017.06.042.

(199) Jada, A.; Ait Akbour, R.; Douch, J. Surface Charge and Adsorption from Water onto Quartz Sand of Humic Acid. *Chemosphere* **2006**, *64* (8), 1287–1295. https://doi.org/10.1016/j.chemosphere.2005.12.063.

(200) Tripathy, S. S.; Raichur, A. M. Enhanced Adsorption Capacity of Activated Alumina by Impregnation with Alum for Removal of As(V) from Water. *Chem. Eng. J.* **2008**, *138* (1–3), 179–186. https://doi.org/10.1016/j.cej.2007.06.028.

(201) Dashtban Kenari, S. L.; Barbeau, B. Size and Zeta Potential of Oxidized Iron and Manganese in Water Treatment: Influence of PH, Ionic Strength, and Hardness. *J. Environ. Eng.* **2016**, *142* (5), 04016010. https://doi.org/10.1061/(asce)ee.1943-7870.0001101.

(202) Hanson, A.; Bates, J.; Heil, D.; Bristol, A. Arsenic Removal from Water Using Manganese Greensand: Laboratory Scale Batch and Column Studies. *New Mex. State Univ.* **1999**, No. 142596-{FC}, 81–05016.

(203) Siddique, T. A.; Dutta, N. K.; Choudhury, N. R. Nanofiltration for Arsenic Removal: Challenges, Recent Developments, and Perspectives. *Nanomaterials* **2020**, *10* (7), 1–37. https://doi.org/10.3390/nano10071323.

(204) Jarma, Y. A.; Karaoğlu, A.; Tekin, Ö.; Baba, A.; Ökten, H. E.; Tomaszewska, B.; Bostancı, K.; Arda, M.; Kabay, N. Assessment of Different Nanofiltration and Reverse Osmosis Membranes for Simultaneous Removal of Arsenic and Boron from Spent Geothermal Water. *J. Hazard. Mater.* **2020**, 124129. https://doi.org/10.1016/j.jhazmat.2020.124129.

(205) Kumar, R.; Kachwaha, M.; Verma, S.; Patidar, D. Quick Detection of Iron in Contaminated Water before Feeding to RO Membranes. *SN Appl. Sci.* **2019**, *1* (5), 1–6. https://doi.org/10.1007/s42452-019-0379-6.

(206) Hoinkis, J.; Valero-Freitag, S.; Caporgno, M. P.; Pätzold, C. Removal of Nitrate and Fluoride by Nanofiltration - A Comparative Study. *Desalin. Water Treat.* **2011**, *30* (1–3), 278–288. https://doi.org/10.5004/dwt.2011.2103.

(207) Gündoğdu, M.; Kabay, N.; Yiğit, N.; Kitiş, M.; Pek, T.; Yüksel, M. Effect of Concentrate

Recirculation on the Product Water Quality of Integrated MBR – NF Process for Wastewater Reclamation and Industrial Reuse. *J. Water Process Eng.* **2019**, *29* (August). https://doi.org/10.1016/j.jwpe.2017.08.023.

(208) US Environmental Protection Agency. *2018 Edition of the Drinking Water Standards and Health Advisories Tables*; 2018.

(209) Bratby, J. R. Optimizing Coagulants and Flocculant Aids for Settling. *J. Am. Water Works Assoc.* **1981**, *73* (6), 312–318. https://doi.org/10.1002/j.1551-8833.1981.tb04720.x.

(210) Cheng, R. C.; Krasner, S. W.; Green, J. F.; Wattier, K. L. Enhanced Coagulation: A Preliminary Evaluation. *J. Am. Water Works Assoc.* **1995**, *87* (2), 91–103. https://doi.org/10.1002/j.1551-8833.1995.tb06321.x.

(211) Qureshi, N.; Nelson, S. Radium Removal by HMO and Manganese Greensand. *J. / Am. Water Work. Assoc.* **2003**, *95* (3), 101–108. https://doi.org/10.1002/j.1551-8833.2003.tb10318.x.

(212) Office of Ground Water and Drinking Water; office of Radiation and Indoor Air U.S. Environmental Protection Agency. *Preliminary Health Risk Reduction and Cost Analysis*; 2000.

(213) Ghosh, D.; Gupta, A. Economic Justification and Eco-Friendly Approach for Regeneration of Spent Activated Alumina for Arsenic Contaminated Groundwater Treatment. *Resour. Conserv. Recycl.* **2012**, *61*, 118–124. https://doi.org/10.1016/j.resconrec.2012.01.005.

(214) Stewart, H. T.; Kessler, K. J. *Evaluation of Arsenic Removal by Activated Alumina Filtration at a Small Community Public Water Supply*; 1989.

(215) Uddin, M. T.; Mozumder, M. S. I.; Figoli, a; Islam, M. A.; Drioli, E. Arsenic Removal by Conventional and Membrane Technology: An Overview. **2007**, *14* (September), 441–450.

(216) Bergman, R. A. Cost of Membrane Softening in Florida. *J. / Am. Water Work. Assoc.* **1996**, *88* (5), 32–43. https://doi.org/10.1002/j.1551-8833.1996.tb06552.x.

(217) Costa, A. R.; de Pinho, M. N. Performance and Cost Estimation of Nanofiltration for Surface Water Treatment in Drinking Water Production. *Desalination* **2006**, *196* (1–3), 55–65. https://doi.org/10.1016/j.desal.2005.08.030.

(218) Elazhar, F.; Tahaikt, M.; Achatei, A.; Elmidaoui, F.; Taky, M.; El Hannouni, F.; Laaziz, I.; Jariri, S.; El Amrani, M.; Elmidaoui, A. Economical Evaluation of the Fluoride Removal by Nanofiltration. *Desalination* **2009**, *249* (1), 154–157. https://doi.org/10.1016/j.desal.2009.06.017.

(219) Odem, W. *Nanofiltration of a High Salinity Groundwater on the Hopi Reservation*; 1995.

(220) Arroyo, J.; Shirazi, S. *Cost of Brackish Groundwater Desalination in Texas*; 2012.

(221) Wittholz, M. K.; O'Neill, B. K.; Colby, C. B.; Lewis, D. Estimating the Cost of Desalination Plants Using a Cost Database. *Desalination* **2008**, *229* (1–3), 10–20. https://doi.org/10.1016/j.desal.2007.07.023.

(222) Owen, G.; Bandi, M.; Howell, J. A.; Churchouse, S. J. Economic Assessment of Membrane Processes for Water and Waste Water Treatment. *J. Memb. Sci.* **1995**, *102* (C), 77–91. https://doi.org/10.1016/0376-7388(94)00261-V.

(223) Gong, W. X.; Qu, J. H.; Liu, R. P.; Lan, H. C. Effect of Aluminum Fluoride Complexation on Fluoride Removal by Coagulation. *Colloids Surfaces A Physicochem. Eng. Asp.* **2012**, *395*, 88–93. https://doi.org/10.1016/j.colsurfa.2011.12.010.

(224) Chauhan, V. S.; Dwivedi, P. K.; Iyengar, L. Investigations on Activated Alumina Based Domestic Defluoridation Units. *J. Hazard. Mater.* **2007**, *139* (1), 103–107. https://doi.org/10.1016/j.jhazmat.2006.06.014.

(225) Ghorai, S.; Pant, K. K. Investigations on the Column Performance of Fluoride Adsorption by Activated Alumina in a Fixed-Bed. *Chem. Eng. J.* **2004**, *98* (1–2), 165–173. https://doi.org/10.1016/j.cej.2003.07.003.

(226) Gebauer, D.; Völkel, A.; Cölfen, H. Stable Prenucleation Calcium Carbonate Clusters. *Science (80-.).* **2008**, *322* (5909), 1819–1822. https://doi.org/10.1126/science.1164271.

(227) Tut Haklidir, F.; Haklidir, M. Fuzzy Control of Calcium Carbonate and Silica Scales in Geothermal Systems. *Geothermics* **2017**, *70* (July), 230–238. https://doi.org/10.1016/j.geothermics.2017.07.003.

(228) Amjad, Z. Calcium Sulfate Dihydrate (Gypsum) Scale Formation on Heat Exchanger Surfaces:

The Influence of Scale Inhibitors. *J. Colloid Interface Sci.* **1988**, *123* (2), 523–536. https://doi.org/10.1016/0021-9797(88)90274-3.

(229) Rioyo, J.; Aravinthan, V.; Bundschuh, J.; Lynch, M. Research on 'High-PH Precipitation Treatment' for RO Concentrate Minimization and Salt Recovery in a Municipal Groundwater Desalination Facility. *Desalination* **2018**, *439* (October 2017), 168–178. https://doi.org/10.1016/j.desal.2018.04.020.

(230) Rahardianto, A.; McCool, B. C.; Cohen, Y. Accelerated Desupersaturation of Reverse Osmosis Concentrate by Chemically-Enhanced Seeded Precipitation. *Desalination* **2010**, *264* (3), 256–267. https://doi.org/10.1016/j.desal.2010.06.018.

(231) Rahardianto, A.; Gao, J.; Gabelich, C. J.; Williams, M. D.; Cohen, Y. High Recovery Membrane Desalting of Low-Salinity Brackish Water: Integration of Accelerated Precipitation Softening with Membrane RO. *J. Memb. Sci.* **2007**, *289* (1–2), 123–137. https://doi.org/10.1016/j.memsci.2006.11.043.

(232) Elimelech, M.; Bhattacharjee, S. A Novel Approach for Modeling Concentration Polarization in Crossflow Membrane Filtration Based on the Equivalence of Osmotic Pressure Model and Filtration Theory. *J. Memb. Sci.* **1998**, *145* (2), 223–241. https://doi.org/10.1016/S0376-7388(98)00078-7.

(233) Kim, S.; Hoek, E. M. V. Modeling Concentration Polarization in Reverse Osmosis Processes. *Desalination* **2005**, *186* (1–3), 111–128. https://doi.org/10.1016/j.desal.2005.05.017.

(234) Kucera, J. Reverse Osmosis Membrane Fouling Control. In *The Science and Technology of Industrial Water Treatment*; Taylor & Francis: London, 2010; pp 247–270. https://doi.org/10.1201/9781420071450.

(235) Liu, Q.; Xu, G. R.; Das, R. Inorganic Scaling in Reverse Osmosis (RO) Desalination: Mechanisms, Monitoring, and Inhibition Strategies. *Desalination* **2019**, *468* (June), 114065. https://doi.org/10.1016/j.desal.2019.07.005.

(236) Younos, T. Environmental Issues of Desalination. *J. Contemp. Water Res. Educ.* **2009**, *132* (1),

11–18. https://doi.org/10.1111/j.1936-704x.2005.mp132001003.x.

(237) Walha, K.; Amar, R. Ben; Firdaous, L.; Quéméneur, F.; Jaouen, P. Brackish Groundwater Treatment by Nanofiltration, Reverse Osmosis and Electrodialysis in Tunisia: Performance and Cost Comparison. *Desalination* **2007**, *207* (1–3), 95–106. https://doi.org/10.1016/j.desal.2006.03.583.

(238) Galanakis, C. M.; Fountoulis, G.; Gekas, V. Nanofiltration of Brackish Groundwater by Using a Polypiperazine Membrane. *Desalination* **2012**, *286*, 277–284. https://doi.org/10.1016/j.desal.2011.11.035.

(239) Badruzzaman, M.; Subramani, A.; DeCarolis, J.; Pearce, W.; Jacangelo, J. G. Impacts of Silica on the Sustainable Productivity of Reverse Osmosis Membranes Treating Low-Salinity Brackish Groundwater. *Desalination* **2011**, *279* (1–3), 210–218. https://doi.org/10.1016/j.desal.2011.06.013.

(240) Rahardianto, A.; Mccool, B. C.; Cohen, Y. Reverse Osmosis Desalting of Inland Brackish Water of High Gypsum Scaling Propensity: Kinetics and Mitigation of Membrane Mineral Scaling. *Environ. Sci. Technol.* **2008**, *42* (12), 4292–4297. https://doi.org/10.1021/es702463a.

(241) Warsinger, D. M.; Tow, E. W.; Maswadeh, L. A.; Connors, G. B.; Swaminathan, J.; Lienhard V, J. H. Inorganic Fouling Mitigation by Salinity Cycling in Batch Reverse Osmosis. *Water Res.* **2018**, *137*, 384–394. https://doi.org/10.1016/j.watres.2018.01.060.

(242) Koo, T.; Lee, Y. J.; Sheikholeslami, R. Silica Fouling and Cleaning of Reverse Osmosis Membranes. *Desalination* **2001**, *139* (1–3), 43–56. https://doi.org/10.1016/S0011-9164(01)00293-4.

(243) Gebauer, D.; Cölfen, H. Prenucleation Clusters and Non-Classical Nucleation. *Nano Today* **2011**, *6* (6), 564–584. https://doi.org/10.1016/j.nantod.2011.10.005.

(244) Saharay, M.; Yazaydin, A. O.; Kirkpatrick, R. J. Dehydration-Induced Amorphous Phases of Calcium Carbonate. *J. Phys. Chem. B* **2013**, *117* (12), 3328–3336. https://doi.org/10.1021/jp308353t.

(245) Saha, A.; Lee, J.; Pancera, S. M.; Bräeu, M. F.; Kempter, A.; Tripathi, A.; Bose, A. New Insights

into the Transformation of Calcium Sulfate Hemihydrate to Gypsum Using Time-Resolved Cryogenic Transmission Electron Microscopy. *Langmuir* **2012**, *28* (30), 11182–11187. https://doi.org/10.1021/la3024474.

(246) Baoxia, M. I.; Elimelech, M. Gypsum Scaling and Cleaning in Forward Osmosis: Measurements and Mechanisms. *Environ. Sci. Technol.* **2010**, *44* (6), 2022–2028. https://doi.org/10.1021/es903623r.

(247) McCool, B. C.; Rahardianto, A.; Faria, J.; Kovac, K.; Lara, D.; Cohen, Y. Feasibility of Reverse Osmosis Desalination of Brackish Agricultural Drainage Water in the San Joaquin Valley. *Desalination* **2010**, *261* (3), 240–250. https://doi.org/10.1016/j.desal.2010.05.031.

(248) Bush, J. A.; Vanneste, J.; Gustafson, E. M.; Waechter, C. A.; Jassby, D.; Turchi, C. S.; Cath, T. Y. Prevention and Management of Silica Scaling in Membrane Distillation Using PH Adjustment. *J. Memb. Sci.* **2018**, *554*, 366–377. https://doi.org/10.1016/j.memsci.2018.02.059.

(249) Sweity, A.; Oren, Y.; Ronen, Z.; Herzberg, M. The Influence of Antiscalants on Biofouling of RO Membranes in Seawater Desalination. *Water Res.* **2013**, *47* (10), 3389–3398. https://doi.org/10.1016/j.watres.2013.03.042.

(250) Vrouwenvelder, J. S.; Manolarakis, S. A.; Veenendaal, H. R.; Van Der Kooij, D. Biofouling Potential of Chemicals Used for Scale Control in RO and NF Membranes. *Desalination* **2000**, *132* (1–3), 1–10. https://doi.org/10.1016/S0011-9164(00)00129-6.

(251) Li, H. Y.; Ma, W.; Wang, L.; Liu, R.; Wei, L. Sen; Wang, Q. Inhibition of Calcium and Magnesium-Containing Scale by a New Antiscalant Polymer in Laboratory Tests and a Field Trial. *Desalination* **2006**, *196* (1–3), 237–247. https://doi.org/10.1016/j.desal.2005.11.024.

(252) Antony, A.; Low, J. H.; Gray, S.; Childress, A. E.; Le-Clech, P.; Leslie, G. Scale Formation and Control in High Pressure Membrane Water Treatment Systems: A Review. *J. Memb. Sci.* **2011**, *383* (1–2), 1–16. https://doi.org/10.1016/j.memsci.2011.08.054.

(253) Drak, A.; Glucina, K.; Busch, M.; Hasson, D.; Laîne, J. M.; Semiat, R. Laboratory Technique for Predicting the Scaling Propensity of RO Feed Waters. *Desalination* **2000**, *132* (1–3), 233–242.

https://doi.org/10.1016/S0011-9164(00)00154-5.

(254) Matin, A.; Rahman, F.; Shafi, H. Z.; Zubair, S. M. Scaling of Reverse Osmosis Membranes Used in Water Desalination: Phenomena, Impact, and Control; Future Directions. *Desalination* **2019**, *455* (January), 135–157. https://doi.org/10.1016/j.desal.2018.12.009.

(255) Venkatesan, A.; Wankat, P. C. Simulation of Ion Exchange Water Softening Pretreatment for Reverse Osmosis Desalination of Brackish Water. *Desalination* **2011**, *271* (1–3), 122–131. https://doi.org/10.1016/j.desal.2010.12.022.

(256) Comstock, S. E. H.; Boyer, T. H.; Graf, K. C. Treatment of Nanofiltration and Reverse Osmosis Concentrates: Comparison of Precipitative Softening, Coagulation, and Anion Exchange. *Water Res.* **2011**, *45* (16), 4855–4865. https://doi.org/10.1016/j.watres.2011.06.035.

(257) Gu, H.; Bartman, A. R.; Uchymiak, M.; Christofides, P. D.; Cohen, Y. Self-Adaptive Feed Flow Reversal Operation of Reverse Osmosis Desalination. *Desalination* **2013**, *308*, 63–72. https://doi.org/10.1016/j.desal.2012.07.041.

(258) Uchymiak, M.; Bartman, A. R.; Daltrophe, N.; Weissman, M.; Gilron, J.; Christofides, P. D.; Kaiser, W. J.; Cohen, Y. Brackish Water Reverse Osmosis (BWRO) Operation in Feed Flow Reversal Mode Using an Ex Situ Scale Observation Detector (EXSOD). *J. Memb. Sci.* **2009**, *341* (1–2), 60–66. https://doi.org/10.1016/j.memsci.2009.05.039.

(259) Bartman, A. R.; McFall, C. W.; Christofides, P. D.; Cohen, Y. Model-Predictive Control of Feed Flow Reversal in a Reverse Osmosis Desalination Process. *J. Process Control* **2009**, *19* (3), 433–442. https://doi.org/10.1016/j.jprocont.2008.06.016.

(260) Xu, X.; Zhang, H.; Yu, M.; Wang, Y.; Gao, T.; Yang, F. Conductive Thin Film Nanocomposite Forward Osmosis Membrane (TFN-FO) Blended with Carbon Nanoparticles for Membrane Fouling Control. *Sci. Total Environ.* **2019**, *697*, 134050. https://doi.org/10.1016/j.scitotenv.2019.134050.

(261) Ahmed, F.; Lalia, B. S.; Kochkodan, V.; Hilal, N.; Hashaikeh, R. Electrically Conductive Polymeric Membranes for Fouling Prevention and Detection: A Review. *Desalination* **2016**, *391*,

1–15. https://doi.org/10.1016/j.desal.2016.01.030.

(262) Hasson, D.; Lumelsky, V.; Greenberg, G.; Pinhas, Y.; Semiat, R. Development of the Electrochemical Scale Removal Technique for Desalination Applications. *Desalination* **2008**, *230* (1–3), 329–342. https://doi.org/10.1016/j.desal.2008.01.004.

(263) Tijing, L. D.; Lee, D. H.; Kim, D. W.; Cho, Y. I.; Kim, C. S. Effect of High-Frequency Electric Fields on Calcium Carbonate Scaling. *Desalination* **2011**, *279* (1–3), 47–53. https://doi.org/10.1016/j.desal.2011.05.072.

(264) Abd-El-Khalek, D. E.; Abd-El-Nabey, B. A. Evaluation of Sodium Hexametaphosphate as Scale and Corrosion Inhibitor in Cooling Water Using Electrochemical Techniques. *Desalination* **2013**, *311*, 227–233. https://doi.org/10.1016/j.desal.2012.11.017.

(265) Dudchenko, A. V.; Rolf, J.; Shi, L.; Olivas, L.; Duan, W.; Jassby, D. Coupling Underwater Superoleophobic Membranes with Magnetic Pickering Emulsions for Fouling-Free Separation of Crude Oil/Water Mixtures: An Experimental and Theoretical Study. *ACS Nano* **2015**, *9* (10), 9930–9941. https://doi.org/10.1021/acsnano.5b04880.

(266) Zhu, X.; Jassby, D. Electroactive Membranes for Water Treatment: Enhanced Treatment Functionalities, Energy Considerations, and Future Challenges. *Acc. Chem. Res.* **2019**, *52*, 1177–1186. https://doi.org/10.1021/acs.accounts.8b00558.

(267) Gao, S.; Zhu, Y.; Gong, Y.; Wang, Z.; Fang, W.; Jin, J. Ultrathin Polyamide Nanofiltration Membrane Fabricated on Brush-Painted Single-Walled Carbon Nanotube Network Support for Ion Sieving. *ACS Nano* **2019**, *13* (5), 5278–5290. https://doi.org/10.1021/acsnano.8b09761.

(268) Duan, W.; Ronen, A.; de Leon, J. V.; Dudchenko, A.; Yao, S.; Corbala-Delgado, J.; Yan, A.; Matsumoto, M.; Jassby, D. Treating Anaerobic Sequencing Batch Reactor Effluent with Electrically Conducting Ultrafiltration and Nanofiltration Membranes for Fouling Control. *J. Memb. Sci.* **2016**, *504*, 104–112. https://doi.org/10.1016/j.memsci.2016.01.011.

(269) Karabelas, A. J.; Mitrouli, S. T.; Kostoglou, M. Scaling in Reverse Osmosis Desalination Plants: A Perspective Focusing on Development of Comprehensive Simulation Tools. *Desalination* **2020**,

474 (November 2019), 114193. https://doi.org/10.1016/j.desal.2019.114193.

(270) Turek, M.; Mitko, K.; Piotrowski, K.; Dydo, P.; Laskowska, E.; Jakóbik-Kolon, A. Prospects for High Water Recovery Membrane Desalination. *Desalination* **2017**, *401*, 180–189. https://doi.org/10.1016/j.desal.2016.07.047.

(271) Jung, B.; Kim, C. Y.; Jiao, S.; Rao, U.; Dudchenko, A. V.; Tester, J.; Jassby, D. Enhancing Boron Rejection on Electrically Conducting Reverse Osmosis Membranes through Local Electrochemical PH Modification. *Desalination* **2020**, *476* (September 2019). https://doi.org/10.1016/j.desal.2019.114212.

(272) Veríssimo, S.; Peinemann, K. V.; Bordado, J. Influence of the Diamine Structure on the Nanofiltration Performance, Surface Morphology and Surface Charge of the Composite Polyamide Membranes. *J. Memb. Sci.* **2006**, *279* (1–2), 266–275. https://doi.org/10.1016/j.memsci.2005.12.014.

(273) Tian, J.; Chang, H.; Gao, S.; Zhang, R. How to Fabricate a Negatively Charged NF Membrane for Heavy Metal Removal via the Interfacial Polymerization between PIP and TMC? *Desalination* **2020**, *491* (March), 114499. https://doi.org/10.1016/j.desal.2020.114499.

(274) Peng, H.; Tang, Q.; Tang, S.; Gong, J.; Zhao, Q. Surface Modified Polyamide Nanofiltration Membranes with High Permeability and Stability. *J. Memb. Sci.* **2019**, *592* (August). https://doi.org/10.1016/j.memsci.2019.117386.

(275) Phuntsho, S.; Lotfi, F.; Hong, S.; Shaffer, D. L.; Elimelech, M.; Shon, H. K. Membrane Scaling and Flux Decline during Fertiliser-Drawn Forward Osmosis Desalination of Brackish Groundwater. *Water Res.* **2014**, *57*, 172–182. https://doi.org/10.1016/j.watres.2014.03.034.

(276) Zhang, W.; Luo, J.; Ding, L.; Jaffrin, M. Y. A Review on Flux Decline Control Strategies in Pressure-Driven Membrane Processes. *Ind. Eng. Chem. Res.* **2015**, *54* (11), 2843–2861. https://doi.org/10.1021/ie504848m.

(277) Fei, J.; Mai, W.; Cheng, P. S.; Shi, J.; Liu, Z.; She, Q. Membrane Structure-Dependent Limiting Flux Behavior and Membrane Selectivity Loss during Gypsum Scaling: Implications for Pressure-

Retarded Osmosis Operation and Membrane Design. *Desalination* **2020**, *492* (August), 114644. https://doi.org/10.1016/j.desal.2020.114644.

(278) Lin, N. H.; Shih, W. Y.; Lyster, E.; Cohen, Y. Crystallization of Calcium Sulfate on Polymeric Surfaces. *J. Colloid Interface Sci.* **2011**, *356* (2), 790–797. https://doi.org/10.1016/j.jcis.2011.01.042.

(279) Jawor, A.; Hoek, E. M. V. Effects of Feed Water Temperature on Inorganic Fouling of Brackish Water RO Membranes. *Desalination* **2009**, *235* (1–3), 44–57. https://doi.org/10.1016/j.desal.2008.07.004.

(280) Shih, W. Y.; Rahardianto, A.; Lee, R. W.; Cohen, Y. Morphometric Characterization of Calcium Sulfate Dihydrate (Gypsum) Scale on Reverse Osmosis Membranes. *J. Memb. Sci.* **2005**, *252* (1–2), 253–263. https://doi.org/10.1016/j.memsci.2004.12.023.

(281) Rahardianto, A.; Shih, W. Y.; Lee, R. W.; Cohen, Y. Diagnostic Characterization of Gypsum Scale Formation and Control in RO Membrane Desalination of Brackish Water. *J. Memb. Sci.* **2006**, *279* (1–2), 655–668. https://doi.org/10.1016/j.memsci.2005.12.059.

(282) Cao, B.; Ansari, A.; Yi, X.; Rodrigues, D. F.; Hu, Y. Gypsum Scale Formation on Graphene Oxide Modified Reverse Osmosis Membrane. *J. Memb. Sci.* **2018**, *552* (January), 132–143. https://doi.org/10.1016/j.memsci.2018.02.005.

(283) Benecke, J.; Haas, M.; Baur, F.; Ernst, M. Investigating the Development and Reproducibility of Heterogeneous Gypsum Scaling on Reverse Osmosis Membranes Using Real-Time Membrane Surface Imaging. *Desalination* **2018**, *428* (November 2017), 161–171. https://doi.org/10.1016/j.desal.2017.11.025.

(284) Porcelli, N.; Judd, S. Chemical Cleaning of Potable Water Membranes: A Review. *Sep. Purif. Technol.* **2010**, *71* (2), 137–143. https://doi.org/10.1016/j.seppur.2009.12.007.

(285) Woo, Y. C.; Lee, J. J.; Oh, J. S.; Jang, H. J.; Kim, H. S. Effect of Chemical Cleaning Conditions on the Flux Recovery of Fouled Membrane. *Desalin. Water Treat.* **2013**, *51* (25–27), 5268–5274. https://doi.org/10.1080/19443994.2013.768754.

(286) Tanninen, J.; Platt, S.; Weis, A.; Nyström, M. Long-Term Acid Resistance and Selectivity of NF Membranes in Very Acidic Conditions. *J. Memb. Sci.* **2004**, *240* (1–2), 11–18. https://doi.org/10.1016/j.memsci.2004.04.006.

(287) Simon, A.; Price, W. E.; Nghiem, L. D. Effects of Chemical Cleaning on the Nanofiltration of Pharmaceutically Active Compounds (PhACs). *Sep. Purif. Technol.* **2012**, *88*, 208–215. https://doi.org/10.1016/j.seppur.2011.12.009.

(288) Huang, J.; Luo, J.; Chen, X.; Feng, S.; Wan, Y. How Do Chemical Cleaning Agents Act on Polyamide Nanofiltration Membrane and Fouling Layer? *Ind. Eng. Chem. Res.* **2020**, *59* (40), 17653–17670. https://doi.org/10.1021/acs.iecr.0c03365.

(289) Wadekar, S. S.; Wang, Y.; Lokare, O. R.; Vidic, R. D. Influence of Chemical Cleaning on Physicochemical Characteristics and Ion Rejection by Thin Film Composite Nanofiltration Membranes. *Environ. Sci. Technol.* **2019**, *53* (17), 10166–10176. https://doi.org/10.1021/acs.est.9b02738.

(290) Waly, T. K. A. *Minimizing the Use of Chemicals to Control Scaling in SWRO*; CRC Press, 2011.